



**INSTITUTO POTOSINO DE INVESTIGACIÓN
CIENTÍFICA Y TECNOLÓGICA, A.C.**

POSGRADO EN CONTROL Y SISTEMAS DINÁMICOS

**Generación de comportamientos colectivos
sobre grafos de proximidad**

Tesis que presenta

MCSD. Eber Jafet Ávila Martínez

Para obtener el grado de

Doctor en Control y Sistemas Dinámicos

Director de la Tesis:

Dr. Juan Gonzalo Barajas Ramírez



Constancia de aprobación de la tesis

La tesis **Generación de comportamientos colectivos sobre grafos de proximidad** presentada para obtener el Grado de de Doctor en Control y Sistemas Dinámicos fue elaborada por **Eber Jafet Ávila Martínez** y aprobada el **9 de diciembre de 2021** por los suscritos, designados por el Colegio de Profesores de la División de Control y Sistemas Dinámicos del Instituto Potosino de Investigación Científica y Tecnológica, A.C.

Dr. Juan Gonzalo Barajas Ramírez
(Director de la tesis)

Dr. Cesar Octavio Maldonado Ahumada
(Asesor de la tesis)

Dr. Eric Campos Cantón
(Asesor de la tesis)

Dr. Adrián René Ramírez López
(Asesor de la tesis)

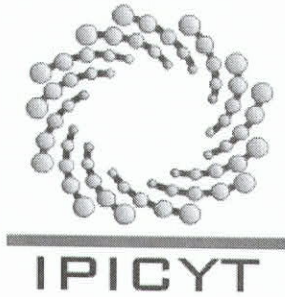
Dr. Juan Ángel Rodríguez Liñan
(Asesor de la tesis)



Créditos Institucionales

Esta tesis fue elaborada en la División de Control y Sistemas Dinámicos del Instituto Potosino de Investigación Científica y Tecnológica, A.C., bajo la dirección del Dr. Juan Gonzalo Barajas Ramírez.

Durante la realización del trabajo el autor recibió una beca académica del Consejo Nacional de Ciencia y Tecnología (No. 279217) y del Instituto Potosino de Investigación Científica y Tecnológica, A. C.



Instituto Potosino de Investigación Científica y Tecnológica, A.C.

Acta de Examen de Grado

El Secretario Académico del Instituto Potosino de Investigación Científica y Tecnológica, A.C., certifica que en el Acta 021 del Libro Primero de Actas de Exámenes de Grado del Programa de Doctorado en Control y Sistemas Dinámicos está asentado lo siguiente:

En la ciudad de San Luis Potosí a los 14 días del mes de enero del año 2022, se reunió a las 12:00 horas en las instalaciones del Instituto Potosino de Investigación Científica y Tecnológica, A.C., el Jurado integrado por:

Dr. Eric Campos Cantón	Presidente	IPICYT
Dr. Juan Gonzalo Barajas Ramírez	Secretario	IPICYT
Dr. Adrián René Ramírez López	Sinodal	IPICYT
Dr. Cesar Octavio Maldonado Ahumada	Sinodal	IPICYT
Dr. Juan Ángel Rodríguez Liñán	Sinodal externo	UANL

a fin de efectuar el examen, que para obtener el Grado de:

DOCTOR EN CONTROL Y SISTEMAS DINÁMICOS

sustentó el C.

Eber Jafet Avila Martínez

sobre la Tesis intitulada:

Generación de comportamientos colectivos sobre grafos de proximidad

que se desarrolló bajo la dirección de

Dr. Juan Gonzalo Barajas Ramírez

El Jurado, después de deliberar, determinó

APROBARLO

Dándose por terminado el acto a las 15:07 horas, procediendo a la firma del Acta los integrantes del Jurado. Dando fe el Secretario Académico del Instituto.

A petición del interesado y para los fines que al mismo convengan, se extiende el presente documento en la ciudad de San Luis Potosí, S.L.P., México, a los 14 días del mes de enero de 2022.


Mtra. Ivonne Lizette Cuevas Vélez
Jefa del Departamento del Posgrado


Dr. Marcial Bonilla Marín
Secretario Académico



IPICYT
SECRETARÍA ACADÉMICA
INSTITUTO POTOSINO DE
INVESTIGACIÓN CIENTÍFICA
Y TECNOLÓGICA, A.C.

A mi esposa y familia.

Agradecimientos

En primer lugar agradezco al Consejo Nacional de Ciencia y Tecnología (CONACYT) y al Instituto Potosino de Investigación Científica y Tecnológica (IPICYT). Al primero, por el apoyo económico brindado durante el periodo de tiempo que comprendió este posgrado. Sin él, estos estudios no hubieran sido posibles. Al segundo, por facilitar la realización del mismo. Las instalaciones, los recursos y el cuerpo académico del instituto, proveyeron de los ingredientes necesarios para el nacimiento de las ideas plasmadas en este documento.

Doy gracias al cuerpo académico de la División de Control y Sistemas Dinámicos (DCS) del IPICYT. La labor de instruir a nuevas generaciones de investigadores es quizá poco reconocida, pero de una importancia inigualable. No se sabe hasta dónde llegaran los conocimientos vertidos en todos los estudiantes de la DCS, pero seguro serán semilla para el nacimiento de nuevas ideas, tecnologías, soluciones a problemas de interés mundial y mucho más. También, doy gracias al M.C. Irwin Allen Díaz Díaz por su apoyo en desarrollo de pruebas de concepto relacionadas con los resultados reportados en esta tesis.

Agradezco especialmente a mi asesor. El Dr. Juan Gonzalo Barajas Ramírez quien no solo me orientó en la realización de esta tesis, sino que lo ha hecho desde mis inicios en el campo de la investigación científica. Doy gracias por su apoyo en el desarrollo de todo el trabajo aquí reportado y en la difusión de los mismos en diferentes congresos. Su guía ha sido incondicional y por ello estaré eternamente agradecido.

También, doy gracias a mi familia; No solo por este, si no por todos los logros personales y académicos obtenidos. Primero, a mis hermanos. Siempre que fuese necesario, incansables, me apoyaron. A mi madre que, con todo su amor y dedicación, estuvo al pendiente de mi salud e integridad física y mental. A mi padre, el principal culpable de la ávida curiosidad que me llevó al camino de la ciencia.

Finalmente, pero no por ello menos importante, doy gracias a mi esposa Roxana Jasso Tenorio. No tengo palabras para describir lo importante que es en mi vida. Respetó mi decisión de continuar mis estudios y me apoyó durante la realización de los mismos; Siempre incondicional. A ella debo mi amor eterno.

Resumen

El control distribuido de sistemas de múltiples robots ha sido estudiado ampliamente durante las pasadas décadas. Modelando las interacciones locales a través de grafos, marcos teóricos han sido desarrollados para analizar y sintetizar movimientos coordinados. En ellos, la principal inspiración del diseño de controladores distribuidos son los comportamientos colectivos observados en insectos sociales, peces, aves y algunos mamíferos. Codificando reglas de interacción local, los controladores dirigen el movimiento de los sistemas de múltiples robots hacia un comportamiento deseado tal como sincronización, consenso o flocking.

En esta tesis diseñamos controladores distribuidos para dirigir sistemas de múltiples robots con restricciones hacia comportamientos de consenso y flocking. La mayor diferencia entre este trabajo y los reportados en la literatura recae en las restricciones de comunicación y de movimiento consideradas en nuestros diseños. Estas restricciones son intrínsecas a los robots, como limitaciones en las entradas de control o los rangos de comunicación, o al espacio de trabajo, como la presencia de obstáculos.

En el capítulo 1 se motiva e introduce el estudio de movimientos colectivos en sistemas de múltiples robots. Se discuten conceptos como *controladores distribuidos* y *comportamientos colectivos*. Posteriormente, se definen los problemas de consenso y flocking. También discutimos los resultados más recientes en ambos temas.

En el capítulo 2 se revisan algunos conceptos básicos de teoría de grafos y se discuten brevemente algunas técnicas de control que permiten describir los modelos de dos tipos de robots móviles como sistemas dinámicos de segundo orden. Posteriormente, se describen los problemas de control de movimiento en los sistemas de múltiples robots para los cuales se diseñan controladores distribuidos. También, se introduce el concepto de grafo de proximidad.

El capítulo 3 se enfoca en los problemas de consenso. Se diseñan controladores para configuraciones sin líder y líder-seguidores en grafos dirigidos fijos y de proximidad bidireccionales. Condiciones necesarias y suficientes son presentadas para garantizar consenso bajo suposiciones leves sobre la conectividad del grafo dirigido. Para el caso de grafos de proximidad bidireccionales, los controladores garantizan la preservación de la conectividad, esto es, solo permiten la adición de enlaces conservando la conectividad inicial del grafo de proximidad.

En el capítulo 4 se estudian los problemas de flocking en grafos de proximidad bidireccionales y dirigidos. Los controladores diseñados satisfacen restricciones heterogéneas en las entradas aún en presencia de obstáculos en el espacio de trabajo para el primer caso. Por otro lado, para grafos dirigidos, se analiza el primer vector propio izquierdo de la matriz Laplaciana asociada con el grafo. Una medida distribuida que refleja la conectividad del grafo completo se construye con las entradas de dicho vector. Luego, se explotan dichas propiedades en el diseño del controlador propuesto.

Por último, se dan algunos comentarios finales y se discuten algunas direcciones futuras de investigación en el capítulo 5.

Abstract

The distributed control of multi-robot systems has been studied extensively in the past few decades. Theoretical frameworks, where graphs model the local interactions between robots, have been developed to analyze and synthesize coordinated motions. There, collective behaviours observed in social insects, fishes, birds and mammals are the main inspiration of the distributed controller designs. Encoding local interaction rules, controllers steer the multi-robot system's motion towards the desired behaviour, such as synchronization, consensus or flocking.

In this thesis, we design distributed controllers to steer a constrained multi-robot system into consensus and flocking. The main difference between our designs and previous works are the communication and motion constraints contemplated for our designs. Such limitations are intrinsic either to the mobile robots, like bounded inputs and detection ranges or to the environment, like obstacles in the workspace.

Chapter 1 motivates and introduces the study of collective motions in multi-robot systems. We discuss concepts like *distributed controllers* and *collective behaviours* in multi-robot systems. Later, the consensus and flocking motion problems are defined. In both cases, we discuss some of the latest published results in these topics.

In Chapter 2, we revise some basic concepts on graph theory and briefly discuss control techniques to model two kinds of mobile robots, namely differential mobile robots and quadcopters, as second-order dynamic systems. Then, we present the multi-robot systems motion control problems to which we design distributed controllers. Here, we also introduce the concept of proximity digraph.

Chapter 3 focuses on consensus problems. We design distributed controllers for leaderless and leader-followers configurations in both fixed digraphs and bidirectional proximity graphs. We derive necessary and sufficient stability conditions for consensus over fixed digraphs with mild connectivity assumptions. As for bidirectional proximity graphs, our designs are connectivity preservers, i.e. allow only edge additions conserving the initial connectivity of the proximity graph.

In Chapter 4, we study flocking motion problems in bidirectional and directed proximity graphs. For the first ones, the designed controllers satisfy heterogeneous input constraints even in the presence of obstacles. On the other hand, for directed proximity graphs, the first-left eigenvector of the matrix Laplacian associated with it is analyzed. With its entries, we build a distributed connectivity measure that reflects the overall network connectivity. We use its properties in our controller designs.

We give some final comments and future research directions in Chapter 5.

Contents

Constancia de Aprobación de la Tesis	iii
Créditos Institucionales	v
Acta de Examen	vii
Dedicatoria	ix
Agradecimientos	xi
Resumen	xiii
Abstract	xiv
1 Introduction	1
1.1 Classification of robots	2
1.1.1 Fixed robots	3
1.1.2 Mobile robots	3
1.2 Interconnected robots	3
1.2.1 Networked robots	3
1.2.2 Network of robots	4
1.2.3 Multi-robot systems	4
1.3 Control of multi-robot systems	5
1.3.1 Motion control	6
1.4 Consensus and flocking motion control of multi-robot systems	8
1.4.1 Consensus on multi-robot systems	9
1.4.2 Flocking motion on multi-robot systems	11
1.5 Problem description	12
1.6 Document description	13
1.7 Published results	14
2 Preliminaries	15
2.1 Graph theory	16
2.1.1 Paths and connectivity	17
2.1.2 Weighted digraphs	18
2.1.3 Algebraic Graph Theory	18
2.2 Mobile robots dynamic models	21

2.2.1	Differential mobile robot	22
2.2.2	Quadrotor	25
2.3	Multi-robot systems control problems	28
2.3.1	Proximity digraphs	29
2.3.2	Consensus	31
2.3.3	Flocking problem	31
3	Consensus Problems	33
3.1	Consensus problem over fixed digraphs	33
3.1.1	Leaderless consensus	34
3.1.2	Leader-followers configuration	39
3.2	Consensus problems over proximity graphs	45
3.2.1	Leaderless configuration	47
3.2.2	Leader-followers configuration	52
4	Flocking Problems	58
4.1	Bidirectional proximity graphs	58
4.1.1	Leaderless configuration	59
4.1.2	Leader-followers configuration	67
4.1.3	Flocking motion with obstacle avoidance	70
4.2	Directed Proximity Graphs	79
4.2.1	Connectivity measure	80
4.2.2	Controller design	85
4.2.3	Stability analysis	86
5	Final Comments	96
5.1	Future work	97
	Bibliography	99

Introduction

Almost a century has passed since the first appearance of the word *robot* in Karel Čapek's play *R. U. R.: Rossum's Universal Robot* back in 1921 [1]. Derived from the word *robota*, which means forced labour or slave worker in Slav languages, the term robot was used to describe artificial human beings; magnificent workers deprived of unnecessary qualities like feelings, creativity and capacity of feeling pain. Although Čapek envisioned robots as human-shaped factory workers, it took decades to introduce actual robots into industrial production processes, not artificial human beings for sure, but mechanical arms developing repetitive tasks, and relegating humans from dangerous environments, mainly in car assembling lines. This humanoid concept of robots inspired many scientific and technological advances over the following years and became a very active research field in its own right.

Robotics, is the engineering field that studies the science and technology of designing, building and using robots [2–4]. This field has advanced by leaps and bounds in recent years [5–7]. Back in 1961, the *Unimate*¹ (Figure 1.1a), the most advanced robotic arm at the time, with commands stored on a magnetic drum, it was used in the car industry to automate metalworking and welding processes. Later, *Shakey*² (Figure 1.1b) was the first mobile robot, build in 1966 and capable of performing task that required planning, route-finding, and rearranging of simple objects. Now, at 2021, *Atlas*³ is one of the most advanced humanoid robots; this amazing machine measures 1.5m height, weights 75kg, is equipped with stereo vision and its body takes advantage of 3D printing technology to save space and weight (Figure 1.1c). Atlas its capable of manipulate objects in the environment and travel on rough terrain. However, nowadays there is not a unified definition of what a robot is. In the literature, one can find different definitions such as:

- (*Oxford dictionary*) A machine capable of carrying out a complex series of actions automatically, especially one programmable by a computer [8].
- (*Cambridge dictionary*) A machine controlled by a computer that is used to

¹www.robotics.org

²www.sri.com

³www.bostondynamics.com

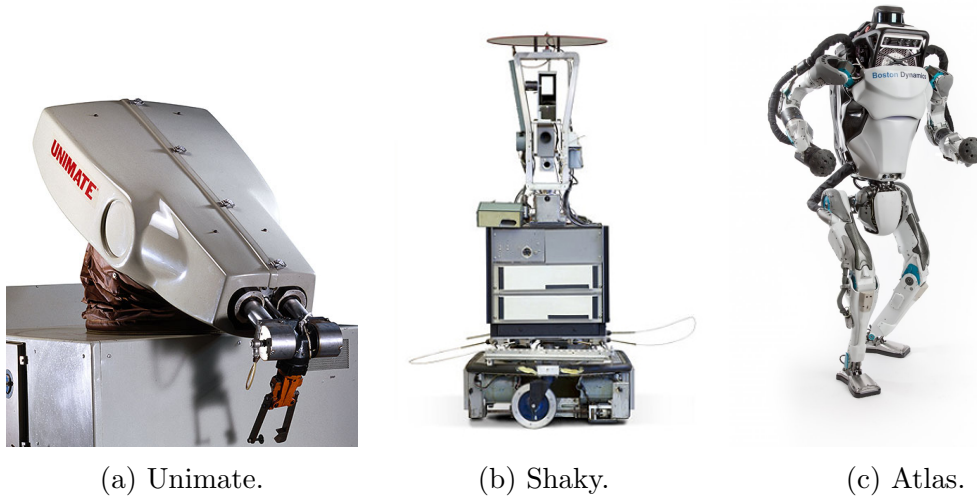


Figure 1.1: Robotics advances: (a) The first industrial robot arm (1961); (b) The first mobile robot (1966); (c) The most advanced humanoid robot (2021).

perform jobs automatically [9].

- (*Random House Webster's dictionary*) A machine that looks something like a human and does mechanical tasks [10].

A *robotic system*, as showed in Figure 1.2, is formed by actuators, sensors and a control unit [2]. The essential component of a robot is the *mechanical system* endowed, in general, with locomotion apparatuses like wheels, crawlers, mechanical legs, and the like, along with a manipulator apparatus such as mechanical arms and effectors, among others. This provides robots with the ability to exert an action over their environment. In a robot, the *actuator unit* is what animates the mechanical components. Thus, this system is in charge of motion control and deals with servomotors, drives and transmissions. The ability to acquire data, either internal (with encoders, temperature sensors, and others) or external (with proximity sensors, cameras, or communication devices, to name a few), is entrusted to the *sensor system*. This unit includes all the signals conditioning and information retrieval. Finally, the *control system* is in charge of the connection between perception and action, *i.e.*, it commands the execution of actions according to the goals set by the given tasks and the collected information through sensors.

1.1 Classification of robots

Robots can be classified concerning the environment in which they operate. *Fixed* and *mobile* robots, is the most common classification. These two robot classes perform tasks on very different working environments and require very distinct capabilities.

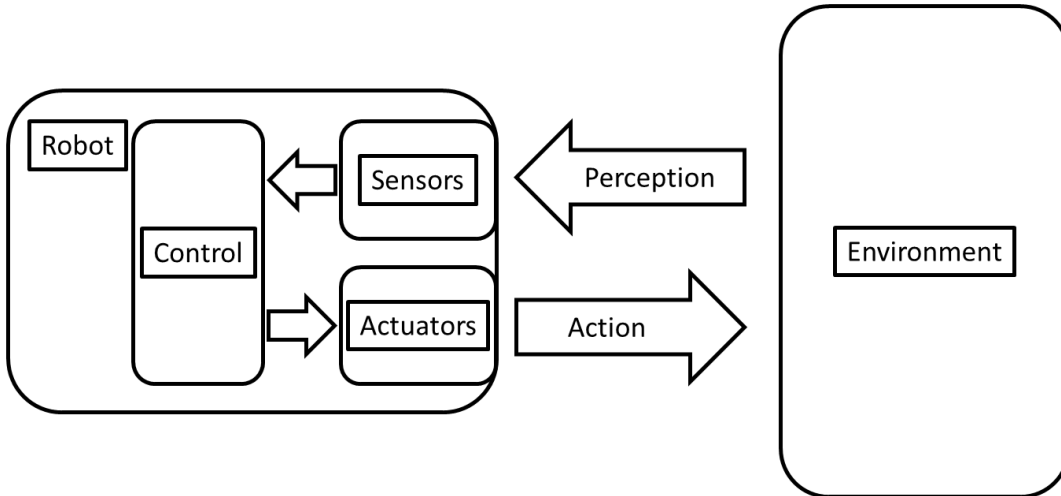


Figure 1.2: Robotic system interacting with the environment.

1.1.1 Fixed robots

Robots attached to a fixed platform on the ground are called *fixed robots*. This type of robot relies on internal sensors to compute its position relative to the surroundings. Most fixed robots are manipulators which consist of a sequence of rigid bodies (links) interconnected through articulations (joints) with industrial applications like soldering, painting, movement of parts and others [4, 11].

1.1.2 Mobile robots

Robotic systems equipped with motion mechanisms are called *mobile robots*. Most implementations of mobile robots depends on their mechanism of motion: aquatic (underwater exploration), terrestrial (vacuum cleaners and self-driving cars) and aerial (aerial photography)[4, 11, 12]. This type of robot relies on its perception of the environment to compute its position and deal with different unknown situations that might change over time. Such environments might include fixed obstacles or unpredictable entities like animals or humans.

1.2 Interconnected robots

1.2.1 Networked robots

A robotic system connected to a communication network, such as the Internet or a local area network (LAN), is called a *networked robot* [11]. Either wired or wireless, the network can be based on any data transport protocol. Applications of these systems range from automation to exploration. There are two classes of networked robots⁴: Teleoperated and autonomous. Teleoperated robots are supervised and managed by

⁴The *IEEE technical committee on networked robots* adopted this classification (www.ieee-ras.org).

a human (the operator). In this class, the operator sends commands to be executed by the robot. And, additionally, he might receive feedback through the network as the internal states of the robot or the task status. Autonomous networked robots use the network to send or receive information without external intervention. Here, robots and sensors exchange data via the network, extending the effective sensing range of robots and allowing them to communicate with each other over long distances to coordinate their activities. Thus, sensing, data process and actuation need no longer be collocated. This autonomy does not impede the existence of a monitoring system that displays relevant information to the manager [13].

Applications of networked robots are vast. Some examples range from coordinated industrial processes, like welding, remote manipulation or manufacturing, to military implementations of coverage and reconnaissance with Unmanned Aerial or Ground Vehicles (UAVs or UGVs) [14, 15]; Even in research areas, networked robots are helpful, like in undersea monitoring with Unmanned Underwater Vehicles (UUVs) [16, 17]. Nonetheless, networked robots pose several challenges for being successfully implemented, especially those related to networks. Often, communication is noisy and have fixed or variable time delays. Even channel congestions and network instability are frequent issues. Therefore, a broad challenge in networked robots is to develop scientific bases that couples communication, perception and control that allow their successful implementations.

1.2.2 Network of robots

A *network of robots* refers to a group of networked robots connected by links through which they share information and work together in a common task [11]. Both teleoperated or autonomous robots might form a network of robots. In a network of robots, a member might be aware of the information of a distant teammate and consider it for task planning. Therefore, to become a system with greater abilities than the sum of its parts, a network of robots combines and complements robot capacities. Some examples of these systems implementations are underwater manipulation and transportation with UUVs [18], precision farming with a combination of UGVs and UAVs [19, 20] and space exploration [21], to name a few.

1.2.3 Multi-robot systems

A multi-robot system consists of an autonomous mobile robots (agents⁵) group with limited information sharing capabilities and computational resources. As a result of implementing coordination laws, a multi-robot system provides several advantages over single robotic systems, including robustness, flexibility and scalability [24]. a) *Robustness* is due to inherent redundancy by considering multiple robots with a common objective with no predefined role for each one; Also, if a robot fails on performing a given task, is damaged or completely lost, the remaining members compensate its role.

⁵*Agent* is anything that can be viewed as perceiving its environment through sensors and acting upon the environment through effectors, *e.g. a robotic system* [22, 23].

b) *Flexibility* is because a multi-robot system can adapt to different tasks and environments without any hardware specialization. c) *Scalability* is due to robots acting based only on local rules and, if the team size increase, they maintain its functionality without any interaction mechanism redefinition.

There are broadly two kinds of multi-robot systems: Homogeneous and heterogeneous. When robots in a multi-robot system have the same abilities, it is called a *homogeneous multi-robot system*. Therefore, they are sometimes called robotic swarms due to the homogeneity observed in nature, where groups of individuals such as ants, bees, fish, and birds, solve complex tasks using the limited information that each individual perceives [25, 26]. These systems fit well when every robot has the same goal and, although incapable of achieving it by itself, the cooperation between them is enough to accomplish it. On the other hand, when robots in a multi-robot system have different abilities, we call it a *heterogeneous multi-robot system*. This kind of system aims to exploit robot differences and achieve goals impossible with a homogeneous group, or at least do it more efficiently.

Recent implementations of multi-robot systems are many and for different tasks. For homogeneous systems, location, navigation and predator-prey tasks with UGVs or UAVs are just some examples [27–30]; They are even used to study and reproduce natural processes as morphogenesis [31, 32] and segregation [33]. On the other hand, heterogeneous multi-robot systems implementations focus on exploiting their properties. Combinations of UGVs and UAVs are often used to solve tasks like reconnaissance and surveillance, urban search and rescue, mapping and detection [34–38].

Physical implementations of multi-robot systems, as the ones recently discussed, most likely require robots to move from one place on their workspace to another. In the following section, we discuss the general schemes to control multi-robot systems. Then, we focus on the controller design approaches to coordinate their motion.

1.3 Control of multi-robot systems

Generally, there are three basic approaches to control multi-robot systems: Centralized, decentralized and distributed. a) The *centralized approach* assumes there exists a sufficiently potent central unit to collect and process the information of every robot. Then, it calculates and applies the individual control to every robot accordingly to the desired reference. This approach, shown in Figure 1.3a, is an extension of the single-system control scheme. b) The *decentralized approach* consists of controllers that receive information from all robots but apply control actions to only a part of them. This approach execute control laws designed in a centralized fashion. Figure 1.3b illustrates this approach. c) The *distributed approach* consists of individual controllers which use only the locally available information shared through an interconnection structure of the overall system. Some of the local controllers might have references, but in general, the control action for each system is based only on the information of its neighbours established by the interconnection structure. This approach allows simpler controller designs but, to achieve global objectives, requires more complex solutions than the centralized and decentralized versions [39]. Figure 1.3c shows this approach.

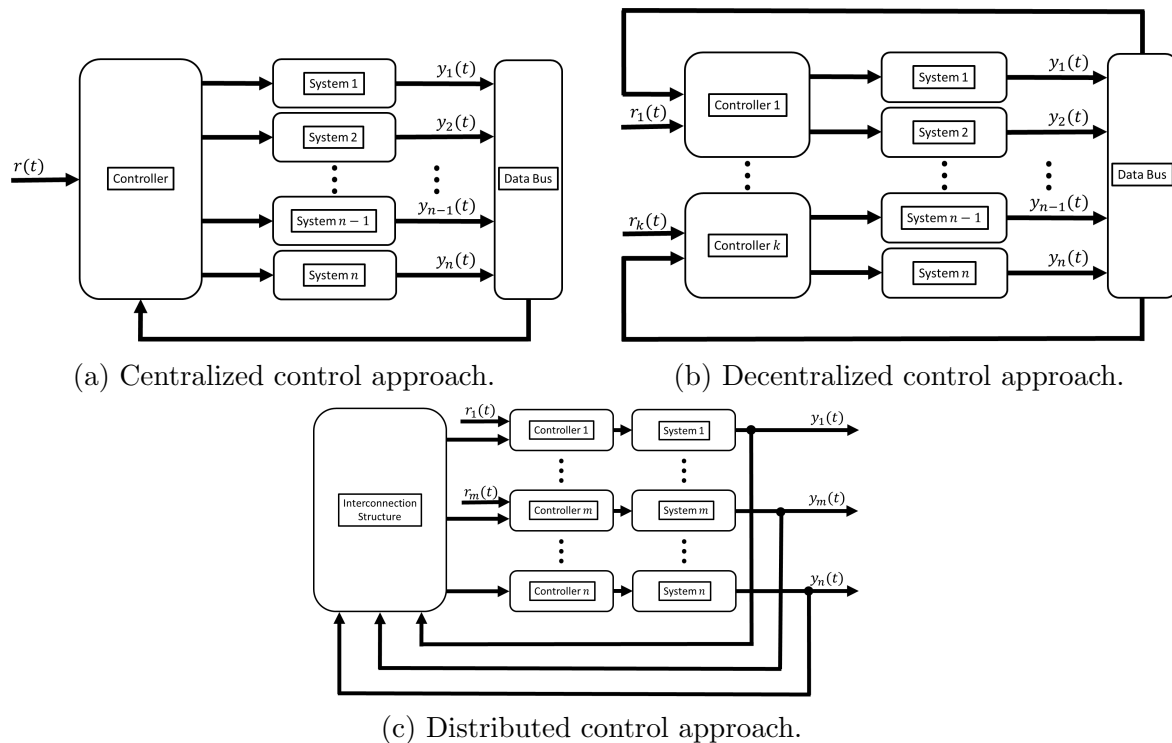


Figure 1.3: Different approaches to multi-robot systems control.

1.3.1 Motion control

A fundamental problem in multi-robot systems is the design of controllers to make the robots move as a group towards a common goal [24, 40]. A seemingly simple task but, when motion constraints are considered, is more complex than it appears. In this section, we present some of these motion limitations. Then, we discuss the two distributed controller's design approaches.

Motion constraints

To better deal with multi-robot systems in real-world applications, it is necessary to consider their intrinsic motion and coordination constraints in the controller design process. These limitations are attributed either to the robots or the environment through which they navigate. Figure 1.4 shows the multi-robot system constraints considered in this thesis. We discuss them in what follows.

On the one hand, robot attributed constraints are those rising from its physical properties and capabilities. In this sense, the masses, sensing ranges and input constraints shown in Figure 1.4a-c are robot attributed. One or all of these constraints usually appear in heterogeneous multi-robot system setups. Robots with different capabilities most likely will have different sizes and thus different masses, sensing ranges and input constraints; Although, when these constraints are equal for every robot, then the multi-robot system is homogeneous. On the other hand, obstacles in the workspace is a constraint attributed to the environment (Figure 1.4d). For safety reasons, robots

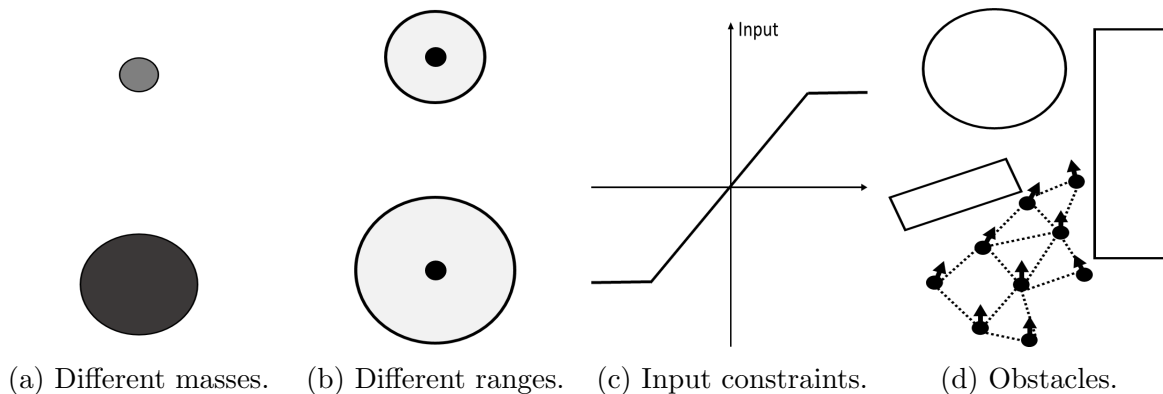


Figure 1.4: Examples of multi-robot systems constraints.

must avoid collisions with these objects. Therefore, they impose limitations on the possible trajectories that the multi-robot system can take. Combinations of these robots and environmental constraints are present in real-world implementations of multi-robot systems. Therefore, to achieve a desired coordinated motion, the controllers' design process must consider them.

Controller design approaches

In the design of controllers to solve the motion coordination problem, there are two approaches: Structural and behavioural [31]. We describe both of them in what follows.

The *structural approach* consists of each robot computing its proper position in a predefined formation (or virtual structure) based on the location of the others. That is, the controller calculates the robot's position error with respect to the desired predefined formation and generates an input vector steering it to its correct location within the virtual structure [40, 41]. In this approach, there are three techniques: 1) The *unit-centre-referenced* (Figure 1.5a), which builds the desired formation around the position centre of the whole group; 2) The *leader-referenced* (Figure 1.5b), which builds the formation around the position of a leader who doesn't follow any other robot; 3) The *neighbourhood-referenced* (Figure 1.5c), which predefines desired distances between each robot and its neighbours, resulting on the desired overall formation. Notice that the unit-centre-referenced and leader-referenced approaches require access to global information, respectively the location of the centre and the position of the leader, which impedes their use on a distributed scheme. The neighbourhood-referenced approach, on the other hand, accepts distributed implementations. However, the structure needs to be previously defined. This requirement precludes its use in a multi-robot system where the information network changes over time since it requires a predefined formation for each possible network configuration.

On the other hand, the collective behaviours observed in nature inspire the *behavioural approach*, hence its name. Figure 1.6 show some of those so-called emergent behaviours where nobody dictates the movement of every single individual nor the final shape of the group. In the behavioural approach, the fulfilment of local rules triggers

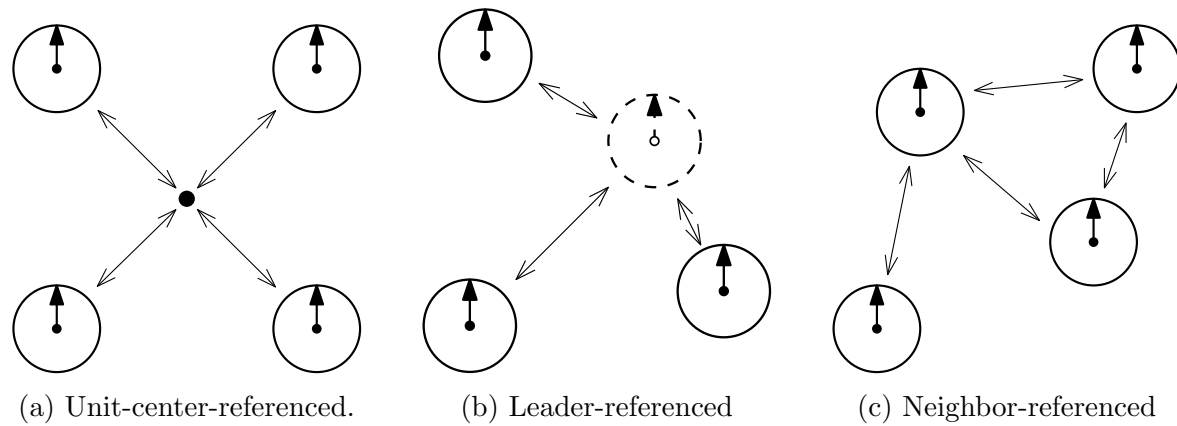


Figure 1.5: The structured approach to motion control of multi-robot systems [40].



(a) Schooling fish.



(b) Flocking birds.

Figure 1.6: Collective behaviors in nature.

each robot's motion, the same way as the emergent behaviours originate in nature. That is, the controller of each robot encodes heuristic rules considering only the locally collected information. As such, and because there is no predefined formation, network configuration changes affect but do not impede the task achievement, as we will see from our results. There are several examples of collective behaviours: Synchronization, rendezvous, consensus and flocking.

In the following section, we define the control and controller design approaches used in this thesis, discuss the desired coordinated motions to be induced in the multi-robot system and review the up to date results in the topic.

1.4 Consensus and flocking motion control of multi-robot systems

A natural approach for motion control of multi-robot systems is the distributed approach, mainly because they are cheaper to implement. The distributed control of multi-robot systems requires less powerful processors, sensors and communication devices than their centralized and decentralized equivalents. However, the complex part is their design, especially when contemplating both robot and environmental motion constraints.

As stated by Cortéz and Egerstedt in [24], to be practical, a distributed controller design for multi-robot systems has to satisfy the following constraints: That is, it must be: 1) *Local*, on information, because is the only available data; 2) *Scalable*, as individual actions, dictated by the controller, cannot depend on team size; 3) *Safe*, for robots, avoiding collisions between individuals and with their surroundings and; 4) *Emergent*, since desired global properties and behaviours should emerge from local interactions. Due to physical and performance constraints is not easy to design distributed controllers with all the above properties [24].

To achieve the distributed controller properties described above, we use the behavioural design approach. This design decision is due to the robot and environmental physical constraints considered in this work. We mainly contemplate multi-robot systems where robots have limited sensing ranges and, because of this consideration, we cannot predefine a virtual structure to steer robots into the desired formation. Also, the neighbourhood within which robots collect information might change over time, and we would need a virtual structure for each possible configuration. In contrast, the behavioural design approach allows us to deal with time-varying neighbourhoods. However, we carefully need to design the local interaction rules and embed them in distributed controllers to steer a multi-robot system towards the desired coordinated motion; This is the main topic of this thesis, widely discussed in the following chapters.

Information sharing is crucial in the design of distributed controllers for multi-robot systems. If a robot is not sharing, receiving, or sensing data from others, the fulfilment of a common objective cannot be guaranteed. Therefore, shared information is a necessary condition for coordination [42]. The information flow, through the onboard communication devices or sensors, between nodes describes the *information network* of the multi-robot system. Robots with unlimited information sharing capabilities can construct fixed networks, even with an all-to-all connection. Meanwhile, if they are distance-limited, the proximity between robots determines the connection topology of the information network with edges that might appear or disappear as robots approach or move away from each other; In consequence, the distributed controller designs must take into account the information network connection properties and, if necessary, must guarantee them.

In this thesis, we limit our attention to consensus and flocking motions in multi-robot systems. In the following sections, we define these motions and discuss the most recent research on these topics. Our literature review focus on the investigations that contemplate every, or some combinations, of the previously discussed motion constraints.

1.4.1 Consensus on multi-robot systems

Consensus means to reach an agreement regarding a certain quantity of interest that depends on the states of all group members [43]. The agreement must be a result of interactions between agents via an *information network*. To achieve consensus there must be a shared variable of interest, called *information state*, and an interaction rule specifying how individuals share the information called *consensus algorithm or protocol*. In the motion coordination of multi-robot systems, one or both, the robot's position

and velocity vectors define the information state. Meanwhile, the ability of the robots to gather local information through their communication or sensing devices defines the information network. Finally, the distributed controllers embed the consensus algorithm.

Historically, consensus problems were studied in opinion formation [44]. Perhaps the first study of consensus in physically constrained systems was carried out by Vicsek in [45]. He observed a velocity alignment of moving particles implementing a nearest position neighbours algorithms. Later, Jadbabaie provided a theoretical explanation of this emergent behaviour [46]. Since then, there have been many reported studies on consensus problems. A consistent framework in the topic was presented in [43] by Olfati Saber. Surveys like [47–49] summarize the recent consensus problem researches from a control systems perspective.

In this thesis, we contemplate two different setups for consensus in multi-robot systems. First, we consider a group of robots where each has different inertias and unlimited sensing ranges; Allowing us to assume the existence of fixed information networks. The second one contemplates a similar setup but with limited sensing ranges. Therefore, in this case, the information network is time-varying. The following state of knowledge resumes the already reported researches related to both of these setups.

State of knowledge

For robots (agents) with different masses and unlimited sensing ranges, almost all the results give sufficient conditions to achieve consensus; for either fixed or switching strongly connected networks [50, 51]. On the other hand, necessary and sufficient conditions are presented in [52] for *weakly* connected fixed networks with communication time delays. Here, a leader defining the desired agreement position and velocity vectors is contemplated. In contrast, we develop necessary and sufficient consensus conditions for fixed networks with minimum connectivity requirements. Also, the developed controllers support configurations without a leader and with a leader moving at a time-varying velocity.

On the other hand, when contemplating limited sensing ranges, studies often focus on robots with unitary inertias, i.e., heterogeneous multi-robot systems. As the previously reported results, and ours, in fixed networks unveil, the network’s configuration plays a fundamental role in achieving consensus. Not surprisingly, in this scenario, connectivity preservation is a big concern ⁶. Works about it often design distributed controllers generating unbounded control actions [54–57]. Other researchers provide controller designs with bounded magnitude [58–62]. However, in most of the cases, they only contemplate leaderless or leader-followers consensus configurations where the leader moves at a constant velocity. In contrast, our distributed controller designs are for heterogeneous multi-robot systems, where robots might have different inertias. Additionally, we investigate and develop a controller for the leader-followers scenario when the leader’s velocity is time-varying. All of our designs produce bounded control efforts.

⁶See [53] for a survey on this topic

1.4.2 Flocking motion on multi-robot systems

Flocking behaviour receives its name from the collective movement observed in groups of starlings, seagulls and other birds. This term refers to the motion that emerges from local interactions involving a large number of individuals. Although inspired by birds, the name is used to describe the coordinated motion of microorganisms, insects, fish, mammals and groups of autonomous robots. In the case of multi-robot systems, flocking means every robot must fulfil the three following rules: 1) collision avoidance: attempt to avoid collisions with nearby flockmates; 2) velocity matching: attempt to match nearby flockmates velocities; 3) flock centring: attempt to stay close to nearby flock mates. These behavioral rules are also known as *separation*, *alignment* and *cohesion*, and gave birth to the famous Reynolds' *Boids* model [63].

Although a computer graphics animation originated the Boids model, it found its way to the coordinated motion of multi-robot systems. From a control systems point of view, a theoretical framework to study flocking motion in multi-robot systems was developed by Olfati Saber back in 2007 [64]. Under this scheme, Olfati-Saber combines the control systems and graph theories to analyze interconnected dynamic systems and use the gradient-descent approach to synthesize distributed controllers to drive the particle-shaped robots to consistent flocking behaviour. Since then, many controller designs and for different kinds of multi-robot system setups have been reported. A recent survey overviews a collection of those results [65].

In this thesis, we contemplate three different scenarios for flocking in multi-robot systems. The first one is for robots with homogeneously limited sensing ranges and heterogeneous input constraints. Then, we extend our results to consider workspace obstacles, which sets our second scenario. Finally, we drop out the input and environmental constraints to contemplate robots with different sensing ranges. The following state of knowledge resumes the already reported researches related to these setups.

State of knowledge

Up to date, year 2021, almost all existing works in flocking motion in multi-robot systems with homogeneous limited sensing ranges do not contemplate input constraints [66–68]. However, to be useful in real-world implementations, the distributed controller designs must consider restrictions on their magnitudes [69]. Therefore, other researchers designed bounded distributed controllers, but this is a mere result of implementing bounded controller terms [70–76]. A few reported results provide distributed controller designs with predefined magnitude bounds, see [77, 78]. A similar quantity contemplates differences between the robots' input limitations [79, 80]. Nonetheless, the results in [77, 78] implement a model predictive scheme and require a discretization of the robot's motion dynamics. Also, they assume the dynamic network remains connected between discrete steps. On the other hand, the results in [79, 80] only contemplate the position dynamics of the robots, do not guarantee inter-robot collision avoidance and are fragile to single edge failures. In contrast, our designs do not require a discretization process, contemplate both robot's position and velocity dynamics, guarantee inter-robot collision avoidance and are more robust to edge failures, as they consider the whole neighbourhood of each robot and not only one neighbour.

Flocking motion in a workspace that includes obstacles has been studied ever since the theoretical framework to study flocking was proposed. However, they usually do not contemplate any predefined input bounds [64, 81, 82]. To the best of our knowledge, just one work consider such a scenario. In [83], the distributed controller must fulfil a predefined input bound, equal for all robots, but cannot ensure inter-robot collision avoidance. In contrast, the magnitude of our designed controller always remains under predefined individual input constraints, even in the presence of nearby obstacles and inter-robot collision avoidance manoeuvres.

Every of the flocking motion researches cited in this section has as an essential feature the information network's connectivity preservation. As we discussed before, without some basic network connectivity properties, no coordinated motion is achievable. With this requirement, almost every distributed controller design aims to preserve every edge in the initial information network, allowing only the addition of new ones while the system evolves. Connectivity is a global property of the information network. To grant robots the ability to decide which edges preserve and which not, we need to provide them with a local sense of the overall information network configuration. Some researchers use a distributed estimation of a connectivity measure called *algebraic connectivity*; See [84–89] for details on the estimation processes. With minor changes, algebraic connectivity estimations are used in multi-robot systems with homogeneous and heterogeneous sensing capabilities. The gradient, with respect to the robot's position, of the algebraic connectivity points towards its increasing direction. This property allows the controller designs based on the gradient-descent method, allowing even obstacle avoidance features [90–93]. However, this is only the case for multi-robot systems with homogeneous sensing abilities. The relation between the edge weights and the gradient with respect to the robot's position does not hold in the heterogeneous case. In this situation and assuming the sensing range can be increased or decreased as needed, in [89], an estimation of the real part of the algebraic connectivity measure serves as an indicator of which edges to maintain and the distributed controllers design modifies the sensing range to preserve them. On the other hand, a new kind of connectivity measure is presented in [94]. It uses the first-left eigenvector entries of the Laplacian matrix associated with the information network. This measure indicates which edge should be maintained. A tension between connecting edges is built with this measure is proposed as the distributed controller. In contrast, we study the properties of the connectivity measure given in [94]. We also unveil its relation with the distance-dependent edge weights. This property allows us to build a distributed controller using the gradient-descent method to achieve flocking motion in multi-robot systems with heterogeneous sensing constraints.

1.5 Problem description

The main objective of this thesis is the design of distributed controllers for a physically constrained heterogeneous multi-robot system to achieve coordinated motions like consensus or flocking. We propose solutions for multi-robot systems with constraints attributed to both robots and the environment. Regarding the robot attributed limi-

tations, we contemplate limited sensing ranges and bounded actuator devices. Additionally, the inertia and the capacities of a robot might be different from others in the group. On the other hand, environmental constraints are imposed by obstacles in the workspace.

Notice that, for consensus behaviour, each robot aims to align its position and velocity with those robots in the neighbourhood. Meanwhile, for flocking behaviour, robots try to align their velocity vectors while avoiding the group's fragmentation and collision with other robots and obstacles. From the above description of the problem in this thesis, we propose the following hypothesis: *Distributed controllers encoding proper interaction rules lead physically constrained heterogeneous multi-robot systems towards desired collective behaviours such as consensus and flocking.* In particular, we deal with the following objectives. For consensus behaviour, our goal is to steer robots towards a fixed position deviation with velocity alignment. We contemplate two scenarios, both in multi-robot systems where the robot inertias might be different. The first one is for fixed information networks. Our controller designs embed a local rule on each robot of approaching towards the states of its neighbours. We provide necessary and sufficient conditions to ensure consensus with minor network's connectivity conditions. In the second one, we contemplate robots with homogeneously limited sensing ranges. This setup implies time-variant information networks. We use the previously described local interaction rule again. However, to synthesize the distributed controller, we use the gradient-descent method. With our proposal, we guarantee both consensus achievement and the information network's connectivity preservation. For flocking behaviour, our goal is to achieve a coordinated motion free of collisions between robots and with the obstacles in the workspace. There are three setups for this behaviour; In all of them, we implement the three rules of the Reynolds' boids model (separation, alignment and cohesion) and use the gradient-descent method to synthesize the distributed controller. The first one, for multi-robot systems with homogeneous sensing limitations and heterogeneous input constraints. Our design allows robots with higher capabilities to compensate for the coordination movements that their less adept neighbours cannot. We extend this setup to contemplate obstacles in the workspace with the same benefits; This is the second setup. As for the third setup, we consider a multi-robot system with heterogeneous constraints in the sensing ranges, without input limitations or obstacles. In our controller design, a distributed connectivity measure of the overall networks configuration is used to choose the edges to preserve. The proposed controller allows less restrictive network configurations than previously reported results. Based on graph and control theory, we derive conditions over the network configuration and controller properties and gains to guarantee the multi-robot systems achieves the desired behaviour.

1.6 Document description

In Chapter 2, we give some basic concepts of graph theory, briefly describe some control methods to model the motion of mobile robots as second-order systems and define the consensus and flocking problems studied in this thesis. Chapter 3 discuss

the consensus problems. We design distributed controllers for both fixed and proximity graphs of multi-robot systems with different inertias. In Chapter 4, we tackle flocking problems. We present distributed controllers for three different combinations of homogeneous and heterogeneous sensing range limitations, input constraints and obstacles in the workspace. Lastly, we give some final comments about this thesis and future work in Chapter 5.

1.7 Published results

The results presented in this thesis were, or plan to be, published in a few conference proceedings or scientific magazines. Our reported results are:

- A distributed controller design for consensus motion in multi-robot systems with a time-invariant network. The controller design was carried out for a multi-robot system where robots possess different acceleration magnitudes and the information network is directed. This result was presented as part of the *Congreso Nacional de Control Automático (AMCA) 2017* held in Monterrey, Nuevo León, México. And it was published in its conference proceedings under the title *Consenso con líder virtual en sistemas de múltiples agentes inerciales*, reference [95]. The authors are Eber J. Ávila-Martínez and Juan G. Barajas-Ramírez.
- A distributed controller design for consensus motion in multi-robot systems with a time-variant network. The controller design considers a multi-robot system where robots possess different acceleration magnitudes and homogeneous information sharing range limitations. This result was presented as part of the *Second Conference on Modeling, Identification and Control of Nonlinear Systems IFAC MICNON 2018* held in Guadalajara, Jalisco, México. And it was published in its conference proceedings under the title *Distributed control for consensus on leader-followers proximity graphs*, reference [96]. The authors are Eber J. Ávila-Martínez and Juan G. Barajas-Ramírez.
- A distributed controller design for flocking motion in multi-agent systems with a time-variant network. The controller design considers agents with heterogeneous input constraints due to actuator limitations and homogeneous information sharing range limits. This result was published in the *Journal of the Franklin Institute* under the title *Flocking motion in swarms with limited sensing radius and heterogeneous input constraints*, reference [97]. The authors are Eber J. Ávila-Martínez and Juan G. Barajas-Ramírez.

Before we introduce the preliminaries and state the problems tackled in this thesis, some basic notations are introduced.

We respectively denote with \mathbb{R} and \mathbb{C} , the set of real and complex numbers, while $\mathbb{R}_{\geq 0}$ and $\mathbb{R}_{> 0}$ are the sets of nonnegative and positive real numbers. Given a complex number $c \in \mathbb{C}$, $Re(c)$ denotes its real part and $Im(c)$ its imaginary part. The set of $n \times 1$ real vectors is denoted by \mathbb{R}^n , while the set of $m \times n$ real matrices is denoted by $\mathbb{R}^{m \times n}$. We let $\mathbf{1}_n \in \mathbb{R}^n$ and $\mathbf{0}_n \in \mathbb{R}^n$ denote the n -dimensional column vectors with all its entries equal to 1 and 0, respectively. Likewise, I_n and Z_n are the $n \times n$ identity and zero matrices. The Kronecker product of $A \in \mathbb{R}^{m \times n}$ and $B \in \mathbb{R}^{p \times q}$ is defined as

$$A \otimes B := \begin{bmatrix} a_{11}B & \cdots & a_{1n}B \\ \vdots & \ddots & \vdots \\ a_{m1}B & \cdots & a_{mn}B \end{bmatrix} \in \mathbb{R}^{mp \times nq} \quad (2.1)$$

and satisfies the following properties

$$cA \otimes B = A \otimes cB \quad (2.2a)$$

$$(A \otimes B)^T = A^T \otimes B^T \quad (2.2b)$$

$$(A \otimes B)(C \otimes D) = (AC) \otimes (BD) \quad (2.2c)$$

$$A \otimes B + A \otimes C = A \otimes (B + C) \quad (2.2d)$$

$$(A \otimes B)^{-1} = A^{-1} \otimes B^{-1} \quad \text{if and only if } A \text{ and } B \text{ are invertible,} \quad (2.2e)$$

where $c \in \mathbb{R}$ and matrices C and D are assumed to be compatible for matrix multiplication.

Lemma 2.1 ([98]). *For the block-defined matrix*

$$Q = \begin{bmatrix} A & B \\ C & D \end{bmatrix} \in \mathbb{R}^{(p+q) \times (p+q)},$$

with $A \in \mathbb{R}^{p \times p}$, $B \in \mathbb{R}^{p \times q}$, $C \in \mathbb{R}^{q \times p}$ and $D \in \mathbb{R}^{q \times q}$, if C and D commute, i.e. $CD = DC$, then

$$\det(Q) = \det(AD - BC) \quad (2.3)$$

Definition 2.1 (Diagonal dominant matrix [99]). A matrix $E = [e_{ij}] \in \mathbb{R}^{N \times N}$ is said to be diagonally dominant if, for all i ,

$$e_{ii} \geq \sum_{j \neq i} |e_{ij}|, \quad (2.4)$$

additionally, if the above inequalities are all strict, the matrix E is said to be strictly diagonally dominant.

Lemma 2.2 ([100]). If a matrix $A = [a_{ij}] \in \mathbb{R}^{N \times N}$ is irreducible and diagonal dominant such that $a_{ii} > \sum_{j \neq i} |a_{ij}|$ for at least one i , then A is nonsingular. On the other hand, if A is strictly diagonal dominant, then $\text{Re}(\lambda_i) > 0$, where λ_i is its i -th eigenvalue.

2.1 Graph theory

Graphs theory provides natural abstractions for network systems. In this section, some basic concepts and useful previous results on graph theory are provided¹.

A *directed graph* (in short, a *digraph*) of order N , is a pair $\mathcal{D} = (\mathcal{V}, \mathcal{E})$, where $\mathcal{V} = \{1, \dots, N\}$ is a set of elements called *nodes* (or *vertices*) and $\mathcal{E} \subseteq \mathcal{V} \times \mathcal{V}$ is a set of ordered pairs of nodes, called *edges*. For $i, j \in \mathcal{V}$ the ordered pair $(i, j) \in \mathcal{E}$ denotes an edge that starts on node i and ends at node j . An edge in the graph portrays the flow of information between nodes. In an edge $(i, j) \in \mathcal{E}$, i is called a *parent* or an *in-neighbor* of node j , and j is called a *child* or an *out-neighbor* of node i . The in- and out-neighbor sets of node i are defined respectively as

$$\mathcal{N}_i^{\text{in}} := \{j \in \mathcal{V} : (j, i) \in \mathcal{E}, j \neq i\} \quad \text{and} \quad \mathcal{N}_i^{\text{out}} := \{j \in \mathcal{V} : (i, j) \in \mathcal{E}, i \neq j\}. \quad (2.5)$$

For a node i , the *in-degree* $d_{\text{in}}(i)$ and *out-degree* $d_{\text{out}}(i)$ are the number of in-neighbors and out-neighbors of i , respectively. A node is *balanced* if its in-degree is equal to its out-degree. A digraph is *topologically balanced* if all its nodes are balanced. An example of a digraph is shown in Figure 2.1.

A *complete* digraph, denoted by \mathcal{K} , is a digraph such that $\mathcal{E}_{\mathcal{K}} = \mathcal{V} \times \mathcal{V}$. A digraph $\mathcal{D}_a = (\mathcal{V}_a, \mathcal{E}_a)$ is a *subgraph* of $\mathcal{D}_A = (\mathcal{V}_A, \mathcal{E}_A)$ if $\mathcal{V}_a \subseteq \mathcal{V}_A$ and $\mathcal{E}_a \subseteq \mathcal{E}_A$. Additionally, if $\mathcal{V}_a = \mathcal{V}_A$, then \mathcal{D}_a is called a *spanning subgraph* of \mathcal{D}_A .

An *undirected graph* (in short, a *graph*) of order N , is a pair $\mathcal{G} = (\mathcal{V}, \mathcal{E})$ consisting of a set of nodes (or vertices) $\mathcal{V} = \{1, \dots, N\}$ and a set of unordered pairs of nodes $\mathcal{E} \subseteq \mathcal{V} \times \mathcal{V}$. A graph is a bidirectional digraph, in the sense that the edge $(j, i) \in \mathcal{E}$ any time that $(i, j) \in \mathcal{E}$. The neighborhood of vertex i is defined as

$$\mathcal{N}_i := \{j \in \mathcal{V} : (i, j) \in \mathcal{E}, j \neq i\}. \quad (2.6)$$

For graphs, if $j \in \mathcal{N}_i$, it follows that $i \in \mathcal{N}_j$, since the edge set of a graph consists on a unordered vertex pair. The *degree* $d(i)$ of vertex i is numbers of neighbors of i . Figure 2.1 illustrates an example of a graph.

¹This section is mainly based on [42, 100–102]

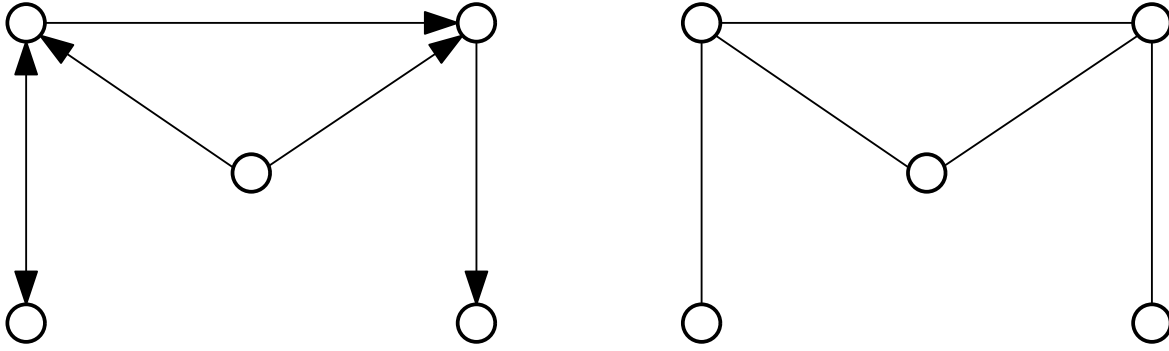


Figure 2.1: A digraph (left) and a graph (right).

2.1.1 Paths and connectivity

In a digraph \mathcal{D} , a *self-loop* is an edge that starts and ends in the same node. A *simple* digraph has no self-loops and no multiple edges between the same pair of nodes. A *directed path* of length m from node i to j is a sequence of edges $(i, k_1), (k_1, k_2), \dots, (k_m, j)$ with distinct nodes k_l and $l = 1, 2, \dots, m$. A directed path is called *simple* if no node appear more than once in it, except possibly for the initial and final node. A *cycle* is a simple path that starts and ends at the same node. A node with in-degree 0 is called a *source*, and every node with out-degree 0 is called a *sink*. If a vertex is simultaneously both, then is called *isolated*. A cycle in a digraph is a simple path that starts and ends in the same node. A digraph is acyclic if it contains no cycles.

A *directed tree* (sometimes called a *rooted tree*) is an acyclic digraph where every node has exactly one parent, except for one called the *root*, which has no parent, and the root has a directed path to every other node. A directed tree is called a *spanning tree* of digraph \mathcal{D} if is a spanning subgraph of it. Rooted trees are denoted by \mathcal{T} .

Denote the set of all digraphs \mathcal{D} of order N as \mathbb{D}^N . The following gives some connectivity notions of digraph and define their respective sets:

1. $\mathcal{D} \in \mathbb{D}^N$ is *weakly connected* if there are no isolated vertices. The set of all weakly connected digraphs is denoted by \mathbb{D}_W^N .
2. $\mathcal{D} \in \mathbb{D}^N$ is *strongly connected* if there exists a directed path connecting every vertex pair. The set of all strongly connected digraphs is denoted by \mathbb{D}_S^N .
3. $\mathcal{D} \in \mathbb{D}^N$ contains a *directed spanning tree* if has a spanning subgraph that is a directed tree. The set of all digraphs that contains a directed spanning tree is denoted by \mathbb{D}_{ST}^N .

Denote the set of all graphs \mathcal{G} of order N as \mathbb{G}^N . A graph $\mathcal{G} \in \mathbb{G}^N$ is *connected* if there exists a path between any two vertices. The set of all connected graphs is denoted by \mathbb{G}_C^N . If a graph is not connected, then is composed of multiple *connected components*, that is, multiple connected subgraphs. A graph with $\mathcal{E} = \mathcal{V} \times \mathcal{V}$ is called fully connected and is denoted as \mathcal{K} .

2.1.2 Weighted digraphs

A *weighted digraph* is a triplet $\mathcal{D} := (\mathcal{V}, \mathcal{E}, \mathcal{W})$, where the pair $(\mathcal{V}, \mathcal{E})$ is a digraph and \mathcal{W} is the collection of strictly positive weights $w_{ij} \in \mathbb{R}_{>0}$ associated to every edge $(i, j) \in \mathcal{E}$. A digraph can be regarded as a weighted digraph by defining its set of weights equal to 1, *i.e.* setting $w_{ij} = 1$ for all $(i, j) \in \mathcal{E}$.

Paths and connectivity notions and definitions of in and out-neighbors of digraphs remain equally valid for weighted digraphs. Although the notions of in- and out-degree are generalized for weighted digraphs. In a weighted digraph, the in- and out-degree of the i -th vertex are defined, respectively as

$$d_{in}(i) := \sum_{j \in \mathcal{N}_i^{in}} w_{ji} \quad \text{and} \quad d_{out}(i) := \sum_{j \in \mathcal{N}_i^{out}} w_{ij}.$$

A weighted digraph is *weight-balanced* if $d_{in}(i) = d_{out}(i)$ for all $i \in \mathcal{V}$. A weighted digraph is *undirected*, also called a *weighted graph*, if $w_{ij} = w_{ji}$ for all $i, j \in \mathcal{V}$. We call \mathcal{D} (correspondingly \mathcal{G}), a *balanced digraph* (*balanced graph*) if it is weight-balanced.

2.1.3 Algebraic Graph Theory

There is a close relation between graph theory and matrix theory, with both fields benefiting from each other. Digraphs admit a representations in terms of matrices. In what follows, these matrices will be examined.

For a digraph $\mathcal{D} \in \mathbb{D}^N$, the *adjacency matrix* $A(\mathcal{D}) := [a_{ij}] \in \mathbb{R}^{N \times N}$ is a nonnegative matrix with rows and columns indexed by the vertices in \mathcal{V} with its elements defined as:

$$a_{ij} := \begin{cases} w_{ji} & \text{if } (j, i) \in \mathcal{E}, \\ 0 & \text{otherwise.} \end{cases} \quad (2.7)$$

The *Laplacian matrix* of a digraph is a zero row sum nonnegative matrix $L(\mathcal{D})$ defined as $L(\mathcal{D}) := D^{in}(\mathcal{D}) - A(\mathcal{D})$ where $D^{in}(\mathcal{D}) := \text{diag}([d_{in}(1), \dots, d_{in}(N)])$ is the matrix of vertex in-degrees². In components, $L(\mathcal{D}) := [l_{ij}] \in \mathbb{R}^{N \times N}$ is defined as

$$l_{ij} := \begin{cases} -a_{ij} & \text{if } i \neq j, \\ \sum_{j \in \mathcal{N}_i^{in}} a_{ij} & \text{if } i = j. \end{cases} \quad (2.8)$$

Both, adjacency and Laplacian matrices, are equally defined for weighted graphs $\mathcal{G} \in \mathbb{G}^N$. However, they have the particular property of being symmetric and balanced, which is not necessary true for digraphs.

Adjacency matrix properties

In what follows, some correspondences between digraphs and adjacency matrices are reviewed. Let $A(\mathcal{D})$ be an adjacency matrix associated to a digraph $\mathcal{D} \in \mathbb{D}^N$. Then, the following statements describe properties of \mathcal{D} that can be extracted from $A(\mathcal{D})$:

²The Laplacian matrix of a directed graph can be defined in other ways, see for instance [102]

1. \mathcal{D} is undirected, that is, a graph \mathcal{G} , if and only if $A(\mathcal{D})$ is symmetric;
2. \mathcal{D} is weight-balanced if and only if $A(\mathcal{D}) \mathbf{1}_N = A(\mathcal{D})^T \mathbf{1}_N$;
3. In a digraph without self-loops, the node i is a sink if and only if the i -th row-sum of $A(\mathcal{D})$ is zero;
4. In a digraph without self-loops, the node i is a source if and only if the i -th column-sum of $A(\mathcal{D})$ is zero;

Laplacian matrix properties

Consider a digraph $\mathcal{D} \in \mathbb{D}^N$ with its associated Laplacian matrix $L(\mathcal{D})$, and a vector $z \in \mathbb{R}^N$. Then, the following conditions are equivalent.

1. The digraph $\mathcal{D} \in \mathbb{D}_{ST}^N$;
2. $\text{rank}(L(\mathcal{D})) = N - 1$;
3. $L(\mathcal{D})z = \mathbf{0}_N$ implies that $z_1 = \dots = z_N$;
4. $L(\mathcal{D})$ has a simple zero eigenvalue with an associated eigenvector $\mathbf{1}_N$.

Denote as $\lambda_i \in \mathbb{C}$ the i -th eigenvalue of its associated Laplacian matrix $L(\mathcal{D})$. Some key properties of the eigenvalues λ_i are enlisted:

1. The eigenvalues can be ordered as $0 = |\lambda_1| \leq |\lambda_2| \leq \dots \leq |\lambda_N|$;
2. The eigenvalues are such that $\text{Re}(\lambda_i) \geq 0$, for all $i \in \mathcal{V}$, if and only if $\mathcal{D} \in \mathbb{D}_{ST}^N$;
3. If $\mathcal{D} \in \mathbb{D}_S^N$, then $\text{Re}(\lambda_2) > 0$. If in addition $\mathcal{D} \in \mathbb{D}_B^N$, then $\text{Re}(\lambda_2) > 0$ if and only if $\mathcal{D} \in \mathbb{D}_S^N$;
4. If the digraph is bidirectional, *i.e.* a graph $\mathcal{G} \in \mathbb{G}^N$ with Laplacian $L(\mathcal{G})$, all its eigenvalues are pure real, that is, $\lambda_i \in \mathbb{R}$ for all $i \in \mathcal{V}$.
5. If the digraph is bidirectional, *i.e.* a graph $\mathcal{G} \in \mathbb{G}^N$ with Laplacian $L(\mathcal{G})$, then $\lambda_2 > 0$ and is a nondecreasing function of the edge weights. This value is known as Fielder's algebraic connectivity or, simply, *algebraic connectivity*.

The Laplacian matrix also have some remarkable properties with respect to its eigenvectors, they are enlisted below.

1. $L(\mathcal{D}) \mathbf{1}_N = \mathbf{0}_N$, *i.e.* $\mathbf{1}_N$ is the right eigenvector associated to $\lambda_1 = 0$;
2. If $\mathcal{D} \in \mathbb{D}_B^N$ then $L(\mathcal{D})^T \mathbf{1}_N = \mathbf{0}_N^T$, *i.e.* $\mathbf{1}_N$ is the left eigenvector associated to $\lambda_1 = 0$;

Some other important results on eigenvectors of Laplacian matrices are given below.

Lemma 2.3 ([100]). *If the digraph $\mathcal{D} \in \mathbb{D}_{ST}$, then, with proper permutation, $L(\mathcal{D})$ can be reduced to the Frobenius normal form [51]*

$$L(\mathcal{D}) = \begin{bmatrix} L_{11} & L_{12} & \cdots & L_{1k} \\ 0 & L_{22} & \cdots & L_{2k} \\ \vdots & \vdots & \ddots & \vdots \\ 0 & 0 & \cdots & L_{kk} \end{bmatrix}$$

where L_{ii} with $i = 1, \dots, k-1$ are irreducible, each L_{ii} has at least one row with positive row sum, and L_{kk} is irreducible or a zero matrix of dimension one.

Lemma 2.4 (Lemma 2.28 [100]). *For a digraph $\mathcal{D} \in \mathbb{D}^N$ with Laplacian $L(\mathcal{D})$ there exists a positive vector $z \in \mathbb{R}_{>0}$ such that $z^T L(\mathcal{D}) = \mathbf{0}_N^T$ if and only if \mathcal{D} is a disjoint union of strongly connected subgraphs.*

Lemma 2.5 (Lemma 2.29 [100]). *Consider a digraph $\mathcal{D} \in \mathbb{D}_{ST}^N$ with Laplacian $L(\mathcal{D})$. Let a nonnegative vector $z \in \mathbb{R}_{\geq 0}$ such that $z^T L(\mathcal{D}) = \mathbf{0}_N^T$. Then $z_i = 0$ for all vertices i that do not have directed paths to all other vertices in \mathcal{D} and $z_i > 0$ otherwise.*

With the lemmas described above, we can build the following ones that relates the positiveness of the elements of a Laplacian's left eigenvector with the topological properties of a digraph.

Lemma 2.6. *For a digraph $\mathcal{D} \in \mathbb{D}_W^N$ with Laplacian $L(\mathcal{D})$, there exists a vector $z \in \mathbb{R}_{>0}$ such that $z^T L(\mathcal{D}) = \mathbf{0}_N^T$ if and only if $\mathcal{D} \in \mathbb{D}_S^N$.*

Proof. For the first part, from lemma 2.4, \mathcal{D} must be a disjoint union of strongly connected graphs, however, since \mathcal{D} is weakly connected, there can be only one component, therefore, $\mathcal{D} \in \mathbb{D}_S^N$.

For the second part, notice that if $\mathcal{D} \in \mathbb{D}_S^N$, then every vertex is a root of a directed spanning tree, therefore, from lemma 2.5, there exists a vector $z \in \mathbb{R}_{>0}$ such that $z^T L(\mathcal{D}) = \mathbf{0}_N^T$. \square

Lemma 2.7. *Let $\mathcal{D} \in \mathbb{D}_{ST}^N$ with Laplacian $L(\mathcal{D})$ and let a nonnegative vector $z \in \mathbb{R}_{>0}$ such that $z^T L(\mathcal{D}) = \mathbf{0}_N^T$. Then, there exists an entry $z_i = 0$ if and only if $\mathcal{D} \notin \mathbb{D}_S^N$.*

Proof. Let $z_i = 0$ for some i . Since $\mathcal{D} \in \mathbb{D}_{ST}^N$ by Lemma 2.5 we know that i do not have a directed path to all other vertices in \mathcal{D} . Thus, there exists a vertex $j \neq i$ such that there is no path from i to j joining them. Therefore, from the definition of a strongly connected digraph, we conclude $\mathcal{D} \notin \mathbb{D}_S^N$.

Let $\mathcal{D} \notin \mathbb{D}_S$. Since $\mathcal{D} \in \mathbb{D}_{ST}^N$, then $\mathcal{D} \in \mathbb{D}_W^N$, implying \mathcal{D} is not a disjoint union of strongly connected digraphs. Also, the eigenvalue zero of $L(\mathcal{D})$ has multiplicity one. Therefore, the matrix $L(\mathcal{D})$ is 1-reducible and can be rewritten in the Frobenius normal form, then satisfies 1) B_1 is irreducible, and 2) one of B_{12}, \dots, B_{1k} is not equal to the zero matrix [100]. Without loss of generality, assume $P = I_N$. One can show that B_1 is nonsingular and any vector such that $z^T L(\mathcal{D}) = \mathbf{0}_N^T$ must be in the form $z = [0, z_2, \dots, z_N]^T$ with $z_k > 0$ for $k = 2, \dots, N$. \square

Additionally, the first left eigenvector has some interesting properties with respect to the matrix Laplacian shown in the following lemmas

Lemma 2.8. (Lemma 3 in [103]) Suppose $\mathcal{D} \in \mathbb{D}_S$. Then, there is a positive eigenvector $z = [z_1, \dots, z_N]^T \in \mathbb{R}^N$ of $L(\mathcal{D})$ associated with the zero eigenvalue and $ZL(\mathcal{D}) + L^T(\mathcal{D})Z \geq 0$, where $Z = \text{diag}(z_1, \dots, z_N)$.

The following lemma describes a generalization of Fielder's algebraic connectivity .

Lemma 2.9. (Lemma 4 in [103]) For a digraph $\mathcal{D} \in \mathbb{D}_S$ with Laplacian matrix $L(\mathcal{D})$, define its generalized algebraic connectivity as $\alpha(L(\mathcal{D})) = \min_{z^T x=0, x \neq 0} \frac{x^T (ZL(\mathcal{D}) + L^T(\mathcal{D})Z)x}{2x^T Zx}$, where z and Z are defined as in Lemma 2.8. Then, $\alpha(L(\mathcal{D})) > 0$. For balanced graphs, $\alpha(L(\mathcal{D})) = \lambda_2 \left(\frac{L(\mathcal{D}) + L^T(\mathcal{D})}{2} \right)$, where $\lambda_2 \left(\frac{L(\mathcal{D}) + L^T(\mathcal{D})}{2} \right)$ denotes the smallest nonzero eigenvalue of $\frac{L(\mathcal{D}) + L^T(\mathcal{D})}{2}$.

Although Lemmas 2.6 and 2.7 prove the existence and positiveness of z it is not clear yet the exact form of its entries. The following proposition gives a way to compute the value of each entry in function of the edge weights and the contained rooted trees inside a strongly connected digraph.

Proposition 2.1 (from Lemma 2.1 in [104]). For a digraph $\mathcal{D} \in \mathbb{D}_S^N$ and vector $z \in \mathbb{R}^N$ such that $z^T L(\mathcal{D}) = \mathbf{0}_N^T$,

$$z_i = \sum_{\mathcal{T} \in \mathbb{T}_i(\mathcal{D})} \prod_{(k,j) \in \mathcal{E}_{\mathcal{T}}} \omega_{kj} \quad \forall i \in \mathcal{V}_{\mathcal{D}} \quad (2.9)$$

where $\mathbb{T}_i(\mathcal{D})$ is the set of all directed spanning trees in \mathcal{D} that are rooted at node i , and $\mathcal{E}_{\mathcal{T}}$ is the set of edges in the tree \mathcal{T} .

The matrix Laplacian also holds a remarkable relation with the number of spanning trees in a graph. Let $M[s]$ denote the submatrix of M obtained by deleting the row and column indexed by s .

Theorem 2.1 (Theorem 13.2.1 in [101]). Let \mathcal{G} be a graph with Laplacian matrix L . If u is an arbitrary vertex of \mathcal{G} , then $\det(L[u])$ is equal to the number of spanning trees of \mathcal{G} .

It follows from Theorem 2.1 the maximum number of spanning trees in a graph.

Corollary 2.1 (Corollary 13.2.2 in [101]). The number of spanning trees of $\mathcal{K} \in \mathbb{G}^N$ is N^{N-2} .

2.2 Mobile robots dynamic models

There is a great variety of mobile robots that can make up a multi-robot system [99]. In this section, we review the dynamic models of differential mobile robots and quadrotors, and we discuss some control techniques allowing us to model the position and velocity dynamics of a point of interest within them through a second-order dynamic system.

2.2.1 Differential mobile robot

Perhaps one of the most popular kinds of mobile robotic systems is the differential mobile robot. This configuration is one of the simplest and cheapest to build; It consists of two independent wheels coupled to DC motors and a caster wheel to keep the robot statically balanced. Translation and rotation of this type of robot are due to wheel angular velocity differences. To model the kinematics of these, we use the well-known unicycle model. The point $r = [r_x, r_y]^T \in \mathbb{R}^2$, located at mid-distance of the actuated wheels (see Figure 2.2), has the following dynamics

$$\begin{bmatrix} \dot{r}_x \\ \dot{r}_y \\ \dot{\theta} \\ \dot{\nu} \\ \dot{\omega} \end{bmatrix} = \begin{bmatrix} \cos(\theta) & 0 \\ \sin(\theta) & 0 \\ 0 & 1 \\ 0 & 0 \\ 0 & 0 \end{bmatrix} \begin{bmatrix} \nu \\ \omega \end{bmatrix} + \begin{bmatrix} 0 & 0 \\ 0 & 0 \\ 0 & 0 \\ \frac{1}{m} & 0 \\ 0 & \frac{1}{J} \end{bmatrix} \begin{bmatrix} F \\ \tau \end{bmatrix}. \quad (2.10)$$

where θ its heading angle, ν its driving velocity, ω its steering velocity, m is the mass of the robot and J its moment of inertia [11, 42]. The variables ν and ω are related to physical kinematic variables as

$$\nu = \frac{\rho}{2} (\omega_r + \omega_l), \quad \omega = \frac{\rho}{l} (\omega_r - \omega_l)$$

where ω_l and ω_r are the angular velocities of the left-side and right-side wheel, respectively, ρ is the radius of the wheels, and l is the distance between them. Therefore, ν and ω serve as control variables. The way these variables relate to the actual inputs of the robot is

$$\omega_r = \frac{2\nu + l\omega}{2\rho} \quad \omega_l = \frac{2\nu - l\omega}{2\rho}.$$

These values serve as references to the wheels angular velocity controllers in the robot (see, for example [28, 30]). Also, notice robot's centre of mass accelerates when turning if it is outside the wheels axis. This effect is not included in the model (2.10) as we assume the centre of mass is in the wheel axis (see [105] for more details).

It has been shown that the differential mobile robots possess a non-holonomic restriction. That is, assuming the robot rolls without side slipping, the robot does not experience any motion along the wheels axle, which is described by the following non-holonomic constraint:

$$\dot{r}_x \sin(\theta) - \dot{r}_y \cos(\theta) = 0. \quad (2.11)$$

This constraint prevents the robot from being stabilized through a continuous and static state feedback controller, *i.e.* robot's position and orientation cannot simultaneously be stabilized [106]. Nonetheless, time-varying and discontinuous control strategies have been proposed to deal with this issue [107–110].

Let $x := [r_x, r_y, \theta, \nu, \omega]^T$ and $\mu := [F, \tau]^T$, be the robot's state and input vector. The equations of motion can be written as

$$\dot{x} = f(x) + g(x)\mu \quad (2.12)$$

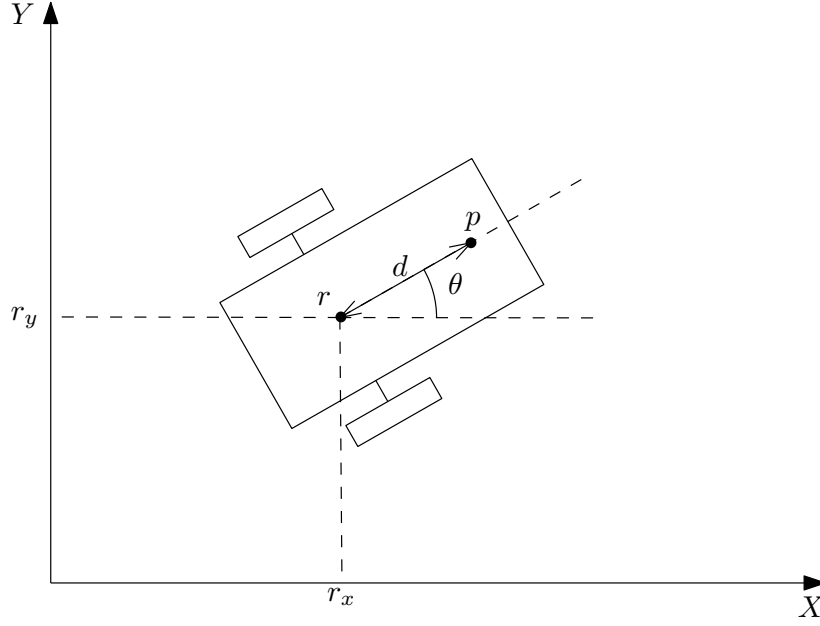


Figure 2.2: Differential mobile robot with hand.

where the definitions of f and g can be inferred from (2.10). Now, define a *point of interest* $p = [p_x, p_y]^T$ within the robot that lies at a distance d along the line that is normal to the wheel axis and intersects it at the center point of the robot r , as shown in Figure 2.2. The point of interest might represent the position of an actuator or sensor mounted on the differential mobile robot, and we aim to control its position. The kinematics of this point of interest is holonomic for $d \neq 0$. From Figure 2.2, notice that the position of h its given as

$$\begin{bmatrix} p_x \\ p_y \end{bmatrix} = \begin{bmatrix} r_x \\ r_y \end{bmatrix} + d \begin{bmatrix} \cos(\theta) \\ \sin(\theta) \end{bmatrix}. \quad (2.13)$$

From equations (2.10) and (2.13) the dynamics of the point of interest is given by

$$\begin{bmatrix} \dot{p}_x \\ \dot{p}_y \end{bmatrix} = \begin{bmatrix} \cos(\theta) & -d \sin(\theta) \\ \sin(\theta) & d \cos(\theta) \end{bmatrix} \begin{bmatrix} \nu \\ \omega \end{bmatrix}. \quad (2.14)$$

Meanwhile, the second-order derivative is

$$\begin{bmatrix} \ddot{p}_x \\ \ddot{p}_y \end{bmatrix} = \begin{bmatrix} -\nu\omega \sin(\theta) - d\omega^2 \cos(\theta) \\ \nu\omega \cos(\theta) - d\omega^2 \sin(\theta) \end{bmatrix} + \begin{bmatrix} \frac{1}{m} \cos(\theta) & -\frac{d}{J} \sin(\theta) \\ \frac{1}{m} \sin(\theta) & \frac{d}{J} \cos(\theta) \end{bmatrix} \begin{bmatrix} F \\ \tau \end{bmatrix}. \quad (2.15)$$

Because

$$\det \left(\begin{bmatrix} \frac{1}{m} \cos(\theta) & -\frac{d}{J} \sin(\theta) \\ \frac{1}{m} \sin(\theta) & \frac{d}{J} \cos(\theta) \end{bmatrix} \right) = \frac{d}{mJ} \neq 0,$$

system (2.10) with output (2.13) has a relative degree of two, therefore, it can be

feedback linearized about the point of interest [111]. Define the map $\psi : \mathbb{R}^5 \mapsto \mathbb{R}^N$ as:

$$\chi = \psi(x) := \begin{bmatrix} r_x + d \cos(\theta) \\ r_y + d \sin(\theta) \\ \nu \cos(\theta - d\omega \sin(\theta)) \\ \nu \sin(\theta) + d\omega \cos(\theta) \\ \theta \end{bmatrix}. \quad (2.16)$$

This map defines a diffeomorphism whose inverse is given by

$$x = \psi^{-1}(\chi) := \begin{bmatrix} \chi_1 - d \cos(\chi_5) \\ \chi_2 - d \sin(\chi_5) \\ \chi_5 \\ \frac{1}{2}\chi_3 \cos(\chi_5) + \frac{1}{2}\chi_4 \sin(\chi_5) \\ -\frac{1}{2d}\chi_3 \sin(\chi_5) + \frac{1}{2d}\chi_4 \cos(\chi_5) \end{bmatrix}.$$

In transformed coordinates, (2.10) and (2.13), are given by

$$\begin{aligned} \begin{bmatrix} \dot{\chi}_1 \\ \dot{\chi}_2 \end{bmatrix} &= \begin{bmatrix} \chi_3 \\ \chi_4 \end{bmatrix} \\ \begin{bmatrix} \dot{\chi}_3 \\ \dot{\chi}_4 \end{bmatrix} &= \begin{bmatrix} -\nu\omega \sin(\theta) - d\omega^2 \cos(\theta) \\ \nu\omega \cos(\theta - d\omega^2 \sin(\theta)) \end{bmatrix} + \begin{bmatrix} \frac{1}{m} \cos(\theta) & -\frac{d}{J} \sin(\theta) \\ \frac{1}{m} \sin(\theta) & \frac{d}{J} \cos(\theta) \end{bmatrix} \mu \\ \dot{\chi}_5 &= -\frac{1}{2d}\chi_3 \sin(\chi_5) + \frac{1}{2d}\chi_4 \cos(\chi_5). \end{aligned}$$

The output feedback linearizing controller is given by

$$\mu = \begin{bmatrix} \frac{1}{m} \cos(\theta) & -\frac{d}{J} \sin(\theta) \\ \frac{1}{m} \sin(\theta) & \frac{d}{J} \cos(\theta) \end{bmatrix}^{-1} \left(u - \begin{bmatrix} -\nu\omega \sin(\theta) - d\omega^2 \cos(\theta) \\ \nu\omega \cos(\theta - d\omega^2 \sin(\theta)) \end{bmatrix} \right)$$

which gives

$$\begin{aligned} \begin{bmatrix} \dot{\chi}_1 \\ \dot{\chi}_2 \end{bmatrix} &= \begin{bmatrix} \chi_3 \\ \chi_4 \end{bmatrix} \\ \begin{bmatrix} \dot{\chi}_3 \\ \dot{\chi}_4 \end{bmatrix} &= u \\ \dot{\chi}_5 &= -\frac{1}{2d}\chi_3 \sin(\chi_5) + \frac{1}{2d}\chi_4 \cos(\chi_5). \end{aligned}$$

The last equation corresponds to the unobservable and uncontrollable internal dynamics of the systems. The zero dynamics is found by setting $\chi_1 = \dots = \chi_4 = 0$ to obtain $\dot{\chi}_5 = 0$. Since $\chi_5 = \theta$ and the vector $[\chi_3, \chi_4]^T$ is the velocity of the point of interest, then it can be conclude that the angle will stop changing when the robot stops moving.

Notice that the position of the point of interest is $p = [\chi_1, \chi_2]$, whose dynamics can be described as a double-integrator systems in the following way

$$\dot{p} = v, \quad \dot{v} = u, \quad (2.17)$$

with u being the new control signal [42, 112].

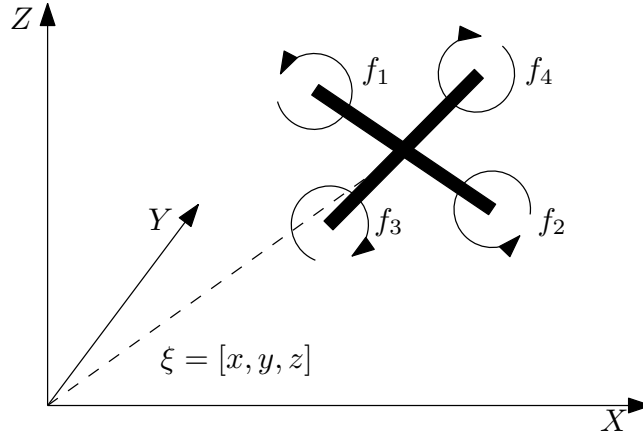


Figure 2.3: A quadrotor.

2.2.2 Quadrotor

A *quadrotor*, shown in Figure 2.3, is a Unmanned Air Vehicle (UAV) classified as a type of multicopter [113]. Due to its simple structure, a quadrotor is easy-to-use and features high reliability and low-cost maintenance. A drone has four propellers providing it with the ability of Vertical Take-Off and Landing (VTOL). Therefore, it has four control inputs which are the four propeller angular speeds. In what follows, we present the quadrotor's dynamic model.

Using the Euler-Lagrange approach (see [114] for the details), the quadrotor's dynamic model is obtained under the following assumptions: The drone is a rigid body, its mass and moment of inertia are constant, the geometric centre and centre of gravity are the same and propellers with odd indices rotate counterclockwise while propellers with even indices rotate clockwise. The model consists of the robot's position $\xi = [x, y, z]^T \in \mathbb{R}^3$, respect to a fixed frame, and its rotation coordinates $\eta = [\phi, \theta, \psi]^T \in \mathbb{R}^3$, respect to its body frame, described by the following equations:

$$m\ddot{\xi} = R \begin{bmatrix} 0 \\ 0 \\ F \end{bmatrix} + \begin{bmatrix} 0 \\ 0 \\ -mg \end{bmatrix} \quad (2.18a)$$

$$\tilde{J}\ddot{\eta} = \tau - C(\eta, \dot{\eta})\dot{\eta} \quad (2.18b)$$

where m is the mass of the quadrotor, F is the force trust applied to its center of mass, g the gravitational constant, $\tau = [\tau_\phi, \tau_\theta, \tau_\psi]^T \in \mathbb{R}^3$ is the vector torque generated by the rotors, $\tilde{J} = JW$ with J the inertial symmetrical matrix and $C(\eta, \dot{\eta}) = J\dot{W}$ is the Coriolis term; The matrices R and W are defined as follows:

$$R = \begin{bmatrix} c\psi c\theta & -c\theta s\psi & s\theta \\ c\phi s\psi + c\psi s\phi s\theta & c\phi c\psi - s\phi s\psi s\theta & -c\theta s\phi \\ s\phi s\psi - c\phi c\psi s\theta & c\psi s\phi + c\phi s\psi s\theta & c\phi c\theta \end{bmatrix} \quad \text{and} \quad W = \begin{bmatrix} 1 & 0 & -s\theta \\ 0 & c\phi & c\theta s\phi \\ 0 & -s\phi & c\theta c\phi \end{bmatrix},$$

where $s\lambda = \sin(\lambda)$ and $c\lambda = \cos(\lambda)$ with $\lambda \in \{\phi, \theta, \psi\}$. According to [114, 115], to simplify equation (2.18b), let be

$$\tau = \tilde{J}\tilde{\tau} + C(\eta, \dot{\eta})\dot{\eta}, \quad (2.19)$$

where $\tilde{\tau} = [\tilde{\tau}_\phi, \tilde{\tau}_\theta, \tilde{\tau}_\psi]^T$ is an auxiliary torque vector. The closed-loop system (2.18)-(2.19) yields to the following dynamics:

$$m\ddot{\xi} = \begin{bmatrix} F \sin(\theta) \\ -F \cos(\theta) \sin(\phi) \\ F \cos(\theta) \cos(\phi) - mg \end{bmatrix} \quad (2.20a)$$

$$\ddot{\eta} = \tilde{\tau} \quad (2.20b)$$

The main thrust force F and the torques τ are related to the thrust forces f_i , with $i \in \{1, 2, 3, 4\}$ generated by each motor in the following way

$$\begin{bmatrix} F \\ \tau \end{bmatrix} = \begin{bmatrix} 1 & 1 & 1 & 1 \\ -l & l & 0 & 0 \\ 1 & 0 & -l & l \\ -\frac{b}{k} & -\frac{b}{k} & \frac{b}{k} & \frac{b}{k} \end{bmatrix} \begin{bmatrix} f_1 \\ f_2 \\ f_3 \\ f_4 \end{bmatrix} \quad (2.21)$$

where l is the length of the quadrotor's arms, b is the drag constant of the rigid body and k is the thrust constant of every rotor-propeller array [114, 115].

Equation (2.20) shows the quadrotor's dynamics admits a decomposition into two hierarchical levels: Posture and orientation dynamics. We assume the rotational dynamics converges faster than the translational dynamics. Hence, we propose a cascade controller. In the inner loop, we have orientation control. The outer loop is in charge of posture control feeding on a generator of the desired trajectory ξ_d . Figure 2.4 shows this control scheme which we describe in the following section.

Orientation control

Let $\eta_d = [\phi_d, \theta_d, \psi_d]^T \in \mathbb{R}^3$ be the twice differentiable desired trajectories for the quadrotor's orientation angles and define the angle errors as follows:

$$e_\phi := \phi - \phi_d, \quad e_\theta := \theta - \theta_d, \quad \text{and} \quad e_\psi := \psi - \psi_d. \quad (2.22)$$

Also, define the auxiliary torque vector elements from equation (2.19) as follows:

$$\begin{aligned} \tilde{\tau}_\phi &= \ddot{\phi}_d - \kappa_1 (\dot{\phi} - \dot{\phi}_d) - \kappa_2 (\phi - \phi_d) \\ \tilde{\tau}_\theta &= \ddot{\theta}_d - \kappa_1 (\dot{\theta} - \dot{\theta}_d) - \kappa_2 (\theta - \theta_d) \\ \tilde{\tau}_\psi &= \ddot{\psi}_d - \kappa_1 (\dot{\psi} - \dot{\psi}_d) - \kappa_2 (\psi - \psi_d). \end{aligned} \quad (2.23)$$

Let $e_1 = [e_\phi, e_\theta, e_\psi]^T \in \mathbb{R}^3$ and $e_2 = [\dot{e}_\phi, \dot{e}_\theta, \dot{e}_\psi]^T \in \mathbb{R}^3$, then the error dynamics of the closed-loop system (2.22)-(2.23) is:

$$\begin{bmatrix} \dot{e}_1 \\ \dot{e}_2 \end{bmatrix} = \left(\begin{bmatrix} 0 & 1 \\ -\kappa_1 & -\kappa_2 \end{bmatrix} \otimes I_3 \right) \begin{bmatrix} e_1 \\ e_2 \end{bmatrix} \quad (2.24)$$

which is exponentially stable for $\kappa_2 > 0$ and $\kappa_1 = \frac{\kappa_2^2}{4}$. A sufficiently large gain κ_2 leads the quadrotor's orientation to the desired one as fast as needed [114, 115].

With this analysis, we establish that the quadrotor can follow desired orientation angle trajectories. We exploit this property in the posture control scheme.

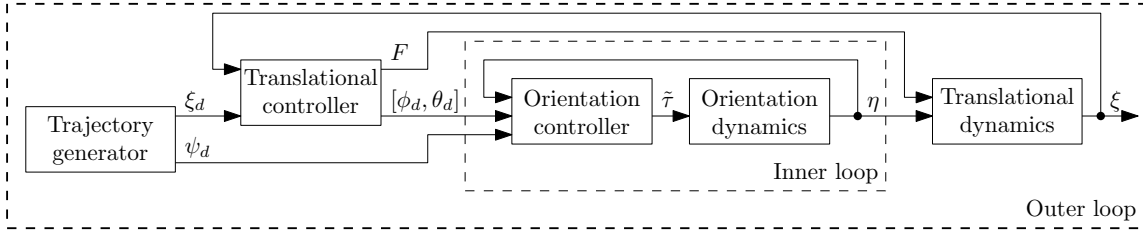


Figure 2.4: Hierarchical control scheme.

Posture control

Given the previous analysis, we will use, whenever needed, the orientation angles as control inputs for the translational coordinates, which describe the desired angle trajectories defined in the previous section. Here, we establish a relation between orientation angles and auxiliary control inputs to transform the quadrotor's translational dynamics into a second-order system.

We begin the posture controller design with the stabilization of the quadrotor's altitude. From equation (2.20) notice that

$$m\ddot{z} = F \cos(\phi) \cos(\theta) - mg. \quad (2.25)$$

We aim to linearize the dynamics of this coordinate. Here, the control signal is introduced through the total thrust F . Thus, let

$$F = \frac{m(u_z + g)}{\cos(\phi) \cos(\theta)}. \quad (2.26)$$

The closed-loop system (2.25)-(2.26) yields to $\ddot{z} = u_z$, where u_z is the auxiliary control. The y -coordinate is governed by the following dynamics:

$$m\ddot{y} = -F \sin(\phi) \cos(\theta). \quad (2.27)$$

Substituting (2.26) in it, we have

$$m\ddot{y} = -m(u_z + g) \tan(\phi). \quad (2.28)$$

Following the same reasoning of the previous case, letting

$$\phi = \arctan\left(-\frac{u_y}{u_z + g}\right) \quad (2.29)$$

yields us to $\ddot{y} = u_y$, where u_y is the auxiliary control. Finally, the x -coordinate dynamics is

$$m\ddot{x} = F \sin(\theta). \quad (2.30)$$

Substituting (2.26) in (2.30) and solving for θ we obtain

$$\theta = \arctan\left(\frac{u_x \cos(\phi)}{u_z + g}\right) \quad (2.31)$$

where u_x is another auxiliary control signal. Thus, the x -coordinate dynamics is $\ddot{x} = u_x$.

In conclusion, letting the angles from equations (2.29) and (2.31) define their corresponding desired values in equation (2.23), we obtain a hierarchical controller that allows describing the posture dynamics as a second-order system; That is:

$$\dot{p} = v, \quad \dot{v} = u \quad (2.32)$$

where $p = [x, y, z]^T \in \mathbb{R}^3$ and $u = [u_x, u_y, u_z]^T \in \mathbb{R}^3$.

2.3 Multi-robot systems control problems

In the previous section, we discussed a way to model the translational dynamics of a mobile robot through a second-order dynamic system. From now on, we state the thesis control problems for the second-order systems.

Consider a multi-robot system consisting of N robots with the i -th mobile robot dynamics given by

$$\dot{p}_i = v_i, \quad \dot{v}_i = u_i, \quad i \in I := \{1, 2, \dots, N\}, \quad (2.33)$$

where $p_i, v_i, u_i \in \mathbb{R}^n$ (with $n = 1, 2$ or 3) are its position, velocity and control input, respectively. For each robot, there is an individual input constraint given by

$$\|u_i\| \leq \hat{u}_i, \quad i \in I. \quad (2.34)$$

where $\hat{u}_i \in \mathbb{R}_{>0}$ is the input constraint of the i th robot. Restriction (2.34) indicates that different robots can move at different speeds. Therefore, some robots might achieve their motion objectives faster than others. Additionally, for each robot, there is a maximum reliable communication/detection distance range $r_i \in \mathbb{R}_{>0}$. Therefore, the relative position between robots determines if a network edge exists among them, which results on a dynamic network topology where edges appear or disappear as robots navigate through the environment. This type of dynamic network topology is known as a *proximity graph* which we describe later in this section.

Usually, multi-robot systems require to travel through the environment following the desired path or to reach an arrival point of interest in a leader-followers scheme. In this case, a leader describing the desired trajectory is identified, and the other robots must follow it. The leader can be either virtual or a member of the group. Virtual leaders are not physical robots, but their motion is transmitted to some members of the group. In this thesis, leaders are always virtual. We consider only one virtual leader with the following dynamics

$$\dot{p}_0 = v_0, \quad \dot{v}_0 = f(t, p_0, v_0), \quad (2.35)$$

where $p_0, v_0 \in \mathbb{R}^n$ (with $n = 1, 2$ or 3) are the position and velocity of the leader, respectively, and a velocity vector field $f : \mathbb{R}_{>0} \times \mathbb{R}^n \times \mathbb{R}^n \mapsto \mathbb{R}^n$ with function f being measurable and locally essentially bounded functions, *i.e.* a solution $v_0(t)$ exists and is unique. We assume that there is only a subset $I_0 \subset I$ of robots in the multi-robot systems having access to the information from the leader, *i.e.* if $i \in I_0$, then

the i th robot has a connection with the virtual leader and access to its information (position and velocity). Those robots are called *informed* members on the group. With this assumption, it is no needed that every robot have dedicated equipment to receive leader's information, allowing a simplest/cheaper design of them.

Notice that the robots in (2.33) have access only to the information collected from within its neighbourhood and from the leader in case it is an informed robot. Therefore, since the only kind of information available to it is local, any controller design for the input vector u_i for all $i \in I$ is a distributed approach. Moreover, since the robots in the neighbourhood might change as robots move through the environment, the distributed controller designs must handle network switches while driving the multi-robot system to the control objective.

Before we present the control objectives, the concept of proximity digraphs, which serves as a way to model dynamic networks, is introduced.

2.3.1 Proximity digraphs

A *proximity digraph* is a state-dependent digraph³ in which the relative position between robots determines the existence of an edge [102]. More precisely, it is a digraph $\mathcal{D} \in \mathbb{D}^N$ that its determine by the configuration $p = [p_1^T, p_2^T, \dots, p_N^T]^T \in \mathbb{R}^{nN}$ of a multi-robot system. That is, we call $\mathcal{D}(p) := (\mathcal{V}, \mathcal{E}(p))$ a proximity digraph with $\mathcal{V} = I$ as the set of nodes (robots) and $\mathcal{E}(p)$ as the set of edges of $\mathcal{D}(p)$. However, the *how* relative position between pair of robots dictates the existence of an edge among them needs to be determinate⁴. In general terms, we consider an indicator function $\sigma_{ij}(p_{ij}) : \mathbb{R}^n \mapsto \{0, 1\}$, where $p_{ij} = p_i - p_j$. That is, $\mathcal{E}(p)$ is a set that depends on the multi-robot system configuration defined as:

$$\mathcal{E}(p) := \{(i, j) \in \mathcal{V} \times \mathcal{V} : \sigma_{ij}(p_{ij}) = 1 \text{ for all } i, j \in \mathcal{V}, j \neq i\}. \quad (2.36)$$

For a configuration p , an edge $(j, i) \in \mathcal{E}(p)$ indicates the i th robot receives (or sense) information from the j th robot. The set of in- and out-neighbours are then defined as

$$\mathcal{N}_i^{in}(p) := \{j \in \mathcal{V} : (j, i) \in \mathcal{E}(p), j \neq i\} \quad (2.37)$$

$$\mathcal{N}_i^{out}(p) := \{j \in \mathcal{V} : (i, j) \in \mathcal{E}(p), i \neq j\}. \quad (2.38)$$

For a case in which $\sigma_{ij}(p_{ij}) \iff \sigma_{ji}(p_{ji})$, the underlying information network can be modeled by means of a proximity undirected graph $\mathcal{G}(p) := (\mathcal{V}, \mathcal{E}(p))$. In such scenario, the neighborhood of the i -th robot is

$$\mathcal{N}_i(p) := \{j \in \mathcal{V} : (i, j) \in \mathcal{E}(p), i \neq j\} = \mathcal{N}_i^{in}(p) = \mathcal{N}_i^{out}(p). \quad (2.39)$$

Notice that every member of the multi-robot system have access only to local information, *i.e.* the data collected within its neighborhood $\mathcal{N}_i^{in}(p)$, and any controller design has to be build from that information.

³A state-dependent digraph is a mapping between the state space of a networked system and the set of all its possible network configurations. See [102] for more details.

⁴In section 3.2 we show how is done in this thesis.

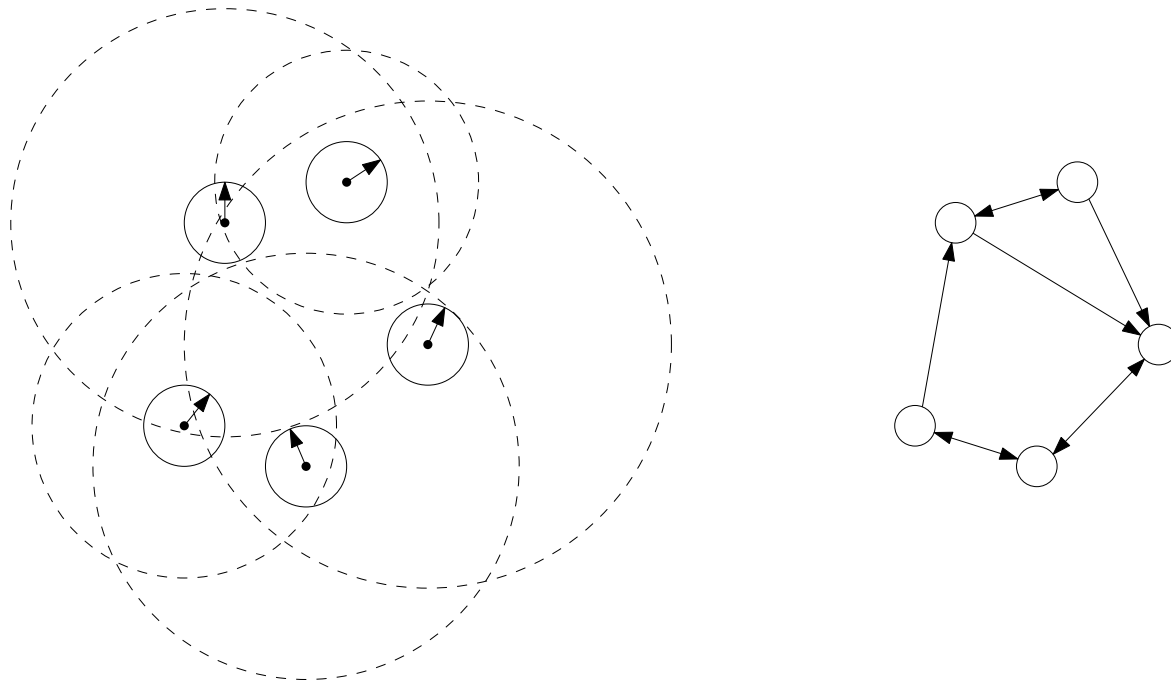


Figure 2.5: A multi-robot system with limited communication/sensing ranges (left) and its induced proximity digraph (right).

Group fragmentation is a phenomenon in multi-robot systems with proximity networks, where the group of robots splits into two or more components [64]. As a consequence of this phenomenon, the global desired behaviour for the entire multi-robot system is hindered. If the neighbourhood of the i th robot is empty, no information can be used by the controller to direct the robot towards a path that allows solving the global task. Therefore, it is necessary to *preserve the connectivity* property of the proximity information network. A kind of distributed controller that address the connectivity preservation issue from an initial time t_0 to a final time t_f , with $0 \leq t_0 < t_f$ is defined as follows.

Definition 2.2 (Strong connectivity preserving distributed controller). *A controller u_i for the multi-robot system (2.33) is a strong connectivity preserving distributed controller if it uses only the locally available information and, for the closed loop system, the proximity digraph $\mathcal{D}(p)$ is strongly connected for all $t \in [t_0, t_f]$. If the information network is bidirectional, the distributed controller u_i is simply called connectivity preserving.*

The main objective in this thesis is the design distributed controllers that drives the multi-robot system (2.33) into a coordinated motion through a behavioral approach. We focus on two collective behaviors: Consensus and flocking. In the following subsections, both behaviors are defined for multi-robot systems described by (2.33), as well as the corresponding control design problem.

2.3.2 Consensus

In the context of multi-robot systems in the form of (2.33), the information state is defined by the position and velocity of every robot. Therefore, the agreement to be reached must be described in terms of these values.

There are in general two different configurations for consensus behavior: leaderless and leader-followers. The leaderless configuration consists on the alignment of positions and velocities of every robot in (2.33), without any specification of the value at which such alignment must occur. This consensus behavior is defined as follows:

Definition 2.3 (Leaderless consensus behavior). *We say that a multi-robot system (2.33) asymptotically reach consensus in position with zero velocity if*

$$\lim_{t \rightarrow \infty} \|p_{ij}\| = \Delta_{ij}, \quad \lim_{t \rightarrow \infty} \|v_{ij}\| = 0 \quad \text{for all } i \in \mathbf{I}. \quad (2.40)$$

where $v_{ij} = v_i - v_j$ and $\Delta_{ij} \geq 0$ denotes the desired position deviation between the i th and j th robot.

On the other hand, for the leader-followers configuration there is a specific value to which the information state of the robots must align. The leader-followers consensus it is defined as follows:

Definition 2.4 (Leader-followers consensus behavior). *We say that a multi-robot system (2.33) asymptotically reaches a consensus with a leader in position with identical velocity if*

$$\lim_{t \rightarrow \infty} \|p_{i0}\| = \Delta_{i0}, \quad \lim_{t \rightarrow \infty} \|v_{i0}\| = 0, \quad \text{for all } i \in \mathbf{I}. \quad (2.41)$$

where $p_{i0} = p_i - p_0$, $v_{i0} = v_i - v_0$, and $\Delta_{i0} \geq 0$ denotes the desired position deviation between the i th robot and the virtual leader.

The consensus problem consists in the design of a *protocol* (controller) to drive the multi-robot system into the desired behaviour. Both leaderless and leader-followers consensus problems are described as follows:

Problem 2.1 (Leaderless (leader-followers) consensus problem). *Design a distributed controller u_i for all $i \in \mathbf{I}$, such that (2.33) reaches a leaderless (leader-followers) consensus behavior.*

2.3.3 Flocking problem

Flocking in multi-robot systems, with dynamics (2.33), consists on the motion of every robot following a cohesive group motion. In terms of the boids model, the members of the group satisfy the heuristic rules: flock centering, collision avoidance and velocity matching. These rules, can be translated to control objectives as we show in this section.

We call a *leaderless flocking motion* to a flocking behavior in which there is no desired path to follow, that is:

Definition 2.5 (Leaderless flocking motion). *We say that a multi-robot system (2.33) is on leaderless flocking motion over a time interval $[t_0, t_f)$ if the following properties are satisfied:*

1. **The group is cohesive:** *There exists a constant $\rho \in \mathbb{R}_{>0}$ such that $\|p_{ij}\| \leq \rho$ for all $i, j \in I$ with $i \neq j$;*
2. **Inter-robot collisions are avoided:** *The distance between robots is never zero;*
3. **Inter-robot velocity mismatches are bounded:** *There exists a constant $v \in \mathbb{R}_{>0}$ such that $\|v_{ij}\| \leq v$ for all $i, j \in I$;*

Additionally, the leaderless flocking motion is called rigid if it results on a fixed configuration where the inter-robot distances remain constant and every robot moves with the same velocity vector.

For the case where there exists a virtual leader, the Definition 2.5 is modified to be:

Definition 2.6 (Leader-followers flocking motion). *A multi-robot system (2.33) is on leader-followers flocking motion, with a leader given by (2.35), over a time interval $[t_0, t_f)$ if the properties (1) and (2) of Definition 2.5 are satisfied and, additionally:*

1. **Robot-leader position tracking errors are bounded:** *There exists a constant $\rho_0 \in \mathbb{R}_{>0}$ such that $\|p_{i0}\| \leq \rho_0$ for all $i \in I$;*
2. **Robot-leader velocity mismatches are bounded:** *There exists a constant $v_0 \in \mathbb{R}_{>0}$ such that $\|v_{i0}\| \leq v_0$ for all $i \in I$.*

Additionally, as before, leader-followers flocking motion is called rigid if the inter-robot distances and the leader-followers deviation are fixed, and every robot moves with the same velocity vector as the leader.

Both leaderless and leader-followers flocking motion describes properties of the entire group that must be enforced through the controllers (protocols) that is designed such that the flocking motion arise from local interplays. Therefore, the flocking motion problems are defined as follows.

Problem 2.2 (Leaderless (leader-followers) flocking motion problem). *Design a controller distributed u_i for all $i \in I$ such that the multi-robot system (2.33) achieves a leaderless (leader-followers) flocking motion.*

In the following Chapters, solutions to Problems 2.1 and 2.2, and some of their variants, are designed under a distributed behavioral approach.

Consensus Problems

In this chapter, we first explore the case of fixed digraphs and design distributed controllers for consensus. Then, we build on top of them to extend these results to information networks modelled through proximity digraphs.

Consider a multi-robot system consisting of N mobile robots described by the following second-order dynamics

$$\dot{p}_i = v_i, \quad m_i \dot{v}_i = u_i \quad i \in \mathbf{I} := \{1, \dots, N\}, \quad (3.1)$$

where $p_i, v_i, u_i \in \mathbb{R}^n$ (with $n = 1, 2$ or 3) are position, velocity and input vector of the i -th robot with $m_i \in \mathbb{R}_{>0}$ as its mass. Robot's dynamics (3.1) is often called an inertial agent [50, 116]. This model captures heterogeneity in the network through the scaling factors m_i to represent different robots.

To design the controllers u_i , we impose the following conditions. It must depend continuously on the relative state deviation among the current robot and its neighbors; if informed, also its deviation from the virtual leader. Considering such restrictions, the following general form is used as controller:

$$u_i = \sum_{j \in \mathcal{N}_i^{in}} g_{ij}(p_{ij}, v_{ij}) + g_{i0}(p_{i0}, v_{i0}), \quad i \in \mathbf{I}, \quad (3.2)$$

where $p_{ij} := p_i - p_j$ and $v_{ij} := v_i - v_j$ are the deviations in position and velocity between the i th robot and its neighbour j , while $p_{i0} := p_i - p_0$ and $v_{i0} := v_i - v_0$ are the position and velocity deviations between the i th robot and the virtual leader. The functions $g_{ij} : \mathbb{R}^n \times \mathbb{R}^n \mapsto \mathbb{R}^n$, with $g_{ik}(p_{ik}, v_{ik}) = \mathbf{0}_n$ for all $k \notin \mathcal{N}_i^{in}$, and $g_{i0} : \mathbb{R}^n \times \mathbb{R}^n \mapsto \mathbb{R}^n$, with $g_{k0}(p_{k0}, v_{k0}) = \mathbf{0}_n$ for all $k \notin \mathbf{I}_0 \subset \mathbf{I}$ and \mathbf{I}_0 the set of informed robots, are all continuous.

For the multi-robot system (3.1), the specific functions g_{ij} and g_{i0} in the distributed controller (3.2) are presented in the following Sections.

3.1 Consensus problem over fixed digraphs

Consider a fixed information network; Figure 3.1, on page 38, shows an example of it. That is, every robot has a fixed set of robots with which it can exchange information.

Denote as \mathcal{D} the fixed digraph that represent the information network of the multi-robot system (3.1). Next, we present the design of distributed controllers for leaderless and leader-followers consensus problems.

3.1.1 Leaderless consensus

For this configuration, the informed robots set I_0 is an empty set since there is no leader. From Definition 2.3, an intuitive approach is to have $g_{i0}(p_{i0}, v_{i0}) = \mathbf{0}_n$ and:

$$u_i = \sum_{j \in \mathcal{N}_i^{in}} g_{ij}(p_{ij}, v_{ij}) = -\kappa_1 \sum_{j \in \mathcal{N}_i^{in}} a_{ij}(p_{ij} - \delta_{ij}) - \kappa_2 \sum_{j \in \mathcal{N}_i^{in}} a_{ij}v_{ij}, \quad i \in I, \quad (3.3)$$

where $\delta_i \in \mathbb{R}^n$ (with $n = 1, 2$ or 3) is called the desired position of the i th robot and $\delta_{ij} = \delta_i - \delta_j$ is the distance between the desired positions of robots i and j (we assume that these vectors exist). Additionally, $\|\delta_{ij}\| = \Delta_{ij} \geq 0$ is the magnitude of the distance between them. The values $a_{ij} \in \mathbb{R}_{\geq 0}$ are the scalar and constant ij th entry of the adjacency matrix $A(\mathcal{D})$. And $\kappa_1, \kappa_2 \in \mathbb{R}_{>0}$ are constant gains to be designed.

Applying (3.3) to (3.1) we have:

$$\dot{p}_i = v_i \quad (3.4a)$$

$$m_i \dot{v}_i = -\kappa_1 \sum_{j \in \mathcal{N}_i^{in}} a_{ij}(p_{ij} - \delta_{ij}) - \kappa_2 \sum_{j \in \mathcal{N}_i^{in}} a_{ij}v_{ij}, \quad i \in I. \quad (3.4b)$$

To analyze the closed-loop system (3.4), first define the i th robot's errors to the desired position and velocities as

$$\tilde{p}_i := p_i - \delta_i \quad \text{and} \quad \tilde{v}_i := v_i - \dot{\delta}_i \quad \text{for all } i \in I. \quad (3.5)$$

where $\dot{\delta}_i = \mathbf{0}_n$, since δ_i is constant. Notice then that if, for all $i \in I$, error \tilde{p}_i approach to the zero vector, then $\|p_{ij}\|$ approximates to Δ_{ij} . Therefore, we must show that the error trajectories approach asymptotically to zero.

The error dynamics are:

$$\dot{\tilde{p}}_i = \tilde{v}_i, \quad (3.6a)$$

$$m_i \dot{\tilde{v}}_i = -\kappa_1 \sum_{j \in \mathcal{N}_i^{in}} a_{ij}\tilde{p}_{ij} - \kappa_2 \sum_{j \in \mathcal{N}_i^{in}} a_{ij}\tilde{v}_{ij}, \quad i \in I, \quad (3.6b)$$

where the fact that $\tilde{p}_{ij} = p_{ij} - \delta_{ij}$ and $\tilde{v}_{ij} = v_{ij} - \dot{\delta}_{ij}$ was used. This error dynamics description is written in terms of the digraph's adjacency matrix entries. An equivalent description, which uses the entries of the Laplacian matrix, defined in (2.8), and which will be useful in demonstrating the stability of the error trajectories, is

$$\dot{\tilde{p}}_i = \tilde{v}_i, \quad (3.7a)$$

$$m_i \dot{\tilde{v}}_i = -\kappa_1 \sum_{j=1}^N l_{ij}\tilde{p}_j - \kappa_2 \sum_{j=1}^N l_{ij}\tilde{v}_j, \quad i \in I, \quad (3.7b)$$

where l_{ij} it's the ij -th entry of the Laplacian matrix $L(\mathcal{D})$. Now, define the vectors $\tilde{p} := [\tilde{p}_1, \dots, \tilde{p}_N]^T \in \mathbb{R}^{nN}$ and $\tilde{v} := [\tilde{v}_1, \dots, \tilde{v}_N]^T \in \mathbb{R}^{nN}$. These vectors collect the error states of every member in the multi-robot system. With these new vectors, and using the Kronecker product (described in section 2), we can rewrite the closed-loop error dynamics (3.7) in a matrix form as

$$\dot{\tilde{p}} = \tilde{v}, \quad (3.8a)$$

$$(M \otimes I_n) \dot{\tilde{v}} = -\kappa_1 (L(\mathcal{D}) \otimes I_n) \tilde{p} - \kappa_2 (L(\mathcal{D}) \otimes I_n) \tilde{v}, \quad i \in I, \quad (3.8b)$$

where $M = \text{diag}(m_1, \dots, m_N) \in \mathbb{R}^{N \times N}$. Notice that M is an invertible matrix, with its inverse given by $M^{-1} = \text{diag}\left(\frac{1}{m_1}, \dots, \frac{1}{m_N}\right)$, therefore, $(M \otimes I_n)$ its also an invertible matrix. Then, using the properties of the Kronecker product, equation (3.8) can be rewritten as

$$\dot{x} = (\Theta \otimes I_n) x, \quad (3.9)$$

where $x = [\tilde{p}^T, \tilde{v}^T]^T \in \mathbb{R}^{2nN}$ and

$$\Theta = \begin{bmatrix} Z_N & I_N \\ -\kappa_1 \Xi & -\kappa_2 \Xi \end{bmatrix} \in \mathbb{R}^{2nN \times 2nN}$$

with $\Xi = [\xi_{ij}] = M^{-1}L(\mathcal{D}) \in \mathbb{R}^{N \times N}$ and $Z_N \in \mathbb{R}^{N \times N}$. Notice that

$$\xi_{ii} = \frac{1}{m_i} \sum_{j \in \mathcal{N}_i^{\text{in}}} a_{ij}, \quad \xi_{ij} = -\frac{a_{ij}}{m_i}, \quad \forall i \in I \text{ and } j \neq i.$$

Therefore, Ξ has the same zero-row sum property of $L(\mathcal{D})$ and, hence, it has a unique zero eigenvalue. The following Lemma generalizes Lemma 4.1 in [42]. There, instead of Ξ , the matrix Laplacian $L(\mathcal{D})$ was considered with the gain $\kappa_1 = 1$. This lemma gives a relation between the zero eigenvalues of Θ and the solutions of (3.9).

Lemma 3.1. *The closed-loop system (3.1)-(3.3) achieves consensus asymptotically if and only if Θ has exactly two zero eigenvalues and all other eigenvalues have negative real parts. Specifically,*

$$\left\| v_i - \sum_{j=1}^N \gamma_j v_j(t_0) \right\| \rightarrow 0 \quad \text{and} \quad \left\| p_i - \sum_{j=1}^N \gamma_j p_j(t_0) - \sum_{j=1}^N \gamma_j v_j(t_0) t \right\| \rightarrow 0 \quad \text{as } t \rightarrow \infty,$$

where $\gamma \in \mathbb{R}_{>0}^N$ is such that of $\gamma^T \Xi = \mathbf{0}_N^T$ satisfying $\gamma^T \mathbf{1}_N = 1$.

Proof. (Sufficiency) We first show that if Θ has an eigenvalue 0 of multiplicity two and all the others have negative real-part, then consensus is reached. Let $q \in \mathbb{R}^{2N}$ be a unit right eigenvector associated to the zero eigenvalue, that is $\Theta q = \mathbf{0}_{2N}$. From equation (3.9) we have that $q = [\mathbf{1}_N^T, \mathbf{0}_N^T]^T$, which is unique. Since there cannot be other right eigenvector associated to the 0 eigenvalue, matrix Θ cannot be diagonal. Therefore,

there exists a nonsingular matrix $Q \in \mathbb{R}^{2N \times 2N}$, such that $Q^{-1}\Theta Q = J$, where J is the Jordan canonical form associated to Θ . Thus, one has

$$\begin{aligned} \Theta &= QJQ^{-1} \\ &= [\xi_1, \dots, \xi_{2N}] \begin{bmatrix} 0 & 1 & Z_{1 \times (2N-n)} \\ 0 & 0 & Z_{1 \times (2N-n)} \\ Z_{(2N-n) \times 1} & Z_{(2N-n) \times 1} & J' \end{bmatrix} \begin{bmatrix} \zeta_1^T \\ \vdots \\ \zeta_{2N}^T \end{bmatrix} \end{aligned} \quad (3.10)$$

where ξ_i and ζ_i , with $i = 1, \dots, 2N$ are respectively the right and left generalized eigenvectors of Θ , and $J' \in \mathbb{R}^{(2n-n) \times (2N-n)}$ is the upper diagonal Jordan block matrix associated with the nonzero eigenvalues $\mu_{i,j}$ for $i = 2, \dots, N$ and $j = 1, 2$.

Without lost of generality, choose $\xi_1 = [\mathbf{1}_N^T, \mathbf{0}_N^T]^T$ as the right eigenvector and $\xi_2 = [\mathbf{0}_N^T, \mathbf{1}_N^T]^T$ as the generalized right eigenvector of matrix Θ associated to the zero eigenvalue. Notice that Θ has exactly two zero eigenvalues, therefore, Ξ has a simple zero eigenvalue, which implies that there exists a positive vector γ such that $\gamma^T \Xi = \mathbf{0}_N^T$ and $\mathbf{1}_N^T \gamma = 1$. It can be verified that $\xi_1 = [\gamma^T, \mathbf{0}_N^T]^T$ and $\xi_2 = [\mathbf{0}_N^T, \gamma^T]^T$ are a left eigenvector, and generalized left eigenvector of Θ associated to the zero eigenvalues, respectively, where $\zeta_1^T \xi_1 = 1$ and $\zeta_2^T \xi_2 = 1$. Since $\mu_{i,j}$ for $i = 2, \dots, N$ and $j = 1, 2$ have negative real parts, and in view of the Kronecker product properties (2.2), therefore,

$$\begin{aligned} \exp^{(\Theta \otimes I_n)t} &= \exp^{(Q \otimes I_n)(Jt \otimes I_n)(Q^{-1} \otimes I_n)} \\ &= (Q \exp^{Jt} Q^{-1}) \otimes I_n \\ &= \left(Q \begin{bmatrix} 1 & t & Z_{1 \times (2N-2)} \\ 0 & 1 & Z_{1 \times (2N-2)} \\ Z_{1 \times (2N-2)} & Z_{1 \times (2N-2)} & J't \end{bmatrix} Q^{-1} \right) \otimes I_n. \end{aligned} \quad (3.11)$$

Notice that, since J' contains all the eigenvalues with negative real part, for a large t , the matrix $\exp(J't) \rightarrow Z_{(2N-2) \times (2N-2)}$; Thus

$$\lim_{t \rightarrow \infty} \exp^{(\Theta \otimes I_n)t} = \begin{bmatrix} \mathbf{1}_N \gamma^T & t \mathbf{1}_N \gamma^T & Z_{1 \times (2N-2)} \\ Z_{N \times N} & \mathbf{1}_N \gamma^T & Z_{1 \times (2N-2)} \\ Z_{1 \times (2N-2)} & Z_{1 \times (2N-2)} & Z_{(2N-2) \times (2N-2)} \end{bmatrix} \otimes I_n.$$

From the previous expression, notice that

$$\begin{aligned} &\lim_{t \rightarrow \infty} \left\| \begin{bmatrix} p(t) \\ v(t) \end{bmatrix} - I_N \otimes \begin{bmatrix} \sum_{i=1}^N \gamma_j p_j(t_0) - \sum_{i=1}^N \gamma_j v_j(t_0)t \\ \sum_{j=1}^N \gamma_j v_j(t_0) \end{bmatrix} \right\| = \\ &\lim_{t \rightarrow \infty} \left\| \exp^{(\Theta \otimes I_n)t} \begin{bmatrix} p(t_0) \\ v(t_0) \end{bmatrix} - I_N \otimes \begin{bmatrix} \sum_{i=1}^N \gamma_j p_j(t_0) - \sum_{i=1}^N \gamma_j v_j(t_0)t \\ \sum_{j=1}^N \gamma_j v_j(t_0) \end{bmatrix} \right\| \\ &= \lim_{t \rightarrow \infty} \left\| \left(\begin{bmatrix} \mathbf{1}_N \gamma^T & t \mathbf{1}_N \gamma^T \\ Z_{N \times N} & \mathbf{1}_N \gamma^T \end{bmatrix} \otimes I_n \right) \begin{bmatrix} p(t_0) \\ v(t_0) \end{bmatrix} \right. \\ &\quad \left. - I_N \otimes \begin{bmatrix} \sum_{i=1}^N \gamma_j p_j(t_0) - \sum_{i=1}^N \gamma_j v_j(t_0)t \\ \sum_{j=1}^N \gamma_j v_j(t_0) \end{bmatrix} \right\| = 0, \end{aligned}$$

which indicates that the (3.3) is a solution to the leaderless consensus Problem 2.1.

(Necessity) If the condition that Θ has exactly one zero eigenvalue of multiplicity two, and every other eigenvalue has positive real part, is not satisfied, then $\lim_{t \rightarrow \infty} \exp^{\Theta t}$ has a rank grater than two, which contradicts the assumption of that the leaderless consensus is reached. \square

The eigenvalues of Θ are extremely important for the stability analysis of (3.9). Therefore, denote as μ_{ij} , with $i = 1, \dots, N$ and $j = 1, 2$, and λ_i , with $i = 1, \dots, N$, the eigenvalues of Θ and Ξ , respectively. The eigenvalues of Θ can be found by solving the characteristic equation $\det(\mu I_{2N} - \Theta) = 0$. Notice that Θ fulfills the property (2.3), therefore

$$\begin{aligned} \det(\mu I_{2N} - \Theta) &= \det \begin{pmatrix} \mu I_N & -I_N \\ \kappa_1 \Xi & \mu I_N + \kappa_2 \Xi \end{pmatrix} \\ &= \det(\mu^2 I_N + (\kappa_2 \mu + \kappa_1) \Xi) \\ &= \prod_{i=1}^N (\mu^2 + (\kappa_2 \mu + \kappa_1) \lambda_i) = 0 \end{aligned} \quad (3.12)$$

Hence, the eigenvalues of Θ can be calculated as

$$\begin{aligned} \mu_{i,1} &= \frac{-\kappa_2 \lambda_i + \sqrt{\kappa_2^2 \lambda_i^2 - 4\kappa_1 \lambda_i}}{2}, \\ \mu_{i,2} &= \frac{-\kappa_2 \lambda_i - \sqrt{\kappa_2^2 \lambda_i^2 - 4\kappa_1 \lambda_i}}{2}. \end{aligned} \quad (3.13)$$

From (3.13), it can be seen that Θ has a zero eigenvalue of algebraic multiplicity $2a$ if and only if Ξ has an eigenvalue zero of algebraic multiplicity a .

With the following result we give conditions over the distributed controller gains κ_1 and κ_2 , and the static digraph \mathcal{D} such that the consensus behavior is asymptotically achieved by the heterogeneous multi-robot system (3.1).

Theorem 3.1. *The closed-loop system (3.1)-(3.3) achieves consensus asymptotically if and only if $\mathcal{D} \in \mathbb{D}_{ST}$ and*

$$\frac{\kappa_2^2}{\kappa_1} > \max_{2 \leq i \leq N} \left\{ \frac{\text{Im}(\lambda_i)^2}{\text{Re}(\lambda_i) (\text{Re}(\lambda_i)^2 + \text{Im}(\lambda_i)^2)} \right\} \quad (3.14)$$

where λ_i with $i = 2, \dots, N$ are the non-zero eigenvalues of Ξ . Specifically,

$$\left\| v_i - \sum_{j=1}^N \gamma_j v_j(t_0) \right\| \rightarrow 0 \quad \text{and} \quad \left\| p_i - \sum_{j=1}^N \gamma_j (p_j(t_0) + v_j(t_0)t) \right\| \rightarrow 0 \quad \text{as} \quad t \rightarrow \infty,$$

where $\gamma \in \mathbb{R}_{>0}^N$ is such that of $\gamma^T \Xi = \mathbf{0}_N^T$ satisfying $\gamma^T \mathbf{1}_N = 1$.

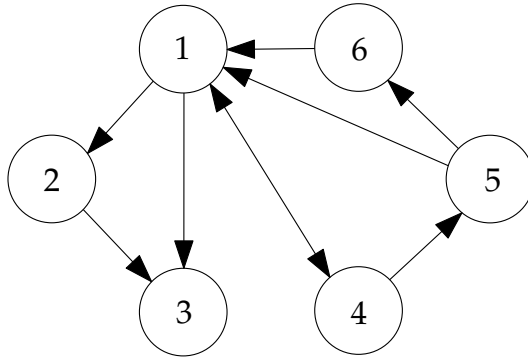


Figure 3.1: Multi-robot system's information network.

Proof. From the discussion on Laplacian matrix properties in Section (2.1.3) we know that $L(\mathcal{D})$ has exactly one zero eigenvalue, therefore, Ξ has a zero eigenvalue of multiplicity two. From Lemma 3.1, we only need to prove that $Re(\mu_{i,j}) < 0$ for all $i = 2, \dots, N$ and $j = 1, 2$ if and only if (3.14) holds and $Re(\lambda_i) > 0$ for all $i = 2, \dots, N$.

Let $\sqrt{\kappa_2^2 \lambda_i^2 - 4\kappa_1 \lambda_i} = a + b\mathbf{i}$, where $a, b \in \mathbb{R}$ and $\mathbf{i} = \sqrt{-1}$. From (3.13), we have that $Re(\mu_{i,j}) < 0$ if and only if $a < \kappa_2 Re(\lambda_i)$ for all $i = 2, \dots, N$. Then, it's sufficient to prove that (3.14) holds if and only if $a^2 < \kappa_2^2 Re(\lambda_i)^2$. Notice that

$$\kappa_2^2 \lambda_i^2 - 4\kappa_1 \lambda_i = (a + b\mathbf{i})^2.$$

Separating real and imaginary parts we obtain

$$\begin{aligned} a^2 - b^2 &= \kappa_2 (Re(\lambda_i)^2 - Im(\lambda_i)^2) - 4\kappa_1 Re(\lambda_i) \\ 2ab &= \kappa_2^2 Re(\lambda_i) Im(\lambda_i) - 4\kappa_1 Im(\lambda_i). \end{aligned}$$

After some algebraic manipulations, we have

$$a^4 - [\kappa_2^2 (Re(\lambda_i)^2 - Im(\lambda_i)^2) - 4\kappa_1 Re(\lambda_i)] a^2 - Im(\lambda_i)^2 [\kappa_2^2 Re(\lambda_i) - 2\kappa_1]^2 = 0,$$

from which it is easy to observe that $a^2 < \kappa_2^2 Re(\lambda_i)^2$ if and only if (3.14) holds. \square

In Theorem 3.1 necessary and sufficient conditions are given for the distributed controller (3.3) being a solution to the leaderless consensus problem. In it, we give a relationship between the gains in (3.3), and the real and imaginary parts of the eigenvalues of the Laplacian matrix associated to the directed information network.

Example 3.1. Consider the closed-loop system (3.1)-(3.3), consisting of $N = 6$ robots moving on a (x, y) -plane (i.e. $n = 2$). The mass for each robot is $m_i = i$, thus $M = \text{diag}(1, 2, 3, 4, 5, 6)$. Suppose the information network is modeled by the digraph shown in Figure 3.1, with edge weights $a_{ij} = 1$ if and only if $(j, i) \in \mathcal{E}$. For simplicity, suppose we want the group to move jointly sharing the same position and velocity vectors, that is $\Delta_{ij} = \dot{\Delta}_{ij} = 0$. Robots cannot share the same location, however, recall that p_i is the position of a point of interest in the robot. Since we consider the motion of the multi-robot system is over a plane, both differential mobile robots and

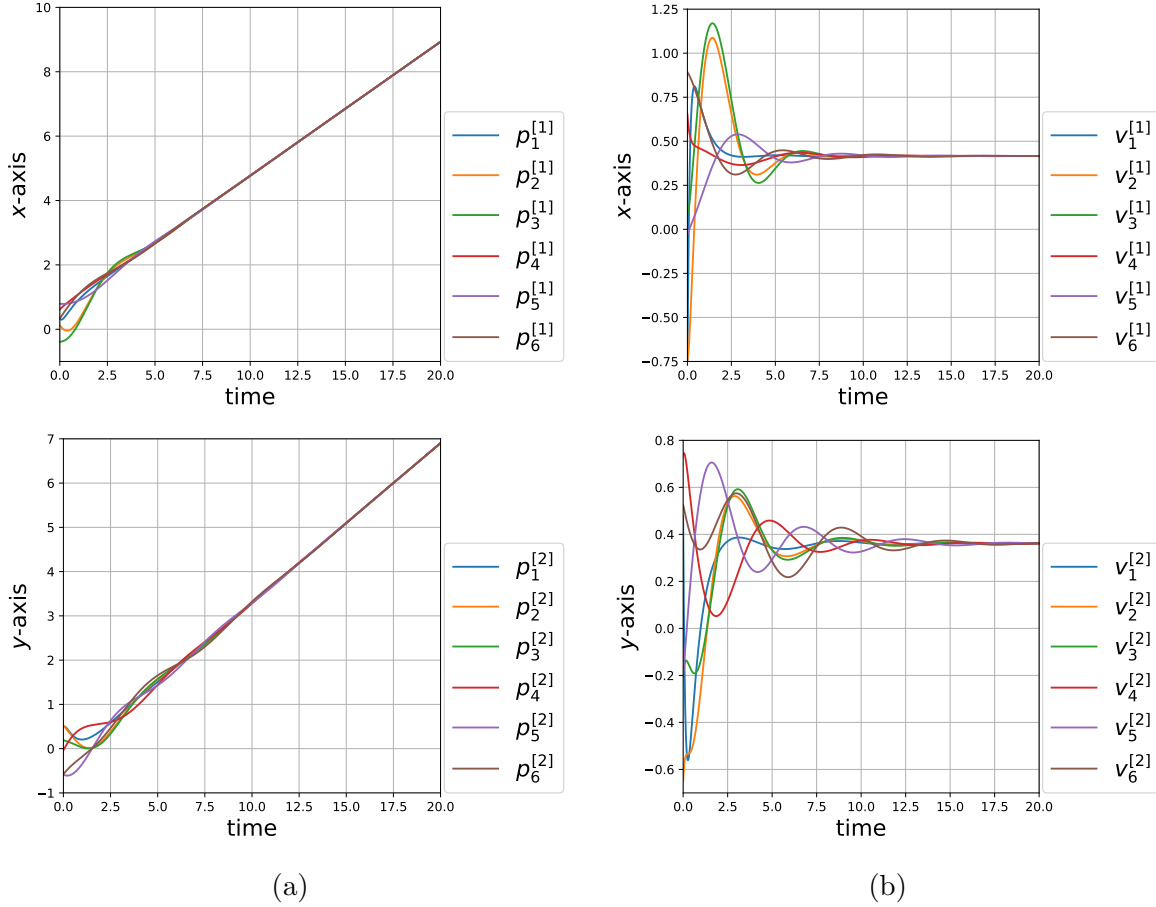


Figure 3.2: Closed-loop system (3.1)-(3.3) of Example 3.1.

drones can be consider here; this is in a case where, for the differential mobile robots, the point of interest is on different heights.

The nonzero eigenvalues of Ξ are $\lambda_{2,3} = 0.267 \pm 0.084i$, $\lambda_4 = 0.5$, $\lambda_5 = 0.666$ and $\lambda_6 = 3.082$. These values define the 12 eigenvalues of Θ through the relation (3.13). To ensure every eigenvalue of Θ has negative real-part, the control gains must fulfill inequality (3.14), that is $\frac{\kappa_2^2}{\kappa_1} > 0.338$. The Figure 3.2 shows the state trajectories for controller gains $\kappa_1 = 4$ and $\kappa_2 = 3$. The trajectories reach a consensus on position and velocity vectors, as desired.

3.1.2 Leader-followers configuration

Consider there is a virtual leader with dynamics described by equations

$$\dot{p}_0 = v_0, \quad \dot{v}_0 = f(t, p_0, v_0), \quad (3.15)$$

where $p_0, v_0 \in \mathbb{R}^n$ are respectively the position and velocity of the leader with a velocity vector field $f : \mathbb{R}_{>0} \times \mathbb{R}^n \times \mathbb{R}^n \mapsto \mathbb{R}^n$, where f is measurable and locally essentially bounded functions, *i.e.* a solution $v_0(t)$ exists and is unique. Every robot will continue

to use the g_{ij} functions defined in (3.3). Additionally, each informed robot (*i.e.* $i \in I_0$) will implements functions g_{i0} in (3.2) to be design.

Virtual leader without acceleration

Consider the virtual leader moves at a constant velocity v_0 , that is, the vector field in (3.15) is $f(p_0, v_0, t) \equiv \mathbf{0}_n$. Notice that, if $v_0(t_0) = \mathbf{0}_n$ the leader describes a fixed position to which the multi-robot system must arrive, meanwhile, if $v_0(t_0) = v_0^*$, with vector $v_0^* \in \mathbb{R}^n$ constant, the leader describes a trajectory that starts at $p_0(t_0)$ and moves with a constant velocity.

Since the objective is to steer informed robots to the leader's state trajectories, we propose to use an error state feedback

$$g_{i0}(p_{i0}, v_{i0}) = -h_i(\kappa_1(p_{i0} - \delta_{i0}) + \kappa_2(v_{i0})), \quad i \in I \quad (3.16)$$

where $p_{i0} = p_i - p_0$ and $v_{i0} = v_i - v_0$ are respectively the position and velocity deviation between the i th robot and the leader; $h_i \in \mathbb{R}_{>0}$ for all $i \in I_0$, with $h_i = 0$ otherwise; and the constant vector $\delta_{i0} = \delta_i - \delta_0 \in \mathbb{R}^n$, with $\|\delta_{i0}\| = \Delta_{i0}$ is the desired position deviation between the i -th robot and the leader. Therefore, the distributed controller (3.2) takes the following form

$$u_i = -\kappa_1 \sum_{j \in \mathcal{N}_i^{in}} a_{ij}(p_{ij} - \delta_{ij}) - \kappa_2 \sum_{j \in \mathcal{N}_i^{in}} a_{ij}(v_{ij} - \dot{\delta}_{ij}) - h_i \left(\kappa_1(p_{i0} - \delta_{i0}) + \kappa_2(v_{i0} - \dot{\delta}_{i0}) \right), \quad i \in I, \quad (3.17)$$

where $\delta_{ij} = \delta_i - \delta_j$. Notice that if $i \notin I_0$ then only the neighborhood information is used, while if $i \in I_0$ the leader's data is also used in the informed robots. The closed-loop system (3.1)-(3.17) is

$$\dot{p}_i = v_i, \quad (3.18a)$$

$$m_i \dot{v}_i = -\kappa_1 \sum_{j \in \mathcal{N}_i^{in}} a_{ij}(p_{ij} - \delta_{ij}) - \kappa_2 \sum_{j \in \mathcal{N}_i^{in}} a_{ij}v_{ij} - h_i(\kappa_1(p_{i0} - \delta_{i0}) + \kappa_2 v_{i0}), \quad i \in I, \quad (3.18b)$$

Define the error states as follows

$$\tilde{p}_i := p_i - (p_0 + \delta_{i0}), \quad \text{and} \quad \tilde{v}_i := v_i - v_0, \quad \text{for all } i \in I. \quad (3.19)$$

The error dynamics is

$$\dot{\tilde{p}}_i = \tilde{v}_i, \quad (3.20a)$$

$$m_i \dot{\tilde{v}}_i = -\kappa_1 \sum_{j \in \mathcal{N}_i^{in}} a_{ij} \tilde{p}_{ij} - \kappa_2 \sum_{j \in \mathcal{N}_i^{in}} a_{ij} \tilde{v}_{ij} - h_i(\kappa_1 \tilde{p}_{i0} + \kappa_2 \tilde{v}_{i0}), \quad i \in I. \quad (3.20b)$$

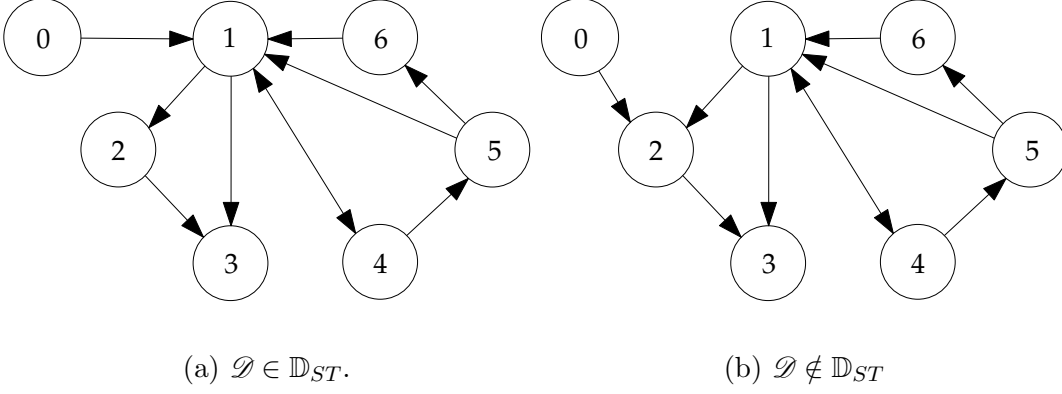


Figure 3.3: Multi-robot system's information network examples with a virtual leader.

An equivalent description in terms of the Laplacian matrix $L(\mathcal{D})$ entries is

$$\dot{\tilde{p}}_i = \tilde{v}_i, \quad (3.21a)$$

$$m_i \dot{\tilde{v}}_i = -\kappa_1 \sum_{j=1}^N l_{ij} \tilde{p}_j - \kappa_2 \sum_{j=1}^N l_{ij} \tilde{v}_j - h_i (\kappa_1 \tilde{p}_{i0} + \kappa_2 \tilde{v}_{i0}), \quad i \in \mathbb{I}. \quad (3.21b)$$

Define the vectors $\tilde{p} := [\tilde{p}_1^T, \dots, \tilde{p}_N^T]^T \in \mathbb{R}^{nN}$ and $\tilde{v} := [\tilde{v}_1^T, \dots, \tilde{v}_N^T]^T \in \mathbb{R}^{nN}$, and let $\hat{L}(\mathcal{D}) = L(\mathcal{D}) + H$ with $H = \text{diag}(h_1, \dots, h_N)$. By using the Kronecker product, equation (3.21) can be written in a matrix form as

$$\dot{\tilde{x}} = \left(\hat{\Theta} \otimes I_n \right) \tilde{x} \quad (3.22)$$

where $\tilde{x} = [\tilde{p}^T, \tilde{v}^T]^T \in \mathbb{R}^{2nN}$ and

$$\hat{\Theta} = \begin{bmatrix} Z_N & I_N \\ -\kappa_1 \hat{\Xi} & -\kappa_2 \hat{\Xi} \end{bmatrix}$$

with $\hat{\Xi} = M^{-1} \hat{L}(\mathcal{D}) \in \mathbb{R}^{N \times N}$.

Now, if $\hat{\Theta}$ is Hurwitz, then we can ensure the error states approach to zero. We have the following definition:

Definition 3.1. Call \mathcal{D}_{N+1} an extended digraph if the virtual leader is considered as the $N + 1$ member of the multi-robot system. Additionally denote as $A(\mathcal{D}_{N+1})$ and $L(\mathcal{D}_{N+1})$ to its corresponding Adjacency and Laplacian matrices.

Consider the information networks shown in Figure 3.3. Notice the extended digraph in Figure 3.3(b) doesn't contain any spanning tree, while in Figure 3.3(a), the leader (node 0) is the root of the only spanning tree contained in the extended digraph.

Lemma 3.2 (Extracted from Theorem 3.8 in [42]). *Matrix $\hat{L}(\mathcal{D})$ is invertible if and only if the extended digraph $\mathcal{D}_{N+1} \in \mathbb{D}_{ST}^{N+1}$ with the leader as the root. Additionally, for all the eigenvalues λ_i of $\hat{L}(\mathcal{D})$, $\text{Re}(\lambda_i) > 0$ with $i = 1, \dots, N$.*

Proof. Let $L(\mathcal{D}_{N+1})$ be the Laplacian matrix associated to it. Notice that the matrix $L(\mathcal{D}_{N+1}) = \begin{bmatrix} L_{N \times (N+1)} \\ Z_{1 \times (N+1)} \end{bmatrix}$ has zero row sum. Therefore, by the Laplacian matrices properties (see Section 2.1.3), $\text{rank}(L(\mathcal{D}_{N+1})) = N$. Thus, if $\mathcal{D}_{N+1} \in \mathbb{D}_{ST}$ then $\text{rank}(L_{N \times (N+1)}) = N$, since the last row of $L(\mathcal{D}_{N+1})$ has all its entries equal to zero. Observe that $L_{N \times (N+1)} = [L^*, h]$, with $L^* = [l_{ij}^*] \in \mathbb{R}^{N \times N}$ defined as $l_{ij}^* = a_{ij}$, for $i \neq j$, $l_{ii}^* = \sum_{j=1, j \neq i}^{N+1} a_{ij}$ and $h = [a_{1(N+1)}, \dots, a_{N(N+1)}]^T \in \mathbb{R}^N$. Since $L_{N \times (N+1)}$ has $N+1$ columns and zero row sum, we have that its last column depends on the first N ones, where $h = -L^* \mathbf{1}_N$. Therefore, $\text{rank}(L^*) = \text{rank}([L^*, h]) = N$ if and only if $\mathcal{D}_{N+1} \in \mathbb{D}_{ST}^N$. Moreover, since $\text{rank}(L^*)$ has full rank, then is invertible. Finally, it can be seen that $L^* = \hat{L}(\mathcal{D})$ has full rank and, hence, is invertible.

In addition, since $\mathcal{D}_{N+1} \in \mathbb{D}_{ST}^{N+1}$ then $L(\mathcal{D}_{N+1})$ has a eigenvalue equal to zero, while the rest have positive real parts. Hence, there exists a matrix P such that $L(\mathcal{D}_{N+1}) = P\Lambda^+P^{-1}$, with $\Lambda^+ = \text{diag}(\lambda_1, \dots, \lambda_{N+1})$. Without lost of generality, the eigenvalues can be ordered as $\lambda_1 \geq \dots \geq \lambda_N > \lambda_{N+1} = 0$. Since $\hat{L}(\mathcal{D})$ has full rank it must contains all nonzero eigenvalues of $L(\mathcal{D}_{N+1})$ implying that every eigenvalue of $\hat{L}(\mathcal{D})$ has positive real part. \square

The conditions on κ_1 and κ_2 such that $\hat{\Theta}$ is Hurwitz are given in the following result:

Theorem 3.2. *The closed-loop system (3.1)-(3.17) achieves leader-followers consensus asymptotically, for a virtual leader (3.15) with $f(p_0, v_0, t) \equiv \mathbf{0}_n$, if and only if $\hat{\Theta}$ is Hurwitz and*

$$\frac{\kappa_2^2}{\kappa_1} > \max_{1 \leq i \leq N} \left\{ \frac{\text{Im}(\lambda_i)^2}{\text{Re}(\lambda_i) (\text{Re}(\lambda_i)^2 + \text{Im}(\lambda_i)^2)} \right\} \quad (3.23)$$

Proof. Notice that the solutions of the error dynamic system (3.22) are

$$\tilde{x}(t) = \exp(\hat{\Theta}t \otimes I_n) \tilde{x}(0) = \left(\exp(\hat{\Theta}t) \otimes I_n \right) \tilde{x}(0),$$

where $\tilde{x}(0)$ is the initial conditions vector. The distributed controller (3.17) is a solution to the leader-followers consensus problem, is equivalent to demonstrate that Θ is Hurwitz. From Lemma 3.2 and the fact that M is a positive definite matrix, is clear that all the eigenvalues of $\hat{\Xi} = M^{-1}\hat{L}(\mathcal{D})$ have positive real part. The eigenvalues of $\hat{\Theta}$ and $\hat{\Xi}$ are such that (3.13) is satisfied. Therefore, to have $\text{Re}(\mu_{i,j}) < 0$, for all $i = 1, \dots, N$ and $j = 1, 2$, the gains κ_1 and κ_2 need to satisfy the condition (3.23) to which we arrive following the same proof of Theorem 3.1. \square

Example 3.2. *Consider the multi-robot system (3.1) consisting of $N = 6$ robots moving in a plane ($n = 2$) with masses such that the matrix $M = \text{diag}(1, 2, 3, 4, 5, 6)$. Apply controller (3.17) with $h_1 = 1$ and $h_i = 0$ for $i = 2, \dots, 6$ and let the information network be the one shown in Figure 3.3a.*

The nonzero eigenvalues of Θ are $\mu_{i,j} = \{0.667, 0.5, 4.062, 0.027, 0.263 \pm 0.077i\}$. Let $\kappa_1 = 1$, condition (3.23) implies that $\kappa_2 > 0.299$. The Figure 3.4 shows the position and velocity error norms which approach to zero and, therefore, the consensus behavior with the virtual leader is reached.

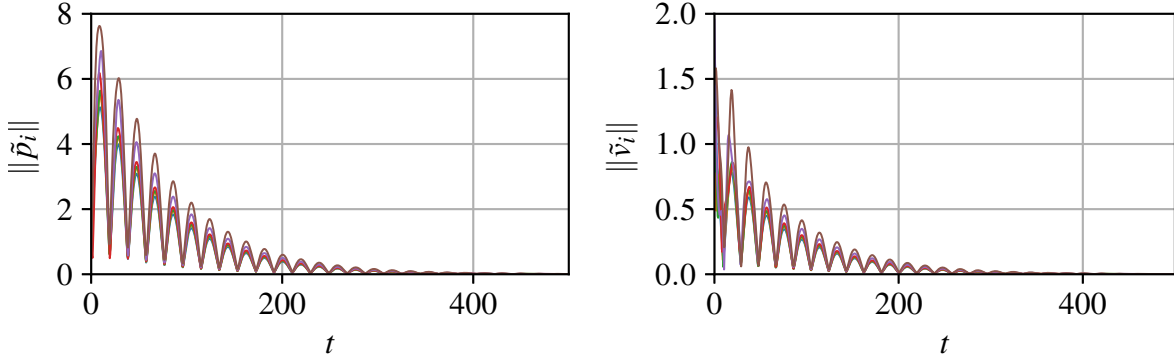


Figure 3.4: Closed-loop system (3.1)-(3.17) of Example 3.2.

Virtual leader with acceleration

Now, consider that the vector field of (3.15) is not equivalent to zero. Then, the velocity of the virtual leader might change over time. One might think the controller (3.17) solves this problem set. The following example shows that's not the case.

Example 3.3. Consider the same multi-robot system set described in the Example 3.2 and let $f(t, p_0, v_0) = [-\cos(t), -\sin(t)]^T$ in (3.15) be the velocity vector field of the virtual leader. With this vector field, the virtual leader's position trajectory describes a unit circle in the xy -plane. Recall we are applying controller (3.17) with suitable gains $\kappa_1 = \kappa_2 = 1$; Example 3.2 shows the effectiveness of (3.17) for a leader moving at a constant speed. The Figure 3.5 shows the position and velocity error norm trajectories. Notice that the state errors, although remain bounded, doesn't approach to zero as required.

The previous example shows that the distributed controller (3.17) is not suitable for the case of a leader with acceleration, since the main objective in Example 3.3 is to drive the error vector norms to zero. Hence, a new solution must be design. Before we create the new one, consider the following assumption.

Assumption 3.1. Each robot share their acceleration \dot{v}_i with its neighbors. Additionally, if informed, the robot also have access to leader's velocity vector field.

Notice that the Assumption 3.1 is equivalent to robots sharing their input vectors. In practical implementations, as the controllers are calculated in a distributed fashion, input vectors are available on each robot to be shared with its neighbors through the information network.

A modified version of the general form of a distributed controller (3.2), considering Assumption 3.1, is

$$u_i = \sum_{j \in \mathcal{N}_i^{in}} g_{ij}(p_{ij}, v_{ij}, \dot{v}_j) + g_{i0}(p_{i0}, v_{i0}, \dot{v}_0), \quad i \in \mathbf{I}, \quad (3.24)$$

where $g_{ij} : \mathbb{R}^n \times \mathbb{R}^n \times \mathbb{R}^n \mapsto \mathbb{R}^n$, with $g_{ik}(p_{ik}, v_{ik}, \dot{v}_k) = \mathbf{0}_n$ for all $k \notin \mathcal{N}_i^{in}$, and $g_{i0} : \mathbb{R}^n \times \mathbb{R}^n \times \mathbb{R}^n \mapsto \mathbb{R}^n$, with $g_{k0}(p_{k0}, v_{k0}, \dot{v}_0) = \mathbf{0}_n$ for all $k \notin \mathbf{I}_0$, are continuous functions.

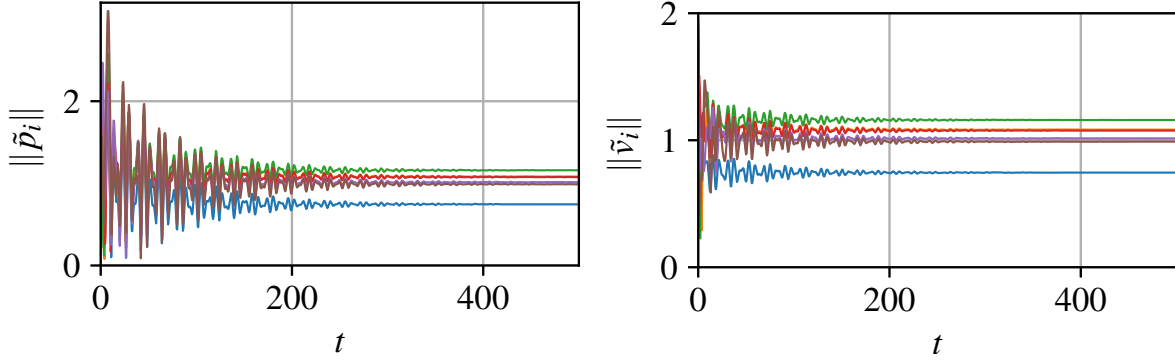


Figure 3.5: Closed-loop system (3.1)-(3.17) of Example 3.3.

As the i -th robot's position still must approach to the desired deviation with respect to its neighbors, we use the terms in equation (3.3) as a basis in the design of g_{ij} functions. However, we add to the i -th robot's input vector the weighted acceleration of its neighbors, with the objective of, once the position and velocity of neighboring robots reach the desired deviation, accelerate the i -th robot with the same input vector as its neighbors. Then, the g_{ij} functions take the form

$$\sum_{j \in \mathcal{N}_i^{in}} g_{ij}(p_{ij}, v_{ij}, \dot{v}_j) := -\frac{\kappa_1}{\eta_i} \sum_{j \in \mathcal{N}_i^{in}} a_{ij}(p_{ij} - \delta_{ij}) - \frac{\kappa_2}{\eta_i} \sum_{j \in \mathcal{N}_i^{in}} a_{ij}v_{ij} + \frac{1}{\eta_i} \sum_{j \in \mathcal{N}_i^{in}} a_{ij}\dot{v}_j \quad (3.25)$$

where $\eta_i = \frac{1}{m_i} \left(h_i + \sum_{j \in \mathcal{N}_i^{in}} a_{ij} \right)$. The functions in (3.25) are well defined for extended digraphs $\mathcal{D}_{N+1} \in \mathbb{D}_{ST}^{N+1}$ with a spanning tree with the leader as the root, since $\eta_i \neq 0$ for all $i \in \mathcal{I}$. Analogously, the functions g_{i0} in the informed robot's controllers are similar to those described in equation (3.16) but this time include leader's velocity vector field.

$$g_{i0}(p_{i0}, v_{i0}, \dot{v}_0) := -\frac{h_i}{\eta_i} (\kappa_1 (p_{i0} - \delta_{i0}) + \kappa_2 v_{i0} - \dot{v}_0) \quad (3.26)$$

where $\dot{v}_0 = f(t, p_0, v_0)$. That is, informed robots must also approach to their desired position deviation with respect to the leader, and to accelerate with the same velocity vector field.

The closed loop system (3.1)-(3.24), with the terms defined in (3.25) and (3.26), takes the following form.

$$\dot{p}_i = v_i, \quad (3.27a)$$

$$m_i \dot{v}_i = -\frac{\kappa_1}{\eta_i} \sum_{j \in \mathcal{N}_i^{in}} a_{ij}(p_{ij} - \delta_{ij}) - \frac{\kappa_2}{\eta_i} \sum_{j \in \mathcal{N}_i^{in}} a_{ij}(v_{ij}) + \frac{1}{\eta_i} \sum_{j \in \mathcal{N}_i^{in}} a_{ij}\dot{v}_j - \frac{h_i}{\eta_i} (\kappa_1 (p_{i0} - \delta_{i0}) + \kappa_2 v_{i0} - \dot{v}_0), \quad i \in \mathcal{I}, \quad (3.27b)$$

Define the error vectors as in equation (3.5), the error dynamics can be described

in a matrix form, and in terms of the Laplacian matrix $L(\mathcal{D})$, as

$$\dot{\tilde{p}} = \tilde{v}, \quad (3.28a)$$

$$\left(\hat{L}(\mathcal{D}) \otimes I_n\right) \dot{\tilde{v}} = -\kappa_1 \left(\hat{L}(\mathcal{D}) \otimes I_n\right) \tilde{p} - \kappa_2 \left(\hat{L}(\mathcal{D}) \otimes I_n\right) \tilde{v}, \quad i \in \mathbf{I}, \quad (3.28b)$$

where $\hat{L}(\mathcal{D}) = L(\mathcal{D}) + H$ with $H = \text{diag}(h_1, \dots, h_N)$.

Theorem 3.3. *The closed-loop system (3.1)-(3.24) achieves leader-followers consensus asymptotically, with a virtual leader (3.15), if and only if the extended digraph $\mathcal{D}_{N+1} \in \mathbb{D}_{ST}^{N+1}$ with the virtual leader as the root of a directed spanning tree. Moreover, if additionally $\kappa_2 \geq 2\sqrt{\kappa_1}$, the errors approach to zero exponentially.*

Proof. Since $\mathcal{D}_{N+1} \in \mathbb{D}_{ST}^{N+1}$ with the virtual leader as the root of a directed spanning tree, from Lemma 3.2, we know that matrix $\hat{L}(\mathcal{D}) \otimes I_n$ is invertible. Therefore, equation (3.28) can be rewritten as

$$\dot{\tilde{p}} = \tilde{v}, \quad (3.29)$$

$$\dot{\tilde{v}} = -\kappa_1 (I_N \otimes I_n) \tilde{p} - \kappa_2 (I_N \otimes I_n) \tilde{v}, \quad i \in \mathbf{I}. \quad (3.30)$$

The system (3.29) can be written, with $\tilde{x} = [\tilde{p}^T, \tilde{v}^T]^T$, like a linear system as

$$\dot{\tilde{x}} = \left(\tilde{\Xi} \otimes I_n\right), \quad \text{where} \quad \tilde{\Xi} = \begin{bmatrix} Z_N & I_N \\ -\kappa_1 I_N & -\kappa_2 I_N \end{bmatrix}.$$

As before, an spectral analysis of matrix $\tilde{\Xi}$ shows that its eigenvalues are

$$\mu_{ij} = \frac{-\kappa_2 \pm \sqrt{\kappa_2^2 - 4\kappa_1}}{2}, \quad i = 1, \dots, N \quad j = 1, 2.$$

Notice that for every $\kappa_1, \kappa_2 > 0$, the eigenvalues of $\tilde{\Xi}$ have negative real part. Moreover, if and only if $\kappa_2 \geq 2\sqrt{\kappa_1}$ the eigenvalues of $\tilde{\Xi}$ are such that $\text{Im}(\mu_{ij}) = 0$. Therefore, the convergence is exponential. \square

Example 3.4. *Consider the multi-robot system set defined in Example 3.2 with $n = 1$ and implementing the distributed controller (3.24), with the terms defined in (3.25) and (3.26). Then, from Theorem 3.3, for any $\kappa_1, \kappa_2 > 0$ the leader-followers consensus is reached. The Figure 3.6 shows the trajectories of the multi-robot system (3.1) where the velocity vector field of the virtual leader is $f(t, p_0, v_0) = -\sin(t)$.*

3.2 Consensus problems over proximity graphs

We design distributed controllers for the leaderless and leader-followers consensus behavior over proximity graphs¹. Here, we consider each member of the multi-robot system (3.1) has a limited communication/sensing radius r , equal for ever robot. Then,

¹Proximity digraphs were described in Section 2.3.1

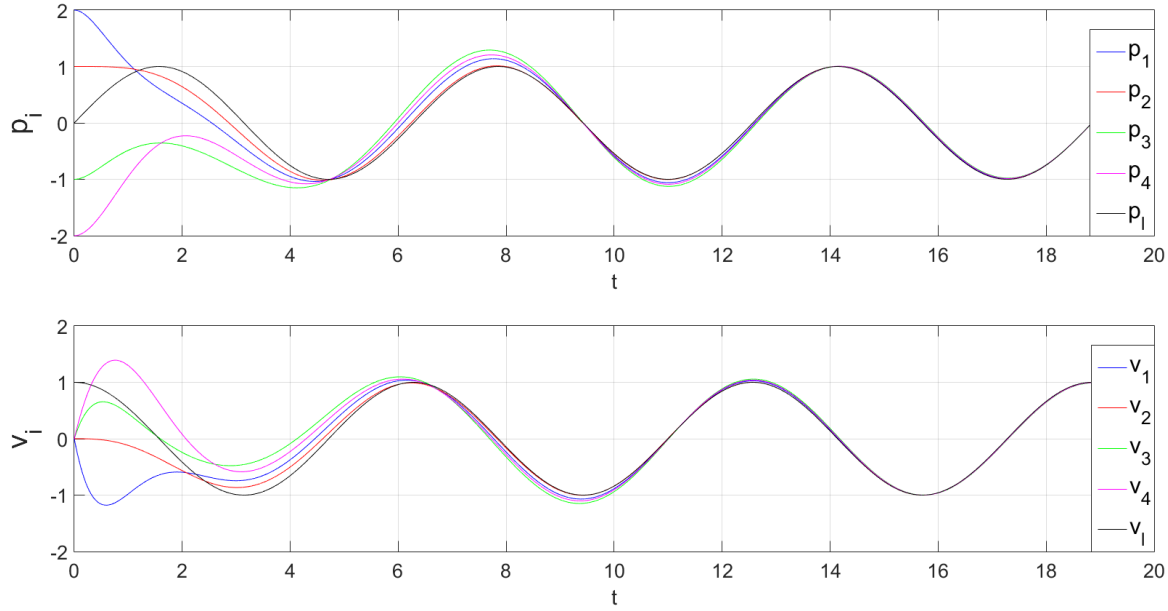


Figure 3.6: Multi-robot system (3.1) implementing controller (3.24).

the information network is bidirectional, since $i \in \mathcal{N}_j^{in}$ always that $j \in \mathcal{N}_i^{in}$, and will be described by means of a graph $\mathcal{G}(p)$.

Our first element of design is not the shape of the controller it self, but the process of addition/deletion of edges in the overall proximity graph from a local process. This is, each robot has embedded a rule on the addition/deletion of robots from its neighborhood set, which modifies the global topology of the information network. Consider the following hysteresis process.

Definition 3.2 (Neighborhood hysteresis process.). *For every robot in (3.1) with a neighborhood $\mathcal{N}_i(p)$, let $\epsilon \in (0, r)$ and $\mathcal{N}_i(p)_{t_0} := \{j \in \mathcal{V} : \|p_{ij}\| < r\}$ at $t = t_0$. We say the i th robot's neighborhood has an hysteresis process when at any time instant $t > t_0$ and $j \in \mathcal{V}$:*

- (Neighbor addition) *if at time t , $\|p_{ij}\| \leq r - \epsilon$ and $j \notin \mathcal{N}_i(p)_{t^-}$, then j is appended to the neighborhood, i.e. $\mathcal{N}_i(p) = \mathcal{N}_i(p)_{t^-} \cup \{j\}$;*
- (Neighbor removal) *if at time t , $\|p_{ij}\| > r$ and $j \in \mathcal{N}_i(p)_{t^-}$, then j is removed from the neighborhood, i.e. $\mathcal{N}_i(p) = \mathcal{N}_i(p)_{t^-} \setminus \{j\}$.*

The neighborhood hysteresis process indicates that, for the i -th robot at any time instant $t \geq t_0$, even when a nearby robot j is closed enough to be available for information exchange, *i.e.* $r - \epsilon < \|p_{ij}\| < r$, it will not be considered as part of $\mathcal{N}_i(p)$ and not will be used to determine the control actions. On the other hand, it will remain as part of $\mathcal{N}_i(p)$ until $\|p_{ij}\| \geq r$. Notice that, if a robot j is appended to (removed from) the i -th robot's neighborhood, then the edge (i, j) is also appended to (removed from) the set $\mathcal{E}(p)$. It also prevents fast creation/deletion of network edges due to inter-robot distances near the sensing radius. The hysteresis process from Definition 3.2 is illustrated in Figure 3.7.

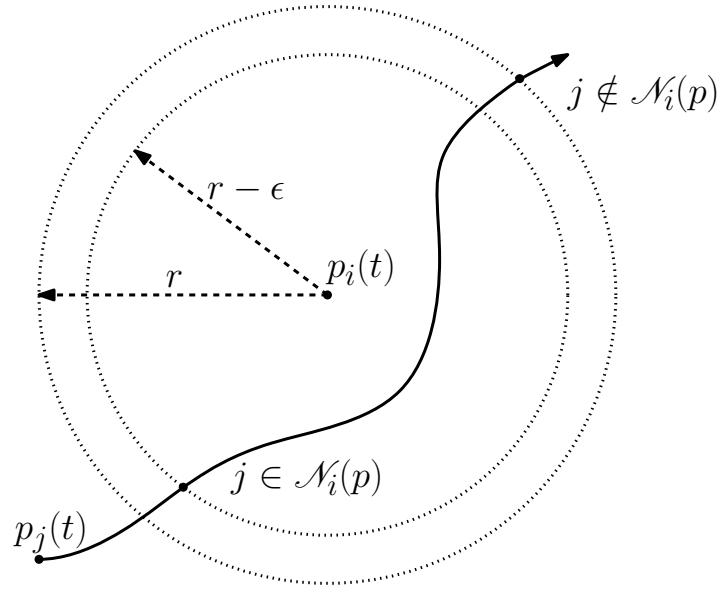


Figure 3.7: Neighborhood hysteresis process.

3.2.1 Leaderless configuration

Our controller design must preserve the connectivity of the proximity network, since the reachability of the consensus state is subject to the topological properties of the proximity graph. Assuming the proximity graph is connected at an initial time t_0 , *i.e.* $\mathcal{G}(p)_{t_0}$, the function g_{ij} must drive the i th robot into a position trajectory such that the distance with its neighbor j , *i.e.* $\|p_{ij}\|$ for $j \in \mathcal{N}_i$, approaches to zero, and remain bounded by r for all $t \in [t_0, t_f]$. If this objective is accomplished by every member of the multi-robot system, then controllers u_i , for $i = 1, \dots, N$, are connectivity preservers and distributed. To achieve this objective, functions g_{ij} are divided into two parts: The first part reduces the inter-robot distances toward zero while maintaining them bounded by r , and the second part forces the velocity error between i and j towards zero.

For the first part, let $s = \|p_{ij}\|$ be the distance between a pair of connected robots, with $(j, i) \in \mathcal{G}(p)$ for $j \neq i$. Consider an Artificial Potential Function (APF) $\psi(s) : [0, r] \mapsto \mathbb{R}_{>0}$ with partial derivative $\varphi(s) = \frac{\partial \psi(s)}{\partial s}$. Define $\psi(s)$ with the following properties:

- (i) $\psi(s) \rightarrow \hat{\psi}$ as $s \rightarrow r$;
- (ii) $\varphi(s) > 0$ for all $s \in (0, r)$;
- (iii) $\lim_{s \rightarrow 0} \left(\frac{\varphi(s)}{s} \right)$ is nonzero and bounded.

Condition (i) states that the APF is bounded by a constant value $\hat{\psi}$. Meanwhile, condition (ii) stipulates that the potential is an increasing function of their relative distance. Finally, condition (iii) requires APF's partial derivative be nonnegative and bounded as pair of robots distance approaches to zero. By taking APF's gradient, *i.e.*

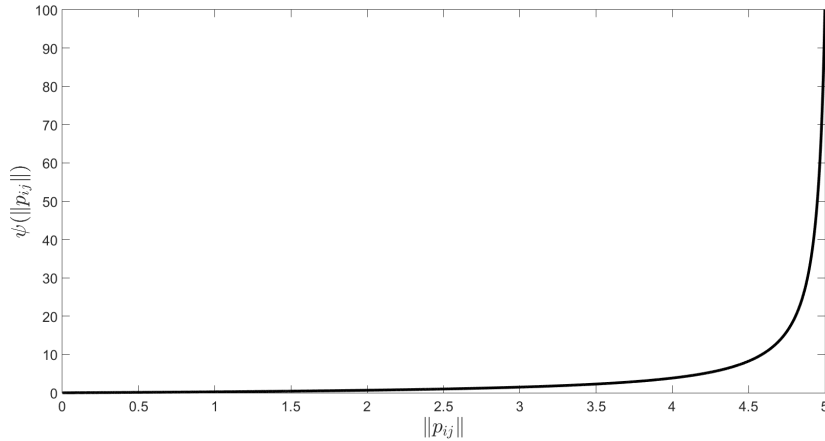


Figure 3.8: Artificial potential function in equation (3.31).

$\nabla_{p_i} \psi(\|p_{ij}\|) = \varphi(\|p_{ij}\|) \frac{p_{ij}}{\|p_{ij}\|}$, a vector force pointing towards its minimum value. That is, as inter-robot distances approach to r , the APF's gradient will force them together, hence, to the desired inter-robot distance. An example of this kind of APF, shown in Figure 3.8, is:

$$\psi(\|p_{ij}\|) := \frac{\hat{\psi} \|p_{ij}\|^2}{\hat{\psi}(r - \|p_{ij}\|) + \|p_{ij}\|^2}. \quad (3.31)$$

For the second part of g_{ij} , consider the deviation state between robot's i velocity and its j -th neighbor. This error is used as a feedback to approach neighboring robots velocity to zero deviation, and will be multiplied by the information network edge weight a_{ij} .

Using the above described terms, the distributed controller is

$$u_i = - \sum_{j \in \mathcal{N}_i(p)} \nabla_{p_i} \psi(\|p_{ij}\|) - \sum_{j \in \mathcal{N}_i(p)} a_{ij} v_{ij}, \quad i \in \mathbf{I}, \quad (3.32)$$

where a_{ij} is the constant weight of the corresponding edge $(j, i) \in \mathcal{E}(p)$. This controller is implemented along with the neighborhood hysteresis process that defines the neighborhood $\mathcal{N}_i(p)$ of the i -th robot.

Notice that the desired coordinated behavior is related to the *internal* configuration (inter-robot positions), rather than with the global frame. To analyze the motion dynamics of the closed loop system (3.1)-(3.32), a mobile coordinate system is necessary. Consider the center of mass (COM) of the multi-robot system (3.1) and denote its position and velocity as

$$\bar{p} := \frac{\sum_{i=1}^N m_i p_i}{\sum_{k=1}^N m_k}, \quad \text{and} \quad \bar{v} := \frac{\sum_{i=1}^N m_i v_i}{\sum_{k=1}^N m_k}. \quad (3.33)$$

Define the errors in position and velocity of the i -th robot with respect to the COM as

$$\tilde{p}_i := p_i - \bar{p}, \quad \text{and} \quad \tilde{v}_i := v_i - \bar{v}, \quad i \in \mathbf{I}. \quad (3.34)$$

From this definition observe that $p_{ij} = \tilde{p}_{ij}$ and $\tilde{v}_{ij} = v_{ij}$. Hence, inter-robot distances in the mobile coordinated system are the same as in the global frame, *i.e.* $\|\tilde{p}_{ij}\| = \|p_{ij}\|$. In consequence, the proximity network can be defined through the vector $\tilde{p} = [\tilde{p}_1^T, \dots, \tilde{p}_N^T]^T \in \mathbb{R}^{nN}$, *i.e.* the proximity graph has the property $\mathcal{G}(\tilde{p}) = \mathcal{G}(p)$. Similarly, the APFs in (3.32) can be written in terms of \tilde{p}_i , since $\psi(\|p_{ij}\|) = \psi(\|\tilde{p}_{ij}\|)$, with its gradient $\nabla_{p_i} \psi(\|p_{ij}\|) = \nabla_{\tilde{p}_i} \psi(\|\tilde{p}_{ij}\|)$. Therefore, the distributed controller can be rewritten in the following form

$$u_i = - \sum_{j \in \mathcal{N}_i(\tilde{p})} \nabla_{\tilde{p}_i} \psi(\|\tilde{p}_{ij}\|) - \sum_{j \in \mathcal{N}_i(\tilde{p})} a_{ij} \tilde{v}_{ij}, \quad i \in \mathbf{I}, \quad (3.35)$$

The dynamical analysis of the closed loop system (3.1)-(3.35) will be done through the total sum of potential and kinetic energy of the multi-robot system in the error coordinates. Define $x = [\tilde{p}^T, \tilde{v}^T]^T \in \mathbb{R}^{2nN}$, with $\tilde{v} = [\tilde{v}_1^T, \dots, \tilde{v}_N^T]^T \in \mathbb{R}^{nN}$, and the total energy of the multi-robot system as follows.

$$V(x) := \frac{1}{2} \sum_{i=1}^N \left(\sum_{j \in \mathcal{N}_i(\tilde{p})} \psi(\|\tilde{p}_{ij}\|) + m_i \tilde{v}_i^T \tilde{v}_i \right). \quad (3.36)$$

Notice that, the energy at an initial instant t_0 is bounded by the value $\bar{V}(x(t_0))$ with

$$V(x(t_0)) \leq \bar{V}(x(t_0)) = \frac{N(N-1)}{2} \psi(r - \epsilon) + \frac{1}{2} \sum_{i=1}^N (m_i \tilde{v}_i^T(t_0) \tilde{v}_i(t_0)). \quad (3.37)$$

We also, define the following set of position and velocities

$$\Omega := \left\{ x \in \mathbb{R}^{2nN} : \bar{V}(x) < \hat{\psi} \right\} \quad (3.38)$$

which are bounded by the maximum value of the APF used in the controller.

Theorem 3.4. *Consider the heterogeneous multi-robot system (3.1). Suppose the initial proximity graph $\mathcal{G}(p)$ is connected and $x(t_0) \in \Omega$, then the distributed controller (3.32), for all $t \in [t_0, \infty)$, is:*

- (i) *Connectivity preserving, and;*
- (ii) *A solution to the leaderless consensus problem*

Proof. First, notice that the closed loop system (3.1)-(3.32) can be rewritten in terms of error states as

$$\begin{aligned} \dot{\tilde{p}}_i &= \tilde{v}_i, \\ m_i \dot{\tilde{v}}_i &= - \sum_{j \in \mathcal{N}_i(\tilde{p})} \nabla_{\tilde{p}_i} \psi(\|\tilde{p}_{ij}\|) - \sum_{j \in \mathcal{N}_i(\tilde{p})} a_{ij} \tilde{v}_{ij}, \quad i \in \mathbf{I}, \end{aligned}$$

Proof of part (i): Notice that the change of $\mathcal{G}(p)$ over time can be interpreted as switching among a set of different fixed network topologies. Assume that $\mathcal{G}(p)$ switches

to a different topology at every time instant t_k with $k = 1, 2, \dots$, and remains fixed over the time interval $[t_{k-1}, t_k)$. Taking the time derivative of (3.36) over time interval $[t_{k-1}, t_k)$ yields

$$\dot{V}(x(t)) = \sum_{i=1}^N \left(\frac{1}{2} \sum_{j \in \mathcal{N}_i(\tilde{p})} \dot{\psi}(\|\tilde{p}_{ij}\|) + m_i \tilde{v}_i^T \dot{\tilde{v}}_i \right).$$

Since

$$\begin{aligned} \frac{1}{2} \sum_{i=1}^N \sum_{j \in \mathcal{N}_i(\tilde{p})} \dot{\psi}(\|\tilde{p}_{ij}\|) &= \sum_{i=1}^N \tilde{v}_i^T \sum_{j \in \mathcal{N}_i(\tilde{p})} \nabla_{\tilde{p}_i} \psi(\|\tilde{p}_{ij}\|) \\ m_i \tilde{v}_i^T \dot{\tilde{v}}_i &= \tilde{v}_i^T u_i, \end{aligned}$$

we have

$$\begin{aligned} \dot{V}(x(t)) &= \sum_{i=1}^N \tilde{v}_i^T \left(\sum_{j \in \mathcal{N}_i(\tilde{p})} \nabla_{\tilde{p}_i} \psi(\|\tilde{p}_{ij}\|) - \sum_{j \in \mathcal{N}_i(\tilde{p})} \nabla_{\tilde{p}_i} \psi(\|\tilde{p}_{ij}\|) - \sum_{j \in \mathcal{N}_i(\tilde{p})} a_{ij} \tilde{v}_{ij} \right) \\ &= - \sum_{i=1}^N \tilde{v}_i^T \sum_{j \in \mathcal{N}_i(\tilde{p})} a_{ij} \tilde{v}_{ij} \\ &= -\tilde{v}^T (L(\mathcal{G}(\tilde{p})) \otimes I_n) \tilde{v}. \end{aligned}$$

Recall that $\mathcal{G}(\tilde{p})$ is connected for all $t \in [t_0, t_1)$, hence $L(\mathcal{G}(\tilde{p}))$ has a unique zero eigenvalue, and every other eigenvalue has positive real part, then

$$-\tilde{v}^T (L(\mathcal{G}(\tilde{p})) \otimes I_n) \tilde{v} \leq 0 \quad (3.39)$$

This implies that $V(x(t)) \leq V(x(t_0)) \leq \bar{V}(x(t_0))$ for all $t \in (t_0, t_1]$. Since $x(t_0) \in \Omega$, then $V(x(t)) \leq \bar{V}(x(t_0)) < \hat{\psi}$. The latter implies that there are no neighboring robots whose distance tends to r for all $t \in (t_0, t_1]$. Since no edges are lost before t_1 , new edges must have been added to the proximity graph on that switching instant. Without loss of generality, assume there are $0 < q_1 \leq \frac{(N-1)(N-2)}{2}$ new edges on the network at t_1 , thus $V(x(t_1)) \leq V(x(t_0)) + q_1 \psi(r - \epsilon) \leq \bar{V}(x(t_0))$. Taking time derivative of $V(x(t))$ for $t \in [t_1, t_2)$ will result on expression (3.39). Once more, there are no distances between neighboring robots that tends to r , hence new edges must have been added at t_2 . The same happens for all switching instant t_k , with $k = 1, 2, \dots$, and time intervals $[t_{k-1}, t_k)$. Finally, since $\mathcal{G}(\tilde{p})$ is connected at t_0 , and no edges are lost from $\mathcal{E}(\tilde{p}(t_0))$ for all $t \in [t_0, \infty)$, then $\mathcal{G}(\tilde{p})$ remains connected for all $t \in [t_0, \infty)$. Hence, controller (3.32) is connectivity preserving.

Proof of part (ii): Assume there are q_k new edges added to $\mathcal{E}(\tilde{p})$ at switching instant t_k . Clearly, $0 < q_k \leq \frac{(N-1)(N-2)}{2}$ thus, from equation (3.39), we have that $V(x(t_1)) \leq V(x(t_0)) + (q_1 + \dots + q_k) \psi(r - \epsilon) \leq \bar{V}(x(t_0))$. Therefore the number of switching instants is finite, which implies that $\mathcal{G}(\tilde{p})$ eventually gets fixed. The remaining analysis is restricted for time interval $[t_k, \infty)$.

To show (3.32) is a solution to the leaderless consensus problem, we will use the LaSalle's invariance principle. Notice, from the previous analysis, that the distance between neighboring robots is no longer than $\psi^{-1}(\bar{V}(x(t_0)))$. Then, the set

$$\Gamma = \left\{ \hat{p} \in D_{\mathcal{G}}, \tilde{v} \in \mathbb{R}^{nN} : V(\hat{p}, \tilde{v}) \leq \bar{V}(x(t_0)) \right\}, \quad (3.40)$$

is positive invariant, where

$$D_{\mathcal{G}} = \left\{ \hat{p} \in \mathbb{R}^{nN^2} : \|\tilde{p}_{ij}\| \in [0, \psi^{-1}(\bar{V}(x(t_0)))] , \quad \forall (j, i) \in \mathcal{E}(\tilde{p}) \right\}$$

and $\hat{p} := [\tilde{p}_{11}^T, \dots, \tilde{p}_{1N}^T, \dots, \tilde{p}_{N1}^T, \dots, \tilde{p}_{NN}^T]^T$. Its clear that, since $V(x(t_0)) \leq \bar{V}(x(t_0))$, then the vector $x(t_0) \in \Gamma$. Now, we will show that Γ is compact. Notice that, since $\mathcal{G}(\tilde{p})$ is connected for all $t \in [t_k, \infty)$, the maximum distance between a pair of robots $i, j \in \mathcal{V}$ is, at most, $\|\tilde{p}_{ij}\| \leq r(N-1)$, then \hat{p} is bounded on every of its entries. Similarly, since $V(x(t)) \leq \bar{V}(x(t_0))$, then $m_i \tilde{v}_i^T \tilde{v}_i \leq 2\bar{V}(x(t_0))$, in consequence, $\|\tilde{v}_i\| \leq \sqrt{\frac{2\bar{V}(x(t_0))}{m_i}}$ for all $i \in \mathcal{V}$. Therefore, Γ is closed and bounded, hence compact. Finally, from LaSalle's invariance principle we know that, since the initial conditions lie in Γ , all trajectories will converge to the largest invariant set inside the region

$$S = \left\{ \hat{p} \in D_{\mathcal{G}}, \tilde{v} \in \mathbb{R}^{nN} : \dot{V}(x(t)) = 0 \right\}. \quad (3.41)$$

From equation (3.39) notice that $\dot{V}(x(t)) = 0$ if and only if $\tilde{v}_i = \dots = \tilde{v}_N$, which implies that $\|v_{ij}\| = 0$. Additionally, in steady state $\tilde{v}_i = \mathbf{0}_n$, this means that, from the definition of distributed controller (3.32), the following expression holds

$$u_i = - \sum_{j \in \mathcal{N}_i(\tilde{p})} \nabla_{\tilde{p}_i} \psi(\|\tilde{p}_{ij}\|) = \mathbf{0}_n, \quad i \in \mathcal{I}.$$

Notice that $\nabla_{\tilde{p}_i} \psi(\|\tilde{p}_{ij}\|) = \varphi(\|\tilde{p}_{ij}\|) \frac{\tilde{p}_{ij}}{\|\tilde{p}_{ij}\|}$. From the definition of $\psi(\cdot)$, we know that $\frac{\varphi(\|\tilde{p}_{ij}\|)}{\|\tilde{p}_{ij}\|}$ is nonzero and bounded, hence the position deviation must be zero, that is $\tilde{p}_{ij} = \mathbf{0}_n$. \square

Example 3.5. Consider an heterogeneous multi-robot system with dynamics (3.1) consisting of $N = 15$ mobile robots in a plane ($n = 2$). The mass and communication/sensing radios of the mobile robots are, respectively, $m_i = i$ and $r = 5$ for all $i = 1, \dots, N$. As for the distributed controller (3.32), consider an APF described by equation (3.31) with a maximum value $\hat{\psi} = 100$. For the neighborhood hysteresis process, let $\epsilon = 1$. As for initial conditions, we randomly choose them from boxes $[0, 10] \times [0, 10]$ for positions and $[0, 1] \times [0, 1]$ for velocities. Before the numerical simulation is initialized, we verify that $\mathcal{G}(p)$ is connected and $V(x(t_0)) \leq \bar{V}(x(t_0))$, if not, new initial conditions are choose.

In Figure 3.9 the proximity graph $\mathcal{G}(p(t_0))$ as well as the state trajectories of the multi-robot system are drawn. In the initial states chart, robots are located at arrow tails, the arrows itself represent the robot velocity vectors, meanwhile, dotted lines symbolize the existence of a proximity network edge among pair of robots. The trajectories and final states chart, shows how robots approach to a position consensus in the (x, y) -plain. Position and velocity vector elements are also drawn. The velocity trajectories chart shows how the multi-robot system finally reach a velocity consensus.

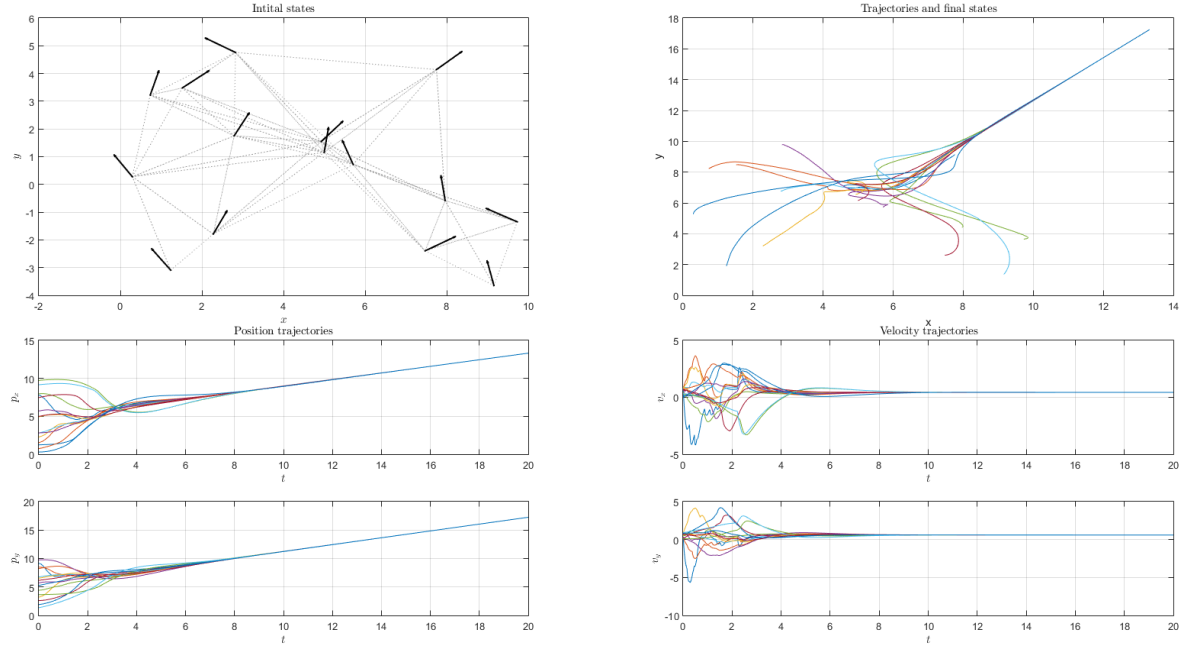


Figure 3.9: Leaderless consensus of the closed-loop system (3.1)-(3.32).

3.2.2 Leader-followers configuration

Consider a virtual leader with dynamics described by equation (3.15) with $I_0 \subset I$ the set of informed robots.

Leader with constant velocity

For this part, we assume the virtual leader, with dynamics (3.15), has its velocity vector field $f(p_0, v_0, t) \equiv \mathbf{0}_n$. Consider the general form of a distributed controller given by equation (3.2). In what follows, the design process for the functions in (3.2) is described.

For the leader-followers configuration let the g_{ij} functions in (3.2) be defined as in (3.32). Then, it only remains to design the g_{i0} functions. To include the robot-leader position and velocity state errors in the g_{i0} functions as to

$$g_{i0} := -h_i(p_{i0} + v_{i0}), \quad i \in I, \quad (3.42)$$

where $h_i \in \mathbb{R}_{>0}$ if $i \in I_0$, with $h_i = 0$ otherwise. Then, the distributed controller is defined as

$$u_i = - \sum_{j \in \mathcal{N}_i(p)} \nabla_{p_i} \psi(\|p_{ij}\|) - \sum_{j \in \mathcal{N}_i(p)} a_{ij} v_{ij} - h_i(p_{i0} + v_{i0}), \quad i \in I. \quad (3.43)$$

Define the state errors between the i -th robot and the virtual leader as

$$\tilde{p}_i := p_i - p_0 \quad \text{and} \quad \tilde{v}_i := v_i - v_0, \quad i \in I. \quad (3.44)$$

Notice that, in this case, the leader states play the role of the COM defined in the previous section as the mobile coordinate system.

Again, the dynamic analysis of the closed loop system (3.1)-(3.43) is analyzed through the total sum of potential and kinetic energy in error coordinates. Define $x = [\tilde{p}^T, \tilde{v}^T]^T \in \mathbb{R}^{2nN}$ and the total energy as follows.

$$V(x) := \frac{1}{2} \sum_{i=1}^N \left(\sum_{j \in \mathcal{N}_i(\tilde{p})} \psi(\|\tilde{p}_{ij}\|) + h_i \tilde{p}_i^T \tilde{p}_i + m_i \tilde{v}_i^T \tilde{v}_i \right), \quad (3.45)$$

which is bounded for any initial conditions as

$$V(x(t_0)) \leq \bar{V}(x(t_0)) = \frac{N(N-1)}{2} \psi(r - \epsilon) + \frac{1}{2} \sum_{i=1}^N (h_i \tilde{p}_i^T(t_0) \tilde{p}_i(t_0) + m_i \tilde{v}_i^T(t_0) \tilde{v}_i(t_0)).$$

Notice that we can relate the states of the multi-robot system to the maximum value of the APF with the set defined in equation (3.38).

Theorem 3.5. *Consider the heterogeneous multi-robot system (3.1) and a virtual leader (3.15) with $f(p_0, v_0, t) \equiv \mathbf{0}_n$. Suppose the initial proximity graph $\mathcal{G}(p)$ is connected and $x(t_0) \in \Omega$, then the distributed controller (3.43), for all $t \in [t_0, \infty)$, is:*

- (i) *Connectivity preserving, and;*
- (ii) *A solution to the leader-followers consensus problem*

Proof. Notice that the closed loop system (3.1)-(3.43), in error states, is

$$\begin{aligned} \dot{\tilde{p}}_i &= \tilde{v}_i, \\ m_i \dot{\tilde{v}}_i &= - \sum_{j \in \mathcal{N}_i(\tilde{p})} \nabla_{\tilde{p}_i} \psi(\|\tilde{p}_{ij}\|) - \sum_{j \in \mathcal{N}_i(\tilde{p})} a_{ij} \tilde{v}_{ij} - h_i (\tilde{p}_i + \tilde{v}_i), \quad i \in \mathbf{I}, \end{aligned}$$

where (3.43) has been written in error states.

Proof of part (i): This part can be proven following the same steps as in its equivalent in Theorem 3.4. We only must notice that the time derivative of energy function $V(x(t))$ in the time interval $[t_{k-1}, t_k)$ between switching instants t_{k-1} and t_k for $k = 1, 2, \dots$, is

$$\begin{aligned} \dot{V}(x(t)) &= \sum_{i=1}^N \left(\frac{1}{2} \sum_{j \in \mathcal{N}_i(\tilde{p})} \dot{\psi}(\|\tilde{p}_{ij}\|) + h_i \tilde{p}_i^T \dot{\tilde{p}}_i + m_i \tilde{v}_i^T \dot{\tilde{v}}_i \right) \\ &= -\tilde{v}^T \left(\hat{L}(\mathcal{G}(\tilde{p})) \otimes I_n \right) \tilde{v}, \end{aligned} \quad (3.46)$$

where $\hat{L}(\mathcal{G}(\tilde{p})) = L(\mathcal{G}(\tilde{p})) + H$ with $H = \text{diag}(h_1, \dots, h_N)$. Consider the virtual leader as an additional member of the multi-robot system and denote as $\mathcal{G}_{N+1}(\tilde{p})$ its corresponding proximity graph. Then, from lemma 3.2 we know the matrix $\hat{L}(\mathcal{G}(\tilde{p}))$ has all its eigenvalues with positive real part. Then, the inequality $\dot{V}(x(t)) \leq 0$ holds. Therefore, $V(x(t)) \leq \bar{V}(x(t_0)) < \hat{\psi}$, implying every edge in $\mathcal{G}(\tilde{p}(t_0))$ is maintained.

Since only new edges are appended to $\mathcal{E}(\tilde{p})$ at switching instants t_k , then $\mathcal{G}(\tilde{p})$ is connected. Hence, controller (3.43) is connectivity preserving.

Proof of part (ii): As in theorem 3.4, we can use the LaSalle's invariance principle. Considering the set Γ , defined in equation (3.40), it can be seen that is a positively invariant set. Since $\|\tilde{p}_{ij}\| \leq r(N-1)$ and $\|\tilde{p}_i\| \leq \sqrt{\frac{2\bar{V}(x(t_0))}{h_i}}$ for $i \in I_0$, and $\|\tilde{v}_i\| \leq \sqrt{\frac{2\bar{V}(x(t_0))}{m_i}}$, then Γ is compact. As such, and since the initial conditions start in Γ , the trajectories converge to the largest set inside region S , defined in (3.41). From equation (3.46) we can see that

$$\dot{V}(x(t)) = -\tilde{v}^T \left(\hat{L}(\mathcal{G}(\tilde{p})) \otimes I_n \right) \tilde{v} = 0$$

which implies that $\tilde{v}_1 = \dots = \tilde{v}_N$ and $\tilde{v}_i = \mathbf{0}_n$ for informed robots, *i.e.* for all i such that $h_i > 0$. In consequence, $v_1 = \dots = v_N = v_0$. Also, in steady state, where $\dot{\tilde{v}}_i = \mathbf{0}_n$, this means that distributed controller (3.43) is such that

$$u_i = - \sum_{j \in \mathcal{N}_i(\tilde{p})} \nabla_{\tilde{p}_i} \psi(\|\tilde{p}_{ij}\|) - h_i \tilde{p}_i = \mathbf{0}_n, \quad i \in I.$$

For uninformed robots, *i.e.* $h_i = 0$, this implies that $\varphi(\|\tilde{p}_{ij}\|) \frac{\tilde{p}_{ij}}{\|\tilde{p}_{ij}\|} = \mathbf{0}_n$. From APF's definition, this means that $\tilde{p}_{ij} = \mathbf{0}_n$ for all $i \in I \setminus I_0$ and $j \in \mathcal{N}_i(\tilde{p})$. For informed robots, the last means that, in steady state, the distance from the leader is zero, *i.e.* $\tilde{p}_i = \mathbf{0}_n$. Hence $p_1 = \dots = p_N = p_0$. That is, the distributed controller is a solution to the leader followers consensus problem. \square

Example 3.6. Consider the same heterogeneous multi-robot system described in Example 3.5 and apply the distributed controller (3.43) with the APF described in it.

Figure 3.10 illustrate the numerical simulation of this example. Again, the initial proximity graph is shown, where the leader's robot position is marked with an asterisk, dotted lines to another robot positions imply that those robots are informed. The state trajectories of the multi-robot system, and the leader, is also portrait. Additionally, the position and velocity vector entries are drawn, showing that every robot asymptotically approach to the leader's states, hence, reach a leader-followers consensus motion.

Leader with time-varying velocity

Once more, consider the Assumption 3.1. This design is based in the general form (3.24). Consider the following g_{ij} functions

$$g_{ij} := -\nabla_{p_i} \psi(\|p_{ij}\|) - a_{ij} v_{ij} + a_{ij} \dot{v}_j. \quad (3.47)$$

Notice that this functions is similar as in section 3.2.1 but it adds the acceleration of the j -th robot. For informed robots and functions g_{i0} , we take a similar version of (3.42) as

$$g_{i0} := -h_i (p_{i0} + v_{i0} - \dot{v}_0) \quad (3.48)$$

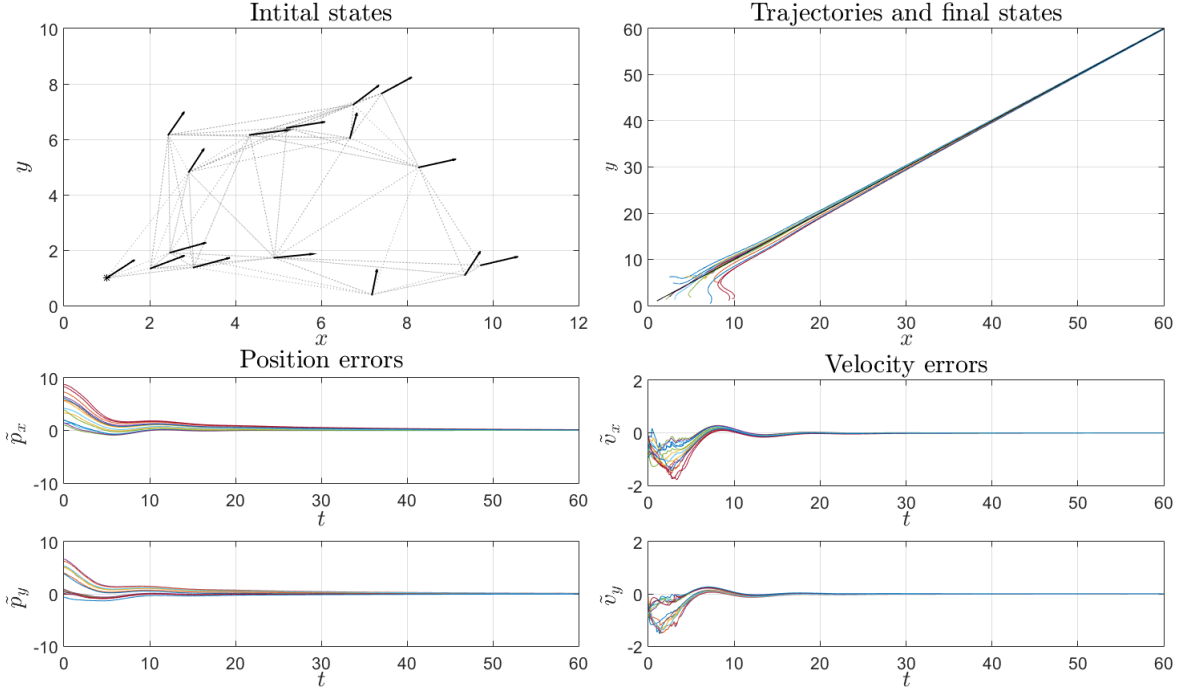


Figure 3.10: Leader-followers consensus of the closed-loop system (3.1)-(3.43).

that adds the leader's acceleration to the controller.

Using the functions defined above, we build the following controller

$$\begin{aligned}
 u_i = & -\frac{1}{\eta_i} \sum_{j \in \mathcal{N}_i(p)} \nabla_{p_i} \psi(\|p_{ij}\|) - \frac{1}{\eta_i} \sum_{j \in \mathcal{N}_i(p)} a_{ij} v_{ij} + \frac{1}{\eta_i} \sum_{j \in \mathcal{N}_i(p)} a_{ij} \dot{v}_j \\
 & - \frac{h_i}{\eta_i} (p_{i0} + v_{i0} - \dot{v}_0), \quad i \in \mathbf{I}, \quad (3.49)
 \end{aligned}$$

where we added the term $\eta_i = \frac{1}{m_i} \left(h_i + \sum_{j \in \mathcal{N}_i(p)} a_{ij} \right)$. notice that, if $\mathcal{G}(p)$ is connected, then η_i is always positive for all $i \in \mathbf{I}$.

Consider the error states defined in equation (3.44). Also, define $x = [\tilde{p}^T, \tilde{v}^T]^T \in \mathbb{R}^{2nN}$ and the following collective energy function

$$V(x(t)) = \frac{1}{2} \sum_{i=1}^N \left(\sum_{j \in \mathcal{N}_i(\tilde{p})} \psi(\|\tilde{p}_{ij}\|) + h_i \tilde{p}_i^T \tilde{p}_i + \tilde{v}^T \left(\hat{L}(\mathcal{G}(\tilde{p})) \otimes I_n \right) \tilde{v} \right) \quad (3.50)$$

which is bounded for initial conditions as

$$\begin{aligned}
 V(x(t_0)) \leq \bar{V}(x(t_0)) = & \frac{N(N-1)}{2} \psi(r - \epsilon) + \frac{1}{2} \sum_{i=1}^N (h_i \tilde{p}_i^T(t_0) \tilde{p}_i(t_0)) + \\
 & \tilde{v}^T(t_0) \left(\hat{L}(\mathcal{G}(\tilde{p})) \otimes I_n \right) \tilde{v}(t_0).
 \end{aligned}$$

Once more, we can relate the states of the multi-robot system with the maximum value of the APF through the set defined in (3.38).

Theorem 3.6. *Consider the heterogeneous multi-robot system (3.1) and a virtual leader with dynamics (3.15). Suppose the initial proximity graph $\mathcal{G}(p)$ is connected and $x(t_0) \in \Omega$, then the distributed controller (3.49), for all $t \in [t_0, \infty)$, is:*

- (i) *Connectivity preserving, and;*
- (ii) *A solution to the leader-followers consensus problem*

Proof. First, notice that the error dynamics is

$$\dot{\tilde{p}}_i = \tilde{v}_i, \quad m_i \dot{\tilde{v}}_i = u_i - m_i f(t, p_0, v_0), \quad i \in \mathbf{I} \quad (3.51)$$

and the distributed controller (3.49) can be rewritten in error states as

$$u_i = -\frac{1}{\eta_i} \sum_{j \in \mathcal{N}_i(\tilde{p})} \nabla_{\tilde{p}_i} \psi(\|\tilde{p}_{ij}\|) - \frac{1}{\eta_i} \sum_{j \in \mathcal{N}_i(\tilde{p})} a_{ij} \tilde{v}_{ij} + \frac{1}{\eta_i} \sum_{j \in \mathcal{N}_i(\tilde{p})} a_{ij} \dot{v}_j - \frac{h_i}{\eta_i} (\tilde{p}_i + \tilde{v}_i - \dot{v}_0), \quad i \in \mathbf{I}. \quad (3.52)$$

After some manipulations is possible to show that, the closed loop system (3.51)-(3.52), results on

$$\begin{aligned} \dot{\tilde{p}}_i &= \tilde{v}_i \\ \sum_{j \in \mathcal{N}_i(\tilde{p})} a_{ij} \dot{\tilde{v}}_{ij} + h_i \dot{\tilde{v}}_i &= \sum_{j \in \mathcal{N}_i(\tilde{p})} \nabla_{\tilde{p}_i} \psi(\|\tilde{p}_{ij}\|) - \sum_{j \in \mathcal{N}_i(\tilde{p})} a_{ij} \tilde{v}_{ij} - h_i (\tilde{p}_i + \tilde{v}_i). \end{aligned}$$

Rewriting the last equation in a matrix form

$$\begin{aligned} \dot{\tilde{p}} &= \tilde{v} \\ \left(\hat{L}(\mathcal{G}(\tilde{p})) \otimes I_n \right) \dot{\tilde{v}} &= \left(\hat{L}(\mathcal{G}(\tilde{p})) \otimes I_n \right) \tilde{p} - \left(\hat{L}(\mathcal{G}(\tilde{p})) \otimes I_n \right) \tilde{v}. \end{aligned}$$

with $\hat{L}(\mathcal{G}(\tilde{p})) = L(\mathcal{G}(\tilde{p})) + H$ with $H = \text{diag}(h_1, \dots, h_N)$.

Proof of part (i): Taking the time derivative of the energy function (3.50) we obtain

$$\dot{V}(x(t)) = \frac{1}{2} \sum_{i=1}^N \sum_{j \in \mathcal{N}_i(\tilde{p})} \dot{\psi}(\|\tilde{p}_{ij}\|) + \sum_{i=1}^N h_i \tilde{p}_i^T \dot{\tilde{p}}_i + \tilde{v}^T \left(\hat{L}(\mathcal{G}(\tilde{p})) \otimes I_n \right) \dot{\tilde{v}},$$

from where can be shown that

$$\dot{V}(x(t)) = -\tilde{v}^T \left(\hat{L}(\mathcal{G}(\tilde{p})) \otimes I_n \right) \tilde{v} \leq 0 \quad (3.53)$$

Following the same reasoning as in Theorems 3.4 and 3.5, in view of inequality (3.53) we can conclude that no edges are lost in $t \in [t_0, \infty)$. Therefore, the distributed controller (3.49) is connectivity preserving.

Proof of part (ii): Consider the set Γ defined in equation (3.40). From the proof of part (i) it can be seen that Γ is positively invariant. Once more, we aim to use

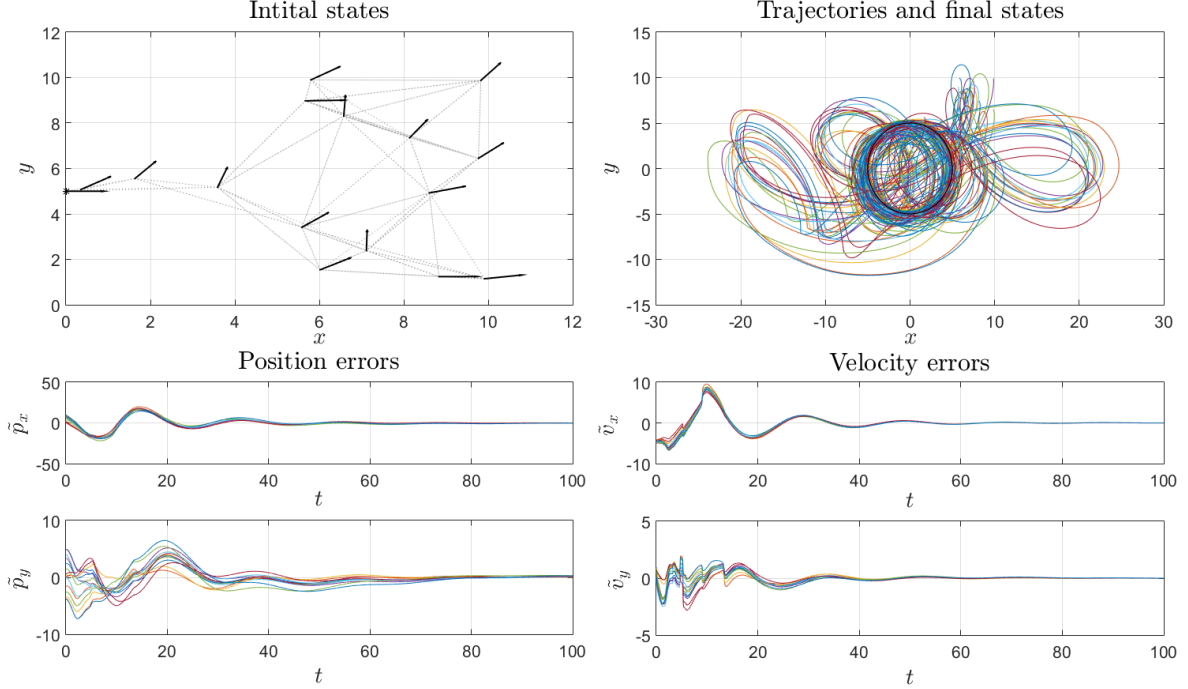


Figure 3.11: Leader-followers consensus of the closed-loop system (2.33)-(3.49).

here the LaSalle's invariance principle, hence, we must show Γ is compact. Notice that $\|\tilde{p}_{ij}\| \leq r(N-1)$, since $\mathcal{G}(\tilde{p})$ is connected. On the other hand, since I_0 is not empty, and H has at least one positive diagonal entry, the matrix $\hat{L}(\mathcal{G}(\tilde{p})) = L(\mathcal{G}(\tilde{p})) + H$ has all its eigenvalues with positive real part. From the expression $\tilde{v}^T (\hat{L}(\mathcal{G}(\tilde{p})) \otimes I_n) \tilde{v} \leq 2\bar{V}(x(0))$ we can conclude that $\|\tilde{v}\| \leq \sqrt{\frac{2\bar{V}(x(0))}{|\lambda_N|}}$, where λ_N is the eigenvalue with the largest magnitude. Hence, Γ is a compact set. Therefore, as the initial conditions lie in Γ , then the trajectories of $x(t)$ will converge to the largest invariant inside region S defined in (3.41). The rest of this proof is carried out following the same reasoning in Theorem 3.5. \square

Example 3.7. *Once more, consider the same heterogeneous multi-robot system described in Example 3.5 and apply the distributed controller (3.49). For this case, let the APF's maximum value $\hat{\psi} = 1000$ and $\epsilon = 1$. Also, let the position and velocity initial values be chosen, respectively, from boxes $[0, 10] \times [0, 10]$ and $[0, 1] \times [0, 1]$. Similarly to the Example 3.5, initial configurations and energy values are verified to meet the graph connectedness and energy conditions.*

Figure 3.11 shows a virtual leader with a velocity vector field defined by $f(t, p_0, v_0) = [-5 \sin(t), -\cos(t)]^T$. Hence, the described position trajectory of the leader is a circle. Clearly, even when the leader's velocity is time varying, the robots manage to approach state errors to zero, reaching to a consensus behavior.

Flocking Problems

We design solutions to the leaderless and leader-followers flocking motion problems, described in Chapter 2, for a multi-robot system with combinations of three different kinds of restrictions: 1) Limited communication/sensing radius, 2) input constraints and 3) environmental obstacles.

Consider a multi-robot system consisting of N mobile robots described by the following second-order dynamics

$$\dot{p}_i = v_i, \quad \dot{v}_i = u_i, \quad i \in \mathbf{I} := \{1, 2, \dots, N\}, \quad (4.1)$$

where $p_i, v_i, u_i \in \mathbb{R}^n$ (with $n = 1, 2$ or 3) are position, velocity and input vector of the i -th robot. Each robot has a limited communication/detection range r_i , therefore, we model the information network with a proximity digraph $\mathcal{D}(p)$.

The controller of each robot u_i uses only local information and group fragmentation is avoided. In the case of environmental obstacles, locally gathered from robots nearby obstacles is used to build the controller. Meanwhile, in case of having a virtual leader, the controller u_i of the informed robots also use its important information in the controller design. In general, we have

$$u_i = \sum_{j \in \mathcal{N}_i^{in}(p)} g_{ij}(p_{ij}, v_{ij}) + \sum_{k \in \mathcal{N}_i^{ob}(p)} h_{ik}(p_{ik}, v_{ik}) + g_{i0}(p_{i0}, v_{i0}), \quad i \in \mathbf{I}, \quad (4.2)$$

where $g_{ij} : \mathbb{R}^n \times \mathbb{R}^n \mapsto \mathbb{R}^n$, $h_{ik} : \mathbb{R}^n \times \mathbb{R}^n \mapsto \mathbb{R}^n$, with $\mathcal{N}_i^{ob}(p)$ the set of robots nearby obstacles, and $g_{i0} : \mathbb{R}^n \times \mathbb{R}^n \mapsto \mathbb{R}^n$, with $g_{k0}(p_{k0}, v_{k0}) = \mathbf{0}_n$ for $k \notin \mathbf{I}_0$, continuous functions to be designed.

4.1 Bidirectional proximity graphs

Consider the multi-robot system (4.1) with a limited communication/sensing radius r and a heterogeneous input constraint given by

$$\|u_i\| \leq \hat{u}_i, \quad i \in \mathbf{I}. \quad (4.3)$$

Notice that the constraints on each controller may be different, and the underlying proximity graph $\mathcal{G}(p)$ is bidirectional. For this setup, we first consider that the workspace of the multi-robot system does not contain obstacles. We design distributed controllers for leaderless and leader-followers schemes. We then modify our designs to include obstacle avoidance manoeuvres.

4.1.1 Leaderless configuration

First of all, we have $I_0 = \emptyset$ and $g_{i0}(p_{i0}, v_{i0}) \equiv \mathbf{0}_n$ for all $i \in I$. Then, we must only design the g_{ij} functions with the information from within $\mathcal{N}_i(p)$ with the neighborhood hysteresis process described in Definition 3.2.

From the leaderless flocking motion described in Definition 2.5, we have that the multi-robot system's configuration $p = [p_1^T, \dots, p_N^T]^T \in \mathbb{R}^{nN}$ must be cohesive, avoid inter-robot collisions, keep inter-robot velocity differences bounded and also connectivity preserving. To achieve the required configuration, we propose the following distributed controller:

$$u_i = - \sum_{j \in \mathcal{N}_i(p)} \nabla_{p_i} \psi_{ij}(\|p_{ij}\|) - \sum_{j \in \mathcal{N}_i(p)} \vartheta_{ij}(\|p_{ij}\|, v_{ij}), \quad i \in I. \quad (4.4)$$

Notice we split functions g_{ij} , in equation (4.2), into two terms. We explain them in what follows.

For the first term in (4.4), consider a distance-dependent APF $\psi_{ij}(\|p_{ij}\|) : [0, r] \mapsto \mathbb{R}_{\geq 0}$ with partial derivative given by $\varphi_{ij}(\|p_{ij}\|) = \frac{\partial \psi_{ij}(\|p_{ij}\|)}{\partial \|p_{ij}\|}$. This APF has the following properties:

- (i) For $s \in [0, r]$, $0 \leq \psi_{ij}(s) \leq \hat{\psi}_{ij}$ with $\hat{\psi}_{ij} = \max_{s \in [0, r]} \{\psi_{ij}(s)\}$ and $\psi_{ij}(d_{ij}) = 0$ for some $d_{ij} \in (0, r]$;
- (ii) For $s \in [0, d_{ij}]$ $\varphi_{ij}(0) \leq \varphi_{ij}(s) < 0$, and $0 < \varphi_{ij}(s) \leq \varphi_{ij}(r)$ for $s \in (d_{ij}, r]$, where $d_{ij} \in (0, r]$ is the unique value such that $\varphi_{ij}(d_{ij}) = 0$. Also, $|\varphi_{ij}(s)| \leq \hat{\varphi}_{ij} = \max_{s \in [0, r]} \{|\varphi_{ij}(s)|\}$.

By condition (i) $\psi_{ij}(\|p_{ij}\|)$ is a positive function of $\|p_{ij}\|$. Due to condition (ii) the APF decreases for $\|p_{ij}\| \in [0, d_{ij})$, increases for $\|p_{ij}\| \in (d_{ij}, r]$, and has only one minimum value at d_{ij} for the whole interval $[0, r]$. Here, d_{ij} is a desired distance between connected robots. Taking the gradient of the APF, *i.e.* $\nabla_{p_i} \psi_{ij}(\|p_{ij}\|) = \varphi_{ij}(\|p_{ij}\|) \frac{p_{ij}}{\|p_{ij}\|}$, a vector force pointing towards the minimum value of $\psi_{ij}(\|p_{ij}\|)$ is obtained. That is, when the inter-robot distance $\|p_{ij}\|$ approaches to zero, it will force them apart, meanwhile, if $\|p_{ij}\|$ approaches to r , then will force them together. For simplicity of presentation, in the APF's definition, we consider robots to be punctual. Therefore, an inter-robot collision occurs when $\|p_{ij}\| = 0$. To account for each robot's volume, we can define a minimum safe distance $\check{d} \in \mathbb{R}_{>0}$ such that the i th robot fits in a ball of radius \check{d} and centred in p_i , for all $i \in I$; Hence collisions occur when $\|p_{ij}\| = \check{d}$. Then, in the APF's definition, instead of $s \in [0, r]$, we set $s \in [\check{d}, r]$, and the analysis done in the following sections is still valid.

For the second term consider a distance-dependent odd function $\vartheta_{ij}(\|p_{ij}\|, v_{ij}) : \mathbb{R}_{\geq 0} \times \mathbb{R}^n \mapsto \mathbf{C}$ defined by elements and bounded, with $\mathbf{C} := \left\{ y \in \mathbb{R}^n : \|y\| \leq \hat{\vartheta}_{ij} \right\}$, where $\hat{\vartheta}_{ij}$ is the biggest norm of any vector in its image.

The closed-loop system (4.1)-(4.4) generates a configuration p that changes over time; decreasing or increasing the relative distance between neighboring robots. In consequence, the proximity graph $\mathcal{G}(p)$ is also time-variant, where edges may appear or disappear as the system evolves. Moreover, since the controller (4.4) relies on the information collected within $\mathcal{N}_i(p)$, the appearance or disappearance of a neighbor changes it. To deal with the effects that a dynamic graph has in (4.4), we use again the neighborhood hysteresis process from Definition 3.2.

To deal with the heterogeneous input constraints condition notice that the i th controller is bounded as follows

$$\|u_i\| \leq \sum_{j \in \mathcal{N}_i(p)} \left(\hat{\varphi}_{ij} + \hat{\vartheta}_{ij} \right), \quad i \in \mathbf{I}, \quad (4.5)$$

where $\hat{\varphi}_{ij}$ and $\hat{\vartheta}_{ij}$ are the bounds of the previously described terms. Such values correspond to a configuration where, for all $j \in \mathcal{N}_i(p)$, the distance $\|p_{ij}\| = r$ and the velocity deviations among neighboring robots is such that $\|\vartheta_{ij}(r, v_{ij})\| = \hat{\vartheta}_{ij}$. From (4.5), conditions such that each robot satisfy its particular input constraint (4.3) can be determine.

Remark 4.1. *The leaderless flocking motion problem was previously addressed in [78, 117]. A discrete distributed controller under homogeneous input constraints condition that requires predictions of the i -th robot neighbor states was provided. However, the proximity graph is assumed to remains connected within the time period where control actions are calculated. In contrast, the controller (4.4), along with the neighborhood hysteresis process, do not need state predictions and does not require any assumption about the proximity graph between the calculation of control actions.*

To analyze the motion dynamics of the closed-loop system (4.1)-(4.4), a mobile coordinate system is necessary. The position and velocity of the weighted center of mass (WCOM) for the swarm are denoted as

$$\bar{p} := \frac{\sum_{i=1}^N \omega_i p_i}{\sum_{k=1}^N \omega_k} \quad \text{and} \quad \bar{v} := \frac{\sum_{i=1}^N \omega_i v_i}{\sum_{k=1}^N \omega_k} \quad (4.6)$$

where $\omega_i \in \mathbb{R}_{>0}$ is the constant influence that the i -th robot exerts over the WCOM of the multi-robot system. Notice that if $\omega_i = 1$ for all $i \in \mathbf{I}$, the WCOM position and velocity are the average position and velocity of the members of the multi-robot system. On the other hand, if the robot is an inertial agent, then $\omega_i = m_i$ and equation (4.6) is the WCOM of the multi-robot system, as in equation (3.33).

the position and velocity errors of the i -th robot with respect to the WCOM are

$$\tilde{p}_i := p_i - \bar{p}, \quad \text{and} \quad \tilde{v}_i := v_i - \bar{v}, \quad i \in \mathbf{I}. \quad (4.7)$$

Notice that $\tilde{p}_{ij} = p_{ij}$, $\tilde{v}_{ij} = v_{ij}$ and that the inter-robot distances norms are the same as in the global frame, *i.e.* $\|\tilde{p}_{ij}\| = \|p_{ij}\|$. In consequence, the proximity graph can be defined through the vector $\tilde{p} = [\tilde{p}_1^T, \dots, \tilde{p}_N^T]^T \in \mathbb{R}^{nN}$, as $\mathcal{G}(\tilde{p}) = \mathcal{G}(p)$. Similarly, the controller (4.4) can be rewritten in error variables as

$$u_i = - \sum_{j \in \mathcal{N}_i(\tilde{p})} \nabla_{\tilde{p}_i} \psi_{ij} (\|\tilde{p}_{ij}\|) - \sum_{j \in \mathcal{N}_i(\tilde{p})} \vartheta_{ij} (\|\tilde{p}_{ij}\|, \tilde{v}_{ij}), \quad i \in \mathbb{I}. \quad (4.8)$$

Another key issue on the analysis of the motion dynamics of the closed-loop system (4.1)-(4.4) is a way to quantify the deviation of the actual multi-robot system position and velocity from the desired configurations. Define the following *collective energy* of the multi-robot system as

$$V(\tilde{p}, \tilde{v}) := \frac{1}{2} \sum_{i=1}^N \omega_i \left(\sum_{j \in \mathcal{N}_i(\tilde{p})} \psi_{ij} (\|\tilde{p}_{ij}\|) + \|\tilde{v}_i\|^2 \right). \quad (4.9)$$

This function adds the potential and the kinetic energies of each robot in the mobile coordinated system. Here, the potential energy is introduced by the controller (4.4) through the APFs of every pair of connected robots.

Since $\mathcal{G}(p)$ is a state-dependent graph, then it might change over time. Then, suppose $\mathcal{G}(p)$ switches on time instants t_k with $k = 1, 2, \dots$, and remains fixed over the time interval $[t_{k-1}, t_k)$. At the time instant t_k , edges might be added to, or deleted from, $\mathcal{E}(p)$. The following lemma, studies the collective energy (4.9) for the time interval in which $\mathcal{G}(p)$ remains fixed.

Lemma 4.1. *Consider the closed-loop system (4.1)-(4.4) and a time interval $[t_{k-1}, t_k)$ in which the proximity graph remains fixed, *i.e.* $\mathcal{G}(p) = \mathcal{G}$ for all $t \in [t_{k-1}, t_k)$. Denote as $V(\tilde{p}, \tilde{v})_{t_{k-1}}$ the collective energy at time instant t_{k-1} . Let the terms in (4.4) be such that*

$$\nabla_{p_i} \psi_{ij} (\|p_{ij}\|) = \kappa_{ij} (\|p_{ij}\|) \nabla_{p_i} \psi (\|p_{ij}\|) \quad \text{and} \quad \vartheta_{ij} (\|p_{ij}\|, v_{ij}) = \kappa_{ij} (\|p_{ij}\|) \vartheta (v_{ij}), \quad (4.10)$$

where $\kappa_{ij} (\|p_{ij}\|) \in \mathbb{R}_{>0}$ for all $\|p_{ij}\| \in [0, r]$, and meet the following condition

$$\omega_i \kappa_{ij} (s) = \omega_j \kappa_{ji} (s), \quad s \in [0, r], \quad (4.11)$$

for all $i, j \in \mathcal{V}$, with $j \neq i$. Then, the collective energy (4.9) doesn't increase in the time interval $[t_{k-1}, t_k)$, *i.e.* $V(\tilde{p}, \tilde{v})_t \leq V(\tilde{p}, \tilde{v})_{t_{k-1}}$ for all $t \in [t_{k-1}, t_k)$.

Proof. First, notice that the error dynamics is given by

$$\dot{\tilde{p}}_i = \tilde{v}_i, \quad \dot{\tilde{v}}_i = u_i, \quad i \in \mathbb{I},$$

where, for the distributed controller rewritten in error terms (4.8) along with properties (4.10) and (4.11), the acceleration of the WCOM is $\dot{\tilde{v}} = \mathbf{0}_n$. Now, taking time derivative

of (4.9) we obtain

$$\begin{aligned}\dot{V}(\tilde{p}, \tilde{v})_t &= -\frac{1}{2} \sum_{i=1}^N \omega_i \left(\sum_{j \in \mathcal{N}_i(\tilde{p})} \dot{\psi}_{ij}(\|\tilde{p}_{ij}\|) + 2\tilde{v}_i^T \dot{\tilde{v}}_i \right) \\ &= -\frac{1}{2} \sum_{i=1}^N \omega_i \left(\sum_{j \in \mathcal{N}_i(\tilde{p})} \tilde{v}_{ij}^T \nabla_{\tilde{p}_i} \psi_{ij}(\|\tilde{p}_{ij}\|) + 2\tilde{v}_i^T u_i \right).\end{aligned}$$

Introducing the distributed controller (4.8) along with properties (4.10) and (4.11), it can be shown that

$$\dot{V}(\tilde{p}, \tilde{v})_t = -\frac{1}{2} \sum_{i=1}^N \omega_i \sum_{j \in \mathcal{N}_i(\tilde{p})} \tilde{v}_{ij}^T \vartheta_{ij}(\|\tilde{p}_{ij}\|, \tilde{v}_{ij}) \leq 0. \quad (4.12)$$

Hence, for all $t \in [t_{k-1}, t_k)$, the collective energy is such that $V(\tilde{p}, \tilde{v})_t \leq V(\tilde{p}, \tilde{v})_{t_{k-1}}$. \square

Remark 4.2. Condition (4.10) states that the terms in (4.4) can be decomposed as a distance-dependent gain $\kappa_{ij}(\|p_{ij}\|)$ multiplying common functions $\psi(\|p_{ij}\|)$ and $\vartheta(v_{ij})$ of artificial potential gradient and velocity consensus, respectively. This is the difference in the controller (4.4) when its applied to the i -th and j -th robot, since $\kappa_{ij}(\|p_{ij}\|)$ and $\kappa_{ji}(\|p_{ji}\|)$ might be different. On the other hand, if the gains $\kappa_{ij}(\|p_{ij}\|)$ are considered as distance-dependent edge weights, then, the property (4.11) is called a detail balance condition, where ω_i are the detail balance parameters [118].

The Lemma 4.1 shows that the collective energy doesn't increase over the time intervals where the proximity graph is fixed. Notice that, if (4.9) remains constant, then the multi-robot system attains fixed inter-robot distances and the error between each robot and the WCOM velocity is constant. On the other hand, if (4.9) decreases, then the inter-robot distances approaches to the desired values d_{ij} described in the APF definition and/or the velocity of every robot approaches to the speed of the WCOM.

As we discussed before, when the proximity graph is initially connected, one way to preserve that property is to prevent the loss of edges, but allowing the creation of new ones. Notice that, given an initial proximity graph $\mathcal{G}(p)_{t_0}$, there exists a finite number of possibly new edges that can be created; this is, there are only $\frac{N(N-1)}{2} - |\mathcal{E}(p)_{t_0}|$ possible new edges.

Define the following value:

$$\bar{V} := V(\tilde{p}, \tilde{v})_{t_0} + \frac{1}{2} \sum_{i=1}^N \omega_i \sum_{j \in \mathcal{N}_i(p)_{t_0}^*} \psi_{ij}(r - \epsilon), \quad (4.13)$$

where $\mathcal{N}_i(p)_{t_0}^* := \{j : (i, j) \in \mathcal{E}_{\mathcal{K}} \setminus \mathcal{E}(p)_{t_0}\}$. The artificial potential $\psi_{ij}(r - \epsilon)$ is provided by an edge (i, j) that doesn't belong to $\mathcal{E}(p)_{t_0}$ but is added to $\mathcal{E}(p)$ at some time instant $t > 0$. Equation (4.13) resume the collective energy of the swarm due to its initial states, plus the potential energy contributed by all the remaining edges such that the proximity graph is complete. Notice that, Lemma 4.1 states that the collective energy doesn't increase as the system evolves, hence (4.13) is the maximum possible energy the closed loop system (4.1)-(4.4) can have.

Theorem 4.1. *Consider the closed-loop system (4.1)-(4.4) along with the neighborhood hysteresis process¹. Suppose the terms in (4.4) meet conditions (4.10) and (4.11). If the proximity graph $\mathcal{G}(p)_{t_0}$ is connected; the initial collective energy is such that*

$$\bar{V} < \hat{V} := \min_{i,j \in \mathcal{V}} \left\{ \frac{\omega_i \hat{\psi}_{ij} + \omega_j \hat{\psi}_{ji}}{2} \right\}; \quad (4.14)$$

and

$$\sum_{j \in \mathcal{N}_i(\tilde{p})} \kappa_{ij} (\|p_{ij}\|) \leq \frac{\hat{u}_i}{\hat{\varphi} + \hat{\vartheta}} \quad (4.15)$$

where $\hat{\varphi} := \max_{s \in [0,r]} \{|\varphi(s)|\}$ and $\hat{\vartheta}$ is the value such that $\|\vartheta(x)\| \leq \hat{\vartheta}$ for all $x \in \mathbb{R}^n$. Then, the following statements simultaneously hold for all $t \geq t_0$:

- (i) *The proximity graph remains connected;*
- (ii) *The multi-robot system is on leaderless flocking motion and asymptotically reaches a rigid configuration and;*
- (iii) *Every robot's control effort satisfy its own input restriction.*

Proof. Proof of (i): Suppose $\mathcal{G}(p)$ switches every time instant t_k with $k = 1, 2, \dots$, and remains fixed over the time interval $[t_{k-1}, t_k)$. The following analysis is done for $k = 1$ and then will be extended for any switching time instant t_k .

Given that the proximity graph doesn't change for all $t \in [t_0, t_1)$, from Lemma 4.1, the collective energy doesn't increase, *i.e.* $V(\tilde{p}, \tilde{v}) \leq V(\tilde{p}, \tilde{v})_{t_0} < \hat{V}$. Notice that \hat{V} is the minimum of every potential energy that a couple of robots $i, j \in \mathcal{V}$ contribute to (4.9) when their distance is $\|p_{ij}\| = r$. Therefore, since $V(\tilde{p}, \tilde{v}) < \hat{V}$ there are no distances between neighboring robots bigger than the sensing range r for all $t \in [t_0, t_1)$; Hence, no edges were lost over the time interval $[t_0, t_1)$. Then, new edges must have been added at the time instant t_1 . Without loss of generality, assume $0 < e_1 \leq \frac{(N-1)(N-2)}{2}$ edges were added to $\mathcal{E}(p)$ at t_1 . Thus, the energy at instant t_1 is

$$V(\tilde{p}, \tilde{v})_{t_1} \leq V(\tilde{p}, \tilde{v})_{t_0} + \frac{1}{2} \sum_{i=1}^N \omega_i \sum_{j \in \mathcal{N}_i^\dagger(p)_{(t_0, t_1)}} \psi_{ij}(r - \epsilon), \quad (4.16)$$

where $\mathcal{N}_i^\dagger(p)_{(t_0, t_1)} := \{j : (i, j) \in \mathcal{E}(p)_{t_1} \setminus \mathcal{E}(p)_{t_0}\}$. From equations (4.13) and (4.14), notice that the collective energy at t_1 is such that $V(\tilde{p}, \tilde{v})_{t_1} \leq \bar{V} < \hat{V}$. Again, since $\mathcal{G}(p)$ doesn't change over the time interval $[t_1, t_2)$, by Lemma 4.1, the energy is non-increasing for all $t \in [t_1, t_2)$. This is, there are no distance among neighboring robots bigger than the sensing range r for all $t \in [t_1, t_2)$. Thus, edges were added to $\mathcal{E}(p)$ at t_2 . Following the same reasoning for every time instant t_k , we can conclude that there are no edges lost from $\mathcal{E}(p)$ at any switching instant. Thus, since the proximity graph is connected and no edges were lost, then $\mathcal{G}(p)$ remains connected for all $t \geq 0$.

¹The neighborhood hysteresis process is described in Definition 3.2

Proof of (ii): For the closed-loop system (4.1)-(4.4) to be in leaderless flocking motion, it must satisfy the properties described in Definition 2.5. We show them separately.

(The group is cohesive) We already show that $\mathcal{G}(p)$ remains connected for all $t \geq 0$. Therefore, the maximum distance among any pair of robots is bounded such that $\|p_{ij}\| \leq \rho = (N-1)r$ for all $i, j \in \mathcal{V}$ and $t \geq 0$. Hence, the group is cohesive.

(Inter-robot collisions are avoided) Notice that, if for any pair of connected robots $\|p_{ij}\| \rightarrow 0$, then $V(\tilde{p}, \tilde{v}) \rightarrow \hat{V}$, since $\psi_{ij}(\|p_{ij}\|) \rightarrow \hat{\psi}_{ij}$ as $\|p_{ij}\| \rightarrow 0$. However, in proof of (ii), we already show that $V(\tilde{p}, \tilde{v}) \leq V(\tilde{p}, \tilde{v})_{t_0} < \hat{V}$ for all $t \geq 0$, therefore, there are no inter-robot distances approaching to zero. Hence, inter-robot collisions are avoided.

(Inter-robot velocity mismatches are bounded) Since $V(\tilde{p}, \tilde{v}) \leq \bar{V}$ for all $t \geq 0$, from equation (4.9) we obtain $\|\tilde{v}_i\| \leq \sqrt{\frac{2\bar{V}}{\omega_i}}$ for all $i \in \mathbf{I}$. Now, notice that $\|v_{ij}\| = \|\tilde{v}_{ij}\| \leq \sqrt{2\bar{V}} \left(\frac{\sqrt{\omega_i} + \sqrt{\omega_j}}{\sqrt{\omega_i \omega_j}} \right)$. Hence, taking $v = \max_{i,j \in \mathcal{V}} \left\{ \sqrt{2\bar{V}} \left(\frac{\sqrt{\omega_i} + \sqrt{\omega_j}}{\sqrt{\omega_i \omega_j}} \right) \right\}$, we conclude that the inter-robot velocity mismatches are bounded

To show the closed-loop system (4.1)-(4.4) asymptotically reach a rigid configuration we use the Lasalle's invariance principle. Therefore, consider the following set

$$\Omega := \{ \tilde{p}, \tilde{v} \in \mathbb{R}^{nN} : V(\tilde{p}, \tilde{v}) \leq \bar{V} \}. \quad (4.17)$$

From the proof of (i), we can conclude that Ω is positively invariant. It remains only to show Ω compactness. We already demonstrate that $\|\tilde{v}_i\| \leq \sqrt{\frac{2\bar{V}}{\omega_i}}$ for all $i \in \mathbf{I}$, after some algebraic manipulations we obtain $\|\tilde{v}\| \leq \sqrt{2\bar{V}} \sum_{i=1}^N \frac{1}{\omega_i}$. On the other hand, from equations (4.6) and (4.7), and the fact that $\mathcal{G}(p)$ is connected for all $t \geq 0$, the position error vector is such that $\|\tilde{p}\| \leq \frac{r(N-1)}{\sum_{i=1}^N \omega_i} \sqrt{\sum_{i=1}^N \left(\sum_{k \neq i}^N \omega_k \right)^2}$. Therefore, Ω is closed and bounded, hence compact. Before we continue, notice that the number of edges added to $\mathcal{E}(p)$ is finite, since $\frac{(N-1)(N-2)}{2}$ is the maximum number of possible new edges appended to it. Therefore, we restrict our analysis to the time interval $[t_k, \infty)$.

From LaSalle's invariance principle, all trajectories of the closed-loop system (4.1)-(4.4) will approach to the largest invariant set inside $S := \{ \tilde{p}, \tilde{v} \in \mathbb{R}^{nN} : \dot{V}(\tilde{p}, \tilde{v}) = 0 \}$.

From the time derivative of the collective energy (4.12) notice that $\dot{V}(\tilde{p}, \tilde{v}) = 0$ if and only if $\tilde{v}_1 = \dots = \tilde{v}_N$, implying that every robot align its velocity with the WCOM and, hence, with each others. This is, the multi-robot velocity mismatches are not only bounded, but every robot asymptotically moves with the same velocity vector. Moreover, in steady state $\dot{\tilde{v}}_i = \mathbf{0}_n$ for all $i \in \mathbf{I}$, therefore

$$u_i = - \sum_{j \in \mathcal{N}_i(p)} \nabla_{\tilde{p}_i} \psi_{ij}(\|p_{ij}\|) = \mathbf{0}_n, \quad i \in \mathbf{I}.$$

Hence, the multi-robot system attains fixed inter-robot distances. That is, the multi-robot system asymptotically reach a rigid leaderless flocking motion.

Proof of (iii). By the property (4.10) the controller (4.4) can be written as

$$u_i = - \sum_{j \in \mathcal{N}_i(p)} \kappa_{ij}(\|p_{ij}\|) (\nabla_{\tilde{p}_i} \psi(\|p_{ij}\|) + \vartheta(v_{ij})), \quad i \in \mathbf{I}.$$

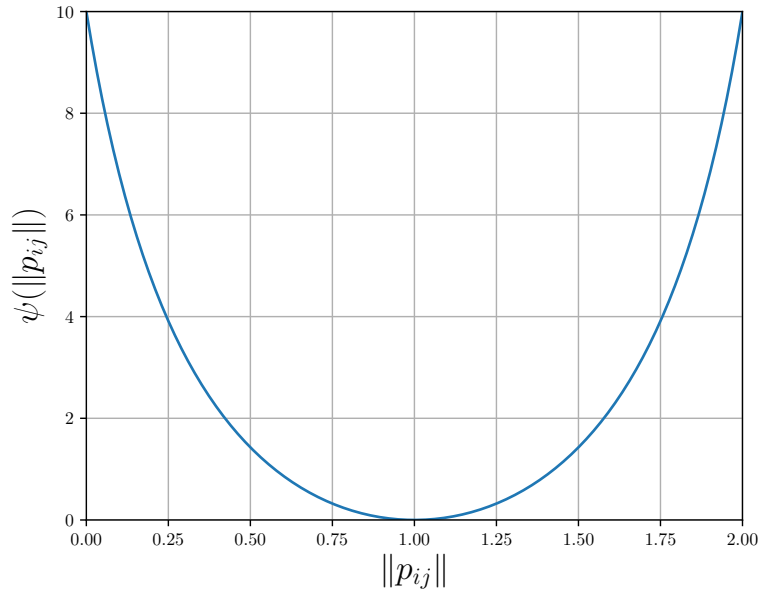


Figure 4.1: Artificial potential function (4.18).

Without loss of generality, assume the i -th robot distance and velocity difference with respect to its neighbors $j \in \mathcal{N}(p)$ are such that $\|p_{ij}\| = r$, and $\|\vartheta(v_{ij})\| = \hat{v}$. Then, the norm of (4.4) is

$$\|u_i\| \leq (\hat{\varphi} + \hat{v}) \sum_{j \in \mathcal{N}_i(p)} \kappa_{ij}(\|p_{ij}\|), \quad i \in \mathbf{I}.$$

From there, condition (4.15) is obtained. \square

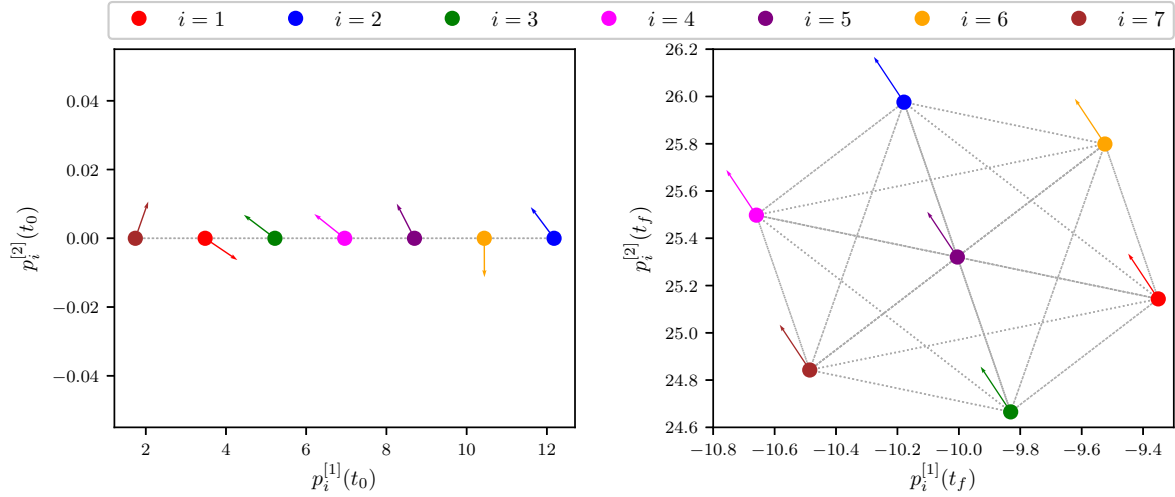
Remark 4.3. Notice that condition (4.15) it can be different for each robot, since it depends on its neighborhood, the values of the gains $\kappa_{ij}(\|p_{ij}\|)$, and its own input bound. Therefore, to fulfill local objectives, the i -th robot's controller u_i might produce different control efforts than those of its neighbors. This is a key feature of our design, where robots with higher capabilities compensate for the requirements of less capable neighbors.

Example 4.1. Consider a multi-robot system with $N = 7$ robots moving on a plane, i.e. $n = 2$, where every robot has a homogeneous communication/detection range $r = 2$ and individual input constraints such that $\hat{u}_1 \leq \dots \leq \hat{u}_7$. The initial robot positions are shown in Figure 4.2a (left), where $\mathcal{G}(p)_{t_0}$ is connected. Meanwhile, the velocity vector v_i for all $i \in \mathbf{I}$ at t_0 is randomly selected within a box $[-1.5, 1.5] \times [-1.5, 1.5]$.

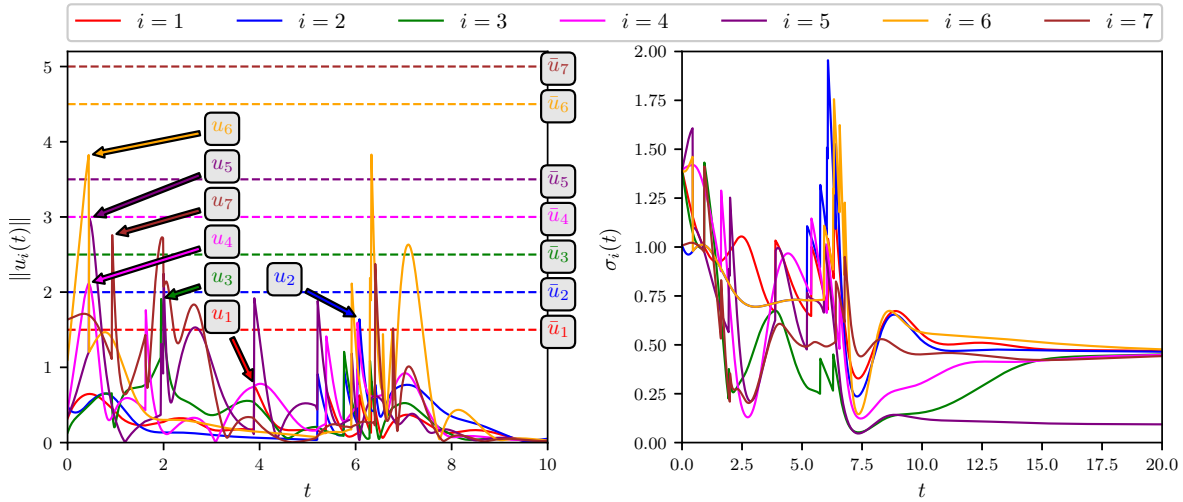
In controller (4.4), the implemented APF is

$$\psi_{ij}(\|p_{ij}\|) = \frac{\hat{\psi}_{ij} (d_{ij} - \|p_{ij}\|)^2}{r (r - \|p_{ij}\|) \|p_{ij}\| + (d_{ij} - \|p_{ij}\|)^2} \quad (4.18)$$

where the desired inter-robot distance is $d_{ij} = \frac{r}{2}$ for all $i, j \in \mathcal{V}$. This APF is shown in Figure 4.1. Meanwhile, the velocity consensus function is an hyperbolic tangent



(a) Initial (left) and final (right) configuration.



(b) Input norms (left) and collision avoidance indicators (right) of the robotic swarm.

Figure 4.2: Leaderless flocking motion with proximity graph.

$\vartheta_{ij}(s, x) = \kappa_{ij}(s) \tanh(x)$, with $\|\vartheta_{ij}(s, x)\| \leq \kappa_{ij}(s) \sqrt{n}$. Additionally, $\epsilon = 0.1$ for the neighborhood hysteresis process. The property (4.10) is fulfilled with $\kappa_{ij}(\|p_{ij}\|) = \hat{\psi}_{ij}$, where $\frac{\hat{u}_i}{r^2 d_{ij}^{(N-1)}(\hat{\varphi} + \hat{\vartheta})}$ is the APF's maximum value, and the WCOM scaling factors are $\omega_i = \frac{N-1}{\hat{u}_i}$ for all $i \in \mathbf{I}$.

To visualize the fulfillment of the collision avoidance objective consider the following indicator

$$\sigma_i := \ln \left(1 + \prod_{j \in \mathcal{N}_i(p)} \|p_{ij}\| \right), \quad i \in \mathbf{I}. \quad (4.19)$$

Notice that $\sigma_i = 0$ if and only if a collision occurs among the i -th robot and any of its neighbors. Therefore, if $\sigma_i > 0$, for all $i \in \mathbf{I}$ and $t \in [0, \infty)$, collisions were avoided at every time instant.

In Figure 4.2a, robots are represented by colored filled circles and arrows. The colored circles are centered at p_i , for all $i \in I$. An arrow, is a scaled normalized velocity vector illustrating the direction of motion of each robot. Dotted gray lines represent the existence of a communication/detection link among pair of robots. Meanwhile, in Figure 4.2b(left) dotted lines stand for the predefined robot input constraints, while solid lines are the input norm trajectories. Meanwhile in Figure 4.2b(right) solid lines represent the trajectories of the collision avoidance indicator (4.19).

Initial and final configurations of the closed-loop system (4.1)-(4.4) are displayed in Figure 4.2a. Notice that, for all $t \in [0, 50]$, every initial edge is preserved and only new edge additions are allowed, hence the connectivity of the proximity graph is preserved. Also, the velocity of every robot in the swarm gets aligned. The control effort of each robot in the swarm is shown in Figure 4.2b. Notice that the control effort applied by each robot satisfy its own individual input constraint. Also, to fulfill local objectives and taking advantage of the heterogeneity of the swarm, robots with higher capacities produce a control effort magnitude greater than the input constraint of their less capable neighbors.

In the following section, we modify our design to consider the existence of a virtual leader.

4.1.2 Leader-followers configuration

Contemplate the existence of a virtual leader with its dynamics described by equation (2.35) moving at a constant speed, *i.e.* $f(t, p_0, v_0) = 0$. Also, consider a nonempty subset of informed robots within the multi-robot system, that is $I_0 \subset I$.

To conduct the design of (4.2), as before, we must guarantee the group remains cohesive without avoid collisions and their velocity differences are bounded, although in this case with respect to the leader's states. Therefore, in (4.2), we keep the designs of functions g_{ij} the same as in (4.4) and only the complementary actions regarded to functions g_{i0} are designed. Here, the complementary actions between the members of the group are key to spread the desired leader-following motion to those robots without direct connection with the leader.

From Definition 2.6, notice that the multi-robot system, to be in leader-followers flocking motion, must keep every robot's position and velocity deferences with the leader bounded. To achieve these objectives, we include driving forces that aims to reach a zero position and velocity error in the informed robots. Hence, the functions g_{i0} are divided into two terms: a position and a velocity consensus function.

For the position consensus function, let $\xi_{i0}(\cdot) : \mathbb{R}^n \mapsto C_\xi$ be defined by elements with $C_\xi := \{y \in \mathbb{R}^n : \|y\| \leq \hat{\xi}_{i0}\}$, where $\hat{\xi}_{i0} > 0$ is the maximum magnitude of any force vector produced by this function, and such that

$$\xi_{i0}(\mathbf{0}_n) = \mathbf{0}_n; \quad \text{and} \quad x^T \xi_{i0}(x) > 0, \quad \forall x \neq \mathbf{0}_n \text{ and } x \in \mathbb{R}^n \quad (4.20)$$

The function $\xi_{i0}(\cdot)$ produces a force that steers an informed robot towards position consensus. On the other hand, for velocity consensus, consider the function $\nu_{i0}(\cdot) : \mathbb{R}^n \mapsto C_\nu$ defined by elements with $C_\nu := \{y \in \mathbb{R}^n : \|y\| \leq \hat{\nu}_{i0}\}$, where $\hat{\nu}_{i0}$

is the maximum magnitude of any vector force produced by this function, and such that

$$\nu_{i0}(\mathbf{0}_n) = \mathbf{0}_n; \quad \text{and} \quad x^T \nu_{i0}(x) > 0, \quad \forall x \neq \mathbf{0}_n \text{ and } x \in \mathbb{R}^n. \quad (4.21)$$

This function drives the informed robot into a velocity consensus trajectory with respect to the leader.

Taking g_{ij} as in (4.4) and adding the previously defined terms for g_{i0} , the distributed controller (4.2) takes the following form

$$u_i = - \sum_{j \in \mathcal{N}_i(p)} \nabla_{p_i} \psi_{ij}(\|p_{ij}\|) - \sum_{j \in \mathcal{N}_i(p)} \vartheta_{ij}(\|p_{ij}\|, v_{ij}) - h_i(\xi_{i0}(p_{i0}) + \nu_{i0}(v_{i0})), \quad i \in \mathbf{I}. \quad (4.22)$$

where $h_i \in \mathbb{R}_{\geq 0}$ with $h_i > 0$ if $i \in \mathbf{I}_0$ and $h_i = 0$ otherwise. Notice that (4.22) is the sum of bounded terms and produce a finite control effort given by

$$\|u_i\| \leq \sum_{j \in \mathcal{N}_i(p)} \left(\hat{\varphi}_{ij} + \hat{\vartheta}_{ij} \right) + h_i \left(\hat{\xi}_{i0} + \hat{\nu}_{i0} \right), \quad i \in \mathbf{I}. \quad (4.23)$$

Consider now the coordinate system as the trajectories of the virtual leader (2.35). Define the errors in position and velocity of the i -th robot with respect to the virtual leader's states as

$$\tilde{p}_i := p_i - p_0 \quad \text{and} \quad \tilde{v}_i := v_i - v_0, \quad i \in \mathbf{I}. \quad (4.24)$$

Define the *collective energy* of the multi-robot system as follows

$$V(\tilde{p}, \tilde{v}) := \frac{1}{2} \sum_{i=1}^N \omega_i \left(\sum_{j \in \mathcal{N}_i(\tilde{p})} \psi_{ij}(\|\tilde{p}_{ij}\|) + \|\tilde{v}_i\|^2 + h_i \int_{\tilde{p}_i} \xi_{i0}(y) \cdot dy \right). \quad (4.25)$$

In addition of the potential energies introduced by the APFs for all connected robots and the kinetic energy of the i -th robot, here the work done by forces $\xi_{i0}(\cdot)$ over the error trajectories \tilde{p}_i for every robot are included.

Once more, since the proximity graph might change over time, with addition/deletion of edges, suppose $\mathcal{G}(p)$ switches every time instant t_k with $k = 1, 2, \dots$, and remains fixed over the time interval $[t_{k-1}, t_k)$. The following Lemma examine the collective energy (4.25) when the proximity graph remains fixed.

Lemma 4.2. *Consider the closed-loop system (4.1)-(4.22), a virtual leader (2.35) with $f_0(p_0, v_0) \equiv \mathbf{0}_n$, a fixed set of informed members $\mathbf{I}_0 \subset \mathbf{I}$, and the time interval $[t_{k-1}, t_k)$ in which the proximity graph remains fixed, i.e. $\mathcal{G}(p) = \mathcal{G}$ for all $t \in [t_{k-1}, t_k)$. Denote as $V(\tilde{p}, \tilde{v})_{t_{k-1}}$ the collective energy at instant t_{k-1} . If the terms in (4.22) meet conditions (4.10) and (4.11), then the collective energy (4.25) is such that $V(\tilde{p}, \tilde{v})_t \leq V(\tilde{p}, \tilde{v})_{t_{k-1}}$ for all $t \in [t_{k-1}, t_k)$.*

Proof. Consider the distributed controller (4.22) rewritten in error terms as

$$u_i = - \sum_{j \in \mathcal{N}_i(\tilde{p})} \nabla_{\tilde{p}_i} \psi_{ij}(\|\tilde{p}_{ij}\|) - \sum_{j \in \mathcal{N}_i(\tilde{p})} \vartheta_{ij}(\|\tilde{p}_{ij}\|, \tilde{v}_{ij}) - h_i(\xi_{i0}(\tilde{p}_i) + \nu_{i0}(\tilde{v}_i)), \quad i \in \mathbf{I}.$$

Then, since $f_0(p_0, v_0) \equiv \mathbf{0}_n$ and (4.22) fulfill conditions (4.10) and (4.11), the error dynamics takes the form

$$\dot{\tilde{p}}_i = \tilde{v}_i \quad \text{and} \quad \dot{\tilde{v}}_i = u_i, \quad i \in \mathcal{I},$$

Taking the time derivative of (4.25), it follows that

$$\dot{V}(\tilde{p}, \tilde{v})_t = \frac{1}{2} \sum_{i=1}^N \omega_i \left(\sum_{j \in \mathcal{N}_i(\tilde{p})} \tilde{v}_{ij}^T \nabla_{\tilde{p}_i} \psi_{ij}(\|\tilde{p}_{ij}\|) + 2\tilde{v}_i^T u_i + h_i \tilde{v}_i^T \xi_{i0}(\tilde{p}_i) \right).$$

Applying controller (4.22), and considering conditions (4.10) and (4.11), after some algebraic manipulations we obtain the following

$$\dot{V}(\tilde{p}, \tilde{v})_t \leq -\frac{1}{2} \sum_{i=1}^N \omega_i \left(\sum_{j \in \mathcal{N}_i(\tilde{p})} \tilde{v}_{ij}^T \vartheta_{ij}(\|\tilde{p}_{ij}\|, \tilde{v}_{ij}) + h_i \tilde{v}_i^T \nu_{i0}(\tilde{v}_i) \right) \leq 0.$$

Therefore, for all $t \in [t_{k-1}, t_k)$, the collective energy decreases, that is, $V(\tilde{p}, \tilde{v})_t \leq V(\tilde{p}, \tilde{v})_{t_{k-1}}$. \square

The following results gives conditions over (4.22) such that its a solution to the leader-followers flocking motion problem for a group of robots with different input constraints.

Theorem 4.2. *Consider the closed-loop system (4.1)-(4.22) with a neighborhood hysteresis process, a fixed set of informed members $\mathcal{I}_0 \subset \mathcal{I}$ and a virtual leader (2.35) with $f_0(p_0, v_0) \equiv \mathbf{0}_n$. Assume (4.22) has properties (4.10) and (4.11). If the proximity graph $\mathcal{G}(p)_{t_0}$ is connected, (4.14) is fulfilled, and*

$$\sum_{j \in \mathcal{N}_i(p)} \kappa_{ij}(\|p_{ij}\|) \leq \frac{\hat{u}_i - h_i \left(\hat{\xi}_{i0} + \hat{\nu}_{i0} \right)}{\hat{\varphi} + \hat{\psi}}, \quad i \in \mathcal{I}, \quad (4.26)$$

with $h_i \in \left(0, \frac{\hat{u}_i}{\hat{\xi}_{i0} + \hat{\nu}_{i0}} \right)$ for all $i \in \mathcal{I}_0$, then the following statements hold for all $t \geq 0$:

- (i) *The proximity graph remains connected for all time;*
- (ii) *The multi-robot system is on leader-followers flocking motion and asymptotically reaches a rigid configuration, and;*
- (iii) *Every robot's control effort satisfy its own input restriction.*

Proof. Proof of statement (i): This statement can be proven following the same reasoning as in Theorem 4.1 applying the results of Lemma 4.2.

Proof of statement (ii): The group cohesiveness, collision avoidance and robot-leader velocity mismatches boundedness proofs can be derived from the reasoning done in Theorem 4.1. It remains to show robot-leader position tracking errors are bounded.

Since $V(\tilde{p}, \tilde{v})_t \leq \bar{V}$ for all $t \geq 0$, notice that $\omega_i h_i \int_{\tilde{p}_i} \xi_{i0}(y) \cdot dy \leq \bar{V}$. From the properties of the controller's function $\xi_{i0}(\cdot)$ it can be shown that

$$\|\tilde{p}_i\| \leq \frac{1}{\sqrt{n}} \left(\frac{\bar{V}}{\omega_i h_i \hat{\xi}_{i0}} - \sum_{i=1}^n \left(\tilde{p}_i^{[k]} \right)_{t_0} \right), \quad i \in I_0.$$

On the other hand, since $\mathcal{G}(p)$ is connected for all $t \geq 0$ then $\|p_{ij}\| \leq r(N-1)$. Therefore, $\|\tilde{p}_i\| \leq \rho_0$ for all $i \in I$ and $t \geq 0$, with

$$\rho_0 = \max_{i \in I_0} \left\{ \frac{1}{\sqrt{n}} \left(\frac{\bar{V}}{\omega_i h_i \hat{\xi}_{i0}} - \sum_{i=1}^n \left(\tilde{p}_i^{[k]} \right)_{t_0} \right) \right\} + r(N-1).$$

Hence, the robot-leader position tracking errors are bounded.

To show the multi-robot system reaches a rigid leader-followers flocking motion, we can follow the same steps as in Theorem 4.1.

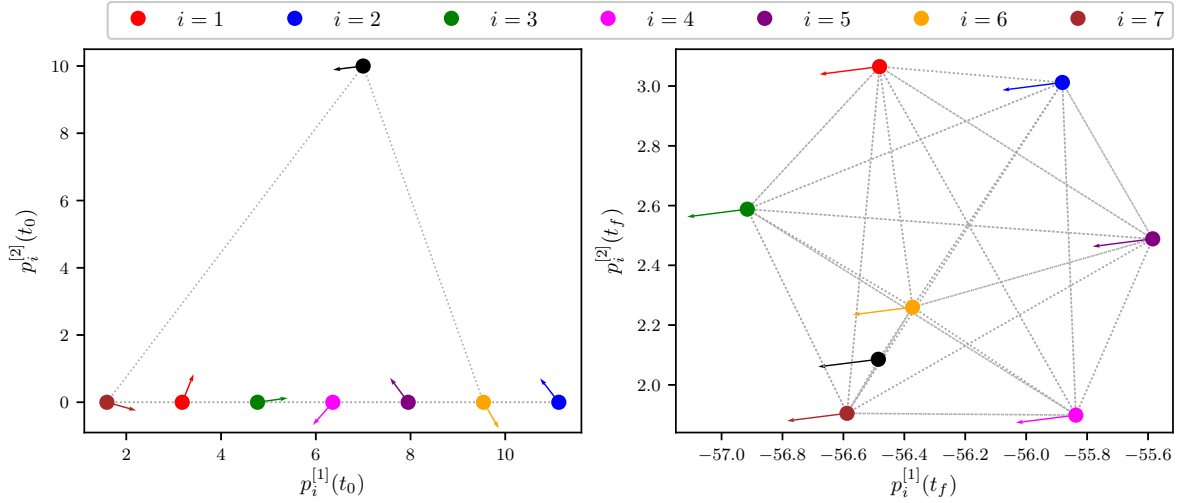
Proof of statement (iii): Following the reasoning done in Theorem 4.1, leads to (4.26). \square

Remark 4.4. *In the literature, the leader-followers flocking motion problem with heterogeneous input constraints condition was addressed in [80, 119]. There, each uninformed robot selects another within its neighborhood that acts as a leader to be followed, this target determination process is done by each robot and, once a target is chosen, it is not changed at any future time. This allow robots to dedicate its entire control effort on maintaining that single network's edge. Nonetheless, with this process, the resulting proximity graph's configuration is susceptible to single node/edge failures that might fragment the group. Moreover, it doesn't guarantee inter-robot collision avoidance. In contrast, the distributed controller (4.22) is designed to avoid inter-robot collisions and, by considering the whole neighborhood of the i -th robot, makes the group less fragile to single node/edge failures that might fragment the swarm.*

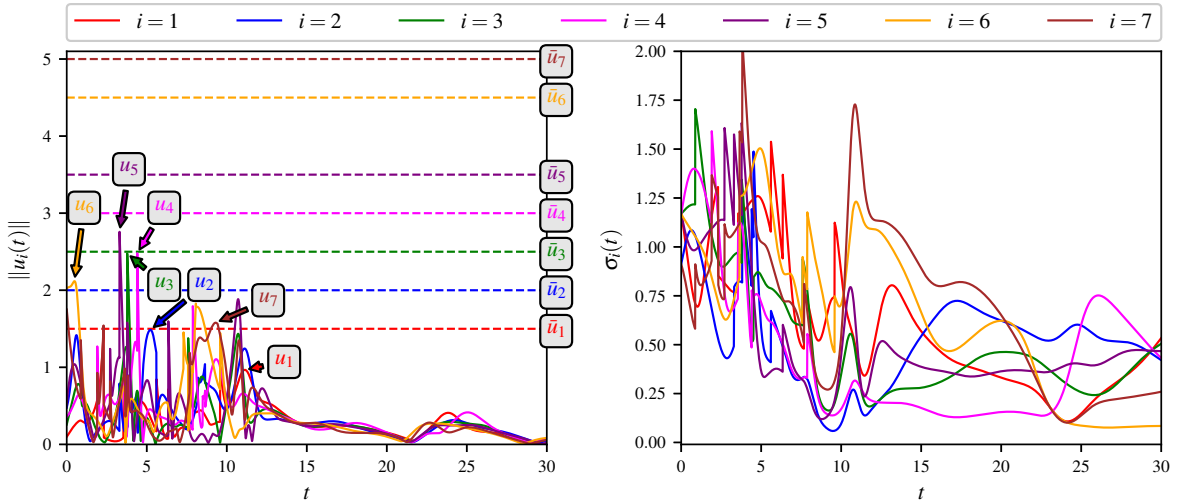
Example 4.2. *Consider the same set of the Example 4.1. The initial and final configurations of the closed-loop system (4.1)-(4.22) are shown in Figure 4.3a. Notice that the connectivity of the proximity graph is preserved for all $t \in [0, 50]$. The robot-leader velocity alignment and position tracking are shown in the final configuration, where the states of the informed robots almost overlaps with the ones of the leader. Observe that $\|p_{k0}\|$ is not zero for informed robots, this is due to the collision avoidance rule among them. The predefined input norms are displayed in Figure 4.3b. Observe that the control effort applied by each robot satisfy its own input constraint and allows robots with higher capabilities to produce control efforts greater than their less capable neighbors to fulfill local objectives.*

4.1.3 Flocking motion with obstacle avoidance

We consider the presence of fixed obstacles in the environment. Before continuing, we make the following assumption:



(a) Initial (left) and final (right) configuration.



(b) Input norms (left) and collision avoidance indicators (right) of the robotic swarm.

Figure 4.3: Leader-followers flocking motion.

Assumption 4.1. *Agents distinguish between teammates and obstacles.*

Assumption 4.1 let us use the obstacle induced virtual agent approach to represent obstacles described in [64, 120]. To include obstacle avoidance objectives, we incorporate additional terms into controllers (4.4) and (4.22). These include the design of a force pushing agents away from nearby obstacles and a consensus force towards the velocity of the obstacle induced virtual agents.

Obstacle induced virtual agents

The main idea for obstacle avoidance is to introduce a virtual agent on the boundary of obstacles and design control efforts to avoid collision with them [64, 120]. We restrict our study to obstacles that are connected convex areas in \mathbb{R}^n (with $n = 1, 2$ or 3) with

boundaries that are smooth manifolds. Specifically, spheres or infinite walls as shown in Figure 4.4. The position of virtual agents are induced by the proximity of real ones with these two types of obstacles. In what follows, we describe how position and velocity of obstacle induced virtual agents are locally computed.

Let $\mathcal{O} := \{o_1, \dots, o_M\}$ denote the index set of obstacles. An agent is called a neighbor of obstacle o_k if and only if a ball of radius r , centered at p_i , overlaps with o_k (see Figure 4.4). The set of nearby obstacles of an agent is defined as follows

$$\mathcal{N}_i^{ob}(p) := \{k \in \mathcal{O} : \|p_i - \check{p}_{i,k}\| \leq r\} \quad (4.27)$$

where $\check{p}_{i,k}$ is the position of the virtual agent induced by the k -th obstacle. The following Lemma describes how position $\check{p}_{i,k}$ and velocity $\check{v}_{i,k}$ vectors are locally computed (more details and proof are found in [64, 120]).

Lemma 4.3. (Lemma 4 in [64]) *Let $\check{p}_{i,k}$ and $\check{v}_{i,k}$ denote the position and velocity of a virtual agent neighbor of obstacle o_k . Then*

- i) *For an obstacle with hyperplane boundary that has a unit normal vector \mathbf{a}_k and passes through the point y_k , the position and velocity of the virtual agent are determined by*

$$\check{p}_{i,k} = Pp_i + (I_n - P)y_k, \quad \check{v}_{i,k} = Pv_i$$

where $P = I_n - \mathbf{a}_k \mathbf{a}_k^T$ is a projection matrix.

- ii) *For a spherical obstacle with radius \check{r}_k centered at y_k , the position and velocity of the virtual agent are given by*

$$\check{p}_{i,k} = \mu p_i + (1 - \mu)y_k, \quad \check{v}_{i,k} = \mu P v_i$$

where $\mu = \frac{\check{r}_k}{\|p_i - y_k\|}$, $\mathbf{a}_k = \frac{(p_i - y_k)}{\|p_i - y_k\|}$, and $P = I_n - \mathbf{a}_k \mathbf{a}_k^T$.

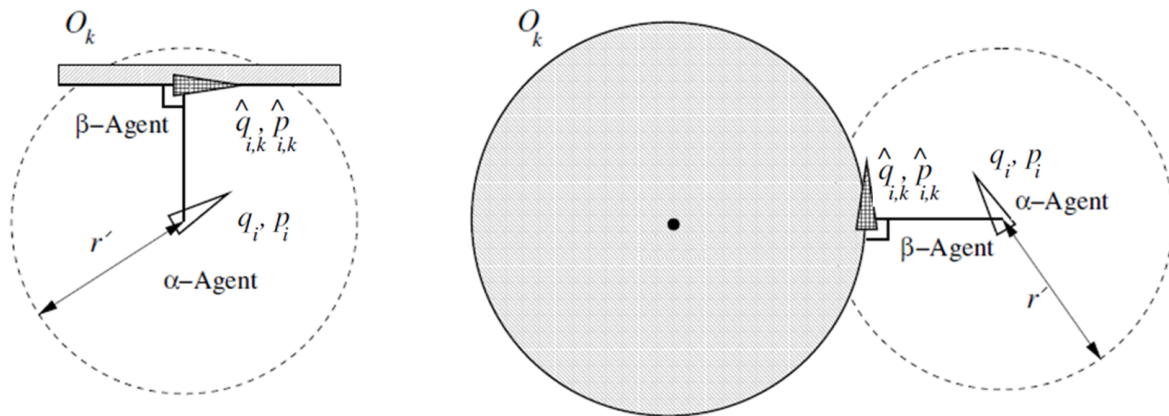


Figure 4.4: Virtual agents induced by nearby obstacles [64, 120].

Obstacle avoidance distributed controller

Since we have a local way of represent environmental obstacles, we now describe how such information is used to design control efforts to induce obstacle avoidance behavior into multi-robot system (4.1).

First, we use the gradient method to design a repelling force between real and obstacle-induced virtual agents. Consider a distance-dependent APF $\psi_{ij}^{ob} : [0, r] \mapsto \mathbb{R}_{\geq 0}$ with partial derivative $\varphi_{ij}^{ob}(s) = \frac{\partial \psi_{ij}^{ob}(s)}{\partial s}$ and the following properties:

- i) For all $s \in [0, r]$, $0 \leq \psi_{ij}^{ob}(s) \leq \bar{\psi}_{ij}^{ob}$ with $\psi_{ij}^{ob}(0) = \bar{\psi}_{ij}^{ob}$ and $\psi_{ij}^{ob}(r) = 0$;
- ii) For all $s \in [0, r]$, $\bar{\varphi}_{ij}^{ob} \leq \varphi_{ij}^{ob}(s) \leq 0$ with $\varphi_{ij}^{ob}(0) = \bar{\varphi}_{ij}^{ob}$ and $\varphi_{ij}^{ob}(r) = 0$.

where $\bar{\psi}_{ij}^{ob}, \bar{\varphi}_{ij}^{ob} \in \mathbb{R}_{>0}$.

The second control effort is an alignment term. Similarly to controllers (4.4) and (4.22), we use velocity consensus functions. Consider a distance-dependent bounded odd function $\vartheta_{ij}^{ob} : \mathbb{R}_{\geq 0} \times \mathbb{R}^n \mapsto \mathbf{C}$ defined by elements with $\mathbf{C} := \left\{ y \in \mathbb{R}^n : \|y\| \leq \hat{\vartheta}_{ij}^{ob} \right\}$, where $\hat{\vartheta}_{ij}^{ob} \in \mathbb{R}_{>0}$ is the biggest norm of any vector on its image.

From the controller described in general form, equation (4.2), we have that functions

$$h_{ik}(p_{ik}, v_{ik}) = \nabla_{p_i} \psi_{ik}^{ob}(\|p_{ik}\|) + \vartheta_{ik}^{ob}(\|p_{ik}\|, v_{ik})$$

where $p_{ik} = p_i - \check{p}_{i,k}$ and $v_{ik} = v_i - \check{v}_{i,k}$ are, respectively, the difference between position and velocity of the i th agent and the k th obstacle-induced virtual agent. Therefore, the distributed controllers including obstacle avoidance objectives are

$$u_i = \nu_i - \sum_{k \in \mathcal{N}_i^{ob}(p)} \nabla_{p_i} \psi_{ik}^{ob}(\|p_{ik}\|) - \sum_{k \in \mathcal{N}_i^{ob}(p)} \vartheta_{ik}^{ob}(\|p_{ik}\|, v_{ik}), \quad i \in \mathbf{I}. \quad (4.28)$$

where ν_i is either the leaderless or leader-followers flocking motion controllers (4.4) and (4.22), respectively. With the following analysis, we establish the convergence of closed-loop system (4.1)-(4.28) for both leaderless and leader-followers flocking motion scenarios at once.

Collective energy

Define the collective energy of of the closed-loop system (4.1)-(4.28) as

$$Q(\tilde{p}, \tilde{v}) := V(\tilde{p}, \tilde{v}) + \sum_{i=1}^N \omega_i \sum_{k \in \mathcal{N}_i^{ob}(\tilde{p})} \psi_{ik}^{ob}(\|\tilde{p}_{ik}\|). \quad (4.29)$$

where $V(\tilde{p}, \tilde{v})$ is the collective energy (4.9) or (4.25) for leaderless or leader-followers flocking motion, respectively. Also, \tilde{p} and \tilde{v} are the errors defined in (4.7) and (4.24) for the leaderless and leader-followers cases. Notice this collective energy summarize

the potential and kinetic energy due to agent interactions plus the APFs on each agent due to nearby obstacles. Notice, the maximum value for $Q(\tilde{p}, \tilde{v})$ is

$$\bar{Q} = \bar{V} + \sum_{i=1}^N \omega_i \sum_{o_k \in \mathcal{O}} \bar{\psi}_{ik}^{ob}$$

where \bar{V} is the bound of collective energies (4.9) or (4.25). We use (4.29) to establish the stability of flocking motion for the closed-loop system (4.1)-(4.28).

Recalling that we are dealing with proximity graphs, the information network might change over time. Then, suppose $\mathcal{G}(p)$ switches on time instants t_k with $k = 1, 2, \dots$, and remains fixed over the time interval $[t_{k-1}, t_k)$. At time instants t_k edges might be added to, or deleted from, $\mathcal{E}(p)$, or agents detect nearby obstacles. The following lemma studies collective energy (4.29) in the time interval $[t_{k-1}, t_k)$.

Lemma 4.4. *For the closed-loop system (4.1)-(4.28) consider time interval $[t_{k-1}, t_k)$. Denote as $Q(\tilde{p}, \tilde{v})_{t_{k-1}}$ the collective energy at instant t_{k-1} . In controller (4.28) suppose ν_i fulfill properties (4.10) and (4.11). Then $Q(\tilde{p}, \tilde{v})_t \leq Q(\tilde{p}, \tilde{v})_{t_{k-1}}$ for all $t \in [t_{k-1}, t_k)$.*

Proof. Take the time-derivative of $Q(\tilde{p}, \tilde{v})_t$ for $t \in [t_{k-1}, t_k)$. We have

$$\begin{aligned} \dot{Q}(\tilde{p}, \tilde{v})_t &= \dot{V}(\tilde{p}, \tilde{v})_t + \sum_{i=1}^N \omega_i \sum_{k \in \mathcal{N}_i^{ob}(\tilde{p})} (\tilde{v}_{ik}^T \nabla_{\tilde{p}_i} \psi_{ik}^{ob}(\|\tilde{p}_{ik}\|) - \tilde{v}_i^T \nabla_{\tilde{p}_i} \psi_{ik}^{ob}(\|\tilde{p}_{ik}\|)) \\ &\quad - \sum_{i=1}^N \omega_i \sum_{k \in \mathcal{N}_i^{ob}(\tilde{p})} \tilde{v}_i^T \vartheta_{ik}^{ob}(\|\tilde{p}_{ik}\|, \tilde{v}_{ik}). \end{aligned}$$

Lemma 4.1 (respectively, Lemma 4.2) states that $\dot{V}(\tilde{p}, \tilde{v})_t \leq 0$ for all $t \in [t_{k-1}, t_k)$. Therefore, we focus on the other terms of $\dot{Q}(\tilde{p}, \tilde{v})_t$.

First, notice that

$$\sum_{i=1}^N \omega_i \sum_{k \in \mathcal{N}_i^{ob}(\tilde{p})} (\tilde{v}_{ik}^T \nabla_{\tilde{p}_i} \psi_{ik}^{ob}(\|\tilde{p}_{ik}\|) - \tilde{v}_i^T \nabla_{\tilde{p}_i} \psi_{ik}^{ob}(\|\tilde{p}_{ik}\|)) = - \sum_{i=1}^N \omega_i \sum_{k \in \mathcal{N}_i^{ob}(\tilde{p})} \tilde{v}_k^T \nabla_{\tilde{p}_i} \psi_{ik}^{ob}(\|\tilde{p}_{ik}\|)$$

where $\tilde{v}_k^T \nabla_{\tilde{p}_i} \psi_{ik}^{ob}(\|\tilde{p}_{ik}\|) = \varphi_{ij}^{ob}(\|\tilde{p}_{ik}\|) \tilde{v}_k^T \frac{\tilde{p}_{ik}}{\|\tilde{p}_{ik}\|}$ with $\tilde{v}_k = \check{v}_{i,k} - \bar{p}$. Notice, from the definition of $\check{v}_{i,k}$, that \tilde{v}_k and \tilde{p}_{ik} are orthogonal, hence the product $\tilde{v}_k^T \frac{\tilde{p}_{ik}}{\|\tilde{p}_{ik}\|} = 0$. In consequence,

$$\sum_{i=1}^N \omega_i \sum_{k \in \mathcal{N}_i^{ob}(\tilde{p})} \tilde{v}_k^T \nabla_{\tilde{p}_i} \psi_{ik}^{ob}(\|\tilde{p}_{ik}\|) = 0$$

On the other hand, the third term of $\dot{Q}(\tilde{p}, \tilde{v})$ is

$$\sum_{i=1}^N \omega_i \sum_{k \in \mathcal{N}_i^{ob}(\tilde{p})} \tilde{v}_i^T \vartheta_{ik}^{ob}(\|\tilde{p}_{ik}\|, \tilde{v}_{ik}) = \sum_{i=1}^N \omega_i \sum_{k \in \mathcal{N}_i^{ob}(\tilde{p})} \tilde{v}_i^T \vartheta_{ik}^{ob}(\|\tilde{p}_{ik}\|, (I_n - \mu P) \tilde{v}_i).$$

Since P is a projection matrix, with eigenvalues either 0 or 1, and noticing $\mu \in [0, 1]$ (see its definition in Lemma 4.3), matrix $I_n - \mu P$ have positive eigenvalues. In consequence, the product $(I_n - \mu P)\tilde{v}_i$ have the same sign of \tilde{v}_i , therefore, the products $\tilde{v}_i^T \vartheta_{ik}^{ob}(\|\tilde{p}_{ik}\|, (I_n - \mu P)\tilde{v}_i) \geq 0$. This implies that

$$\sum_{i=1}^N \omega_i \sum_{k \in \mathcal{N}_i^{ob}(\tilde{p})} \tilde{v}_i^T \vartheta_{ik}^{ob}(\|\tilde{p}_{ik}\|, \tilde{v}_{ik}) \geq 0$$

as the sum of non-negative values.

Finally, we conclude that

$$\dot{Q}(\tilde{p}, \tilde{v})_t = \dot{V}(\tilde{p}, \tilde{v})_t - \sum_{i=1}^N \omega_i \sum_{k \in \mathcal{N}_i^{ob}(\tilde{p})} \tilde{v}_i^T \vartheta_{ik}^{ob}(\|\tilde{p}_{ik}\|, \tilde{v}_{ik}) \leq 0. \quad (4.30)$$

This, implies that $Q(\tilde{p}, \tilde{v})_t \leq Q(\tilde{p}, \tilde{v})_{t_{k-1}}$ for all $t \in [t_{k-1}, t_k]$, finishing our proof. \square

Leaderless flocking motion with obstacle avoidance

Let ν_i in (4.28) be defined by equation (4.4). The following theorem gives conditions for the multi-agent system approach to a leaderless flocking motion with obstacle avoidance abilities.

Theorem 4.3. *Consider the closed-loop system (4.1)-(4.28) along with the neighborhood hysteresis process (described in Definition 3.2). Suppose the terms in ν_i meet conditions (4.10) and (4.11) while the obstacle avoidance terms satisfy*

$$\nabla_{p_i} \psi_{ik}^{ob}(\|p_{ik}\|) = \kappa_{ik}^{ob}(\|p_{ik}\|) \nabla_{p_i} \psi^{ob}(\|p_{ik}\|) \text{ and } \vartheta_{ik}^{ob}(\|p_{ik}\|, v_{ik}) = \kappa_{ik}^{ob}(\|p_{ik}\|) \vartheta^{ob}(v_{ik}), \quad (4.31)$$

where $\kappa_{ik}^{ob}(\|p_{ik}\|) \in \mathbb{R}_{>0}$ for all $\|p_{ik}\| \in [0, r]$. If the proximity graph $\mathcal{G}(p)_{t_0}$ is connected; the initial collective energy is such that $\bar{Q} < \min \{ \hat{V}_{ij}, \hat{\psi}_{ik}^{ob} \}$, where $\hat{V}_{ij} := \frac{\omega_i \hat{\psi}_{ij} + \omega_j \hat{\psi}_{ji}}{2}$; the values $\kappa_{ij}(s)$, for all $s \in [0, r]$ are such that

$$\sum_{j \in \mathcal{N}_i(p)} \kappa_{ij}(\|p_{ij}\|) + \sum_{k \in \mathcal{N}_i^{ob}(p)} \kappa_{ik}^{ob}(\|p_{ik}\|) \leq \frac{\bar{u}_i}{\hat{\varphi} + \hat{\vartheta}} \quad i \in \mathcal{I}. \quad (4.32)$$

where $\hat{\varphi}_{ik}^{ob} = \hat{\varphi} := \max_{s \in [0, r]} \{ |\varphi(s)| \}$ and $\hat{\vartheta}$ is the value such that $\|\vartheta(x)\| \leq \hat{\vartheta}$ for all $x \in \mathbb{R}^n$. Then, the following statements hold for all $t \geq t_0$:

- i) The proximity graph remains connected;
- ii) The multi-robot system is on leaderless flocking motion while avoid environmental obstacles;
- iii) Every robot's control effort satisfy its own input constraint.

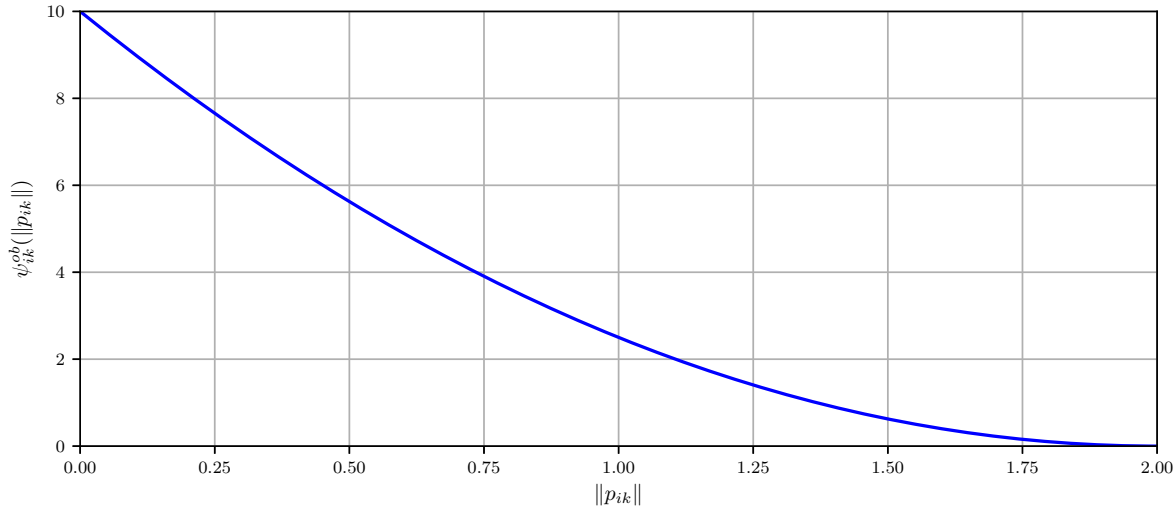


Figure 4.5: Artificial potential function (4.33).

Proof. Proof of statement i) follows the same reasoning of its equivalent in Theorem 4.1 using the non-increasing property of the collective energy shown by Lemma 4.4.

Proof of statement ii) follows the same reasoning of its equivalent in Theorem 4.1. Using LaSalle's invariance principle, it can be seen, from (4.30), that the largest invariant corresponds to a fixed leaderless-flocking motion configuration and, in presence of obstacles, a velocity alignment with obstacle induced virtual agents.

Proof of statement iii) use properties (4.10), (4.11) and (4.34) to compute bound shown in equation (4.35). \square

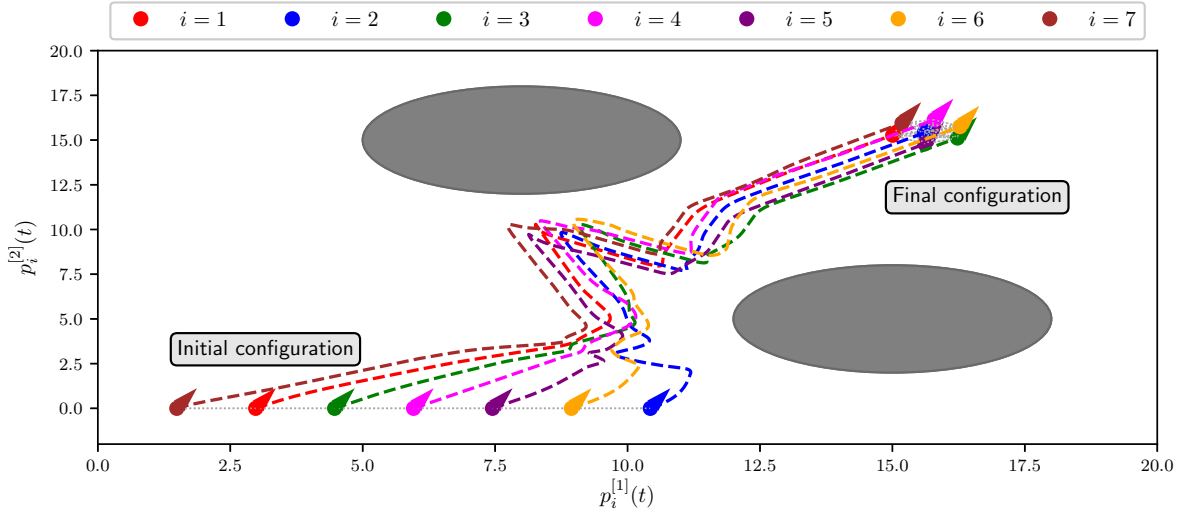
Remark 4.5. Notice, Theorem 4.3 is quite similar to Theorem 4.1; Condition (4.34) allows us to write conditions over the values κ_{ij} and κ_{ik}^{ob} similarly to equation (4.15). Also, the initial energy condition includes the potential induced by nearby obstacles. With these minor modifications to Theorem 4.1, we were able to include obstacle avoidance objectives.

Example 4.3. Consider the same setup of Example 4.1 and choose agents initial velocity vectors such that $v_i \in [0, 0.4] \times [0, 0.4]$ for all $i \in \mathcal{I}$. For the obstacle avoidance terms in (4.28), define the APF as

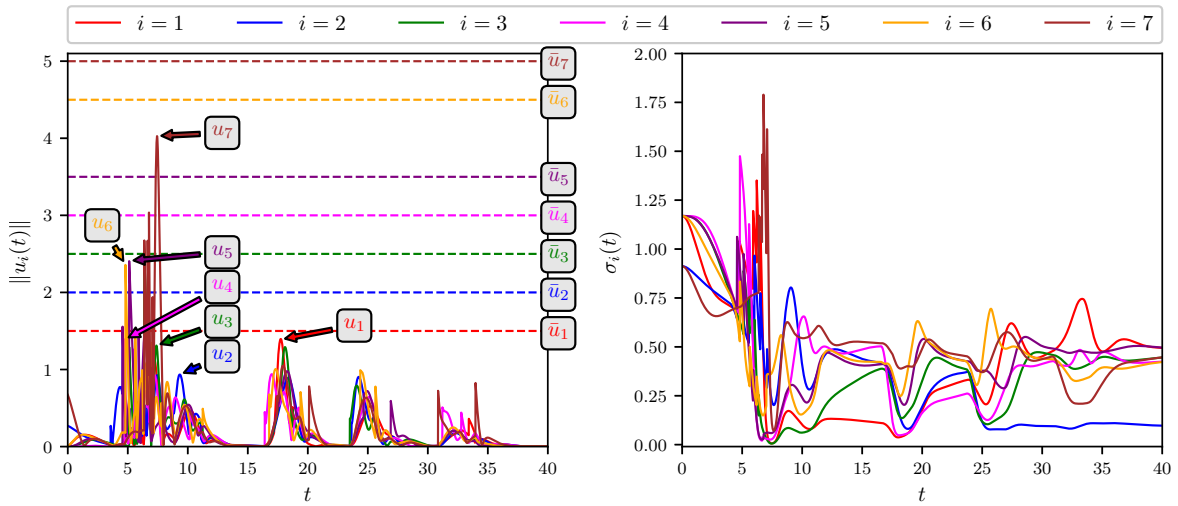
$$\psi_{ik}^{ob}(\|p_{ik}\|) := \frac{\hat{\psi}_{ik}(r - \|p_{ik}\|)^2}{r^2}; \quad (4.33)$$

Figure 4.5 shows its shape. And, for the velocity alignment part, consider $\vartheta_{ik}^{ob}(x, s) = \kappa_{ik}(s) \tanh(x)$, with $\|\vartheta_{ik}(s, x)\| \leq \kappa_{ik}(s) \sqrt{n}$. Also, consider two spherical obstacles of radius $\check{r}_k = 3$, with $k = 1, 2$, located at $y_1 = [8, 15]$ and $y_2 = [15, 5]$, respectively.

In Figure 4.6a agents are represented by coloured circles and arrows and dotted grey lines represent the existence of information exchange between agents. Dotted coloured lines represent each agent's trajectory. The spherical obstacles are illustrated by the dark grey colour circles. Meanwhile, in Figure 4.6b, solid lines represent the trajectories



(a) System trajectories



(b) Input norms (left) and collision avoidance indicators (right).

Figure 4.6: Leaderless flocking motion with obstacle avoidance.

of input norms and collision avoidance indicators from equation (4.19), and dotted lines represent agent's input constraints.

From Figure 4.6a, notice the agents avoid nearby obstacles while preserving connectivity of the proximity graph and avoid inter-agent collisions. In Figure 4.6b, we highlighted the agent's maximum input norms to show the fulfilment of input restrictions as well. Again, agents with higher capacities produce control efforts beyond the input constraint of their neighbours with smaller input constraints.

Leader-followers flocking motion with obstacle avoidance

Let ν_i in (4.28) be defined by equation (4.22). The following theorem gives conditions for the multi-agent system approach to a leader-followers flocking motion with

obstacle avoidance abilities.

Theorem 4.4. *Consider the closed-loop system (4.1)-(4.28) along with the neighborhood hysteresis process (described in Definition 3.2), a fixed set of informed members $\mathcal{I}_0 \subset \mathcal{I}$ with a virtual leader (2.35), where $f_0(p_0, v_0) \equiv \mathbf{0}_n$. Suppose the terms in v_i meet conditions (4.10) and (4.11) while the obstacle avoidance terms satisfy*

$$\nabla_{p_i} \psi_{ik}^{ob}(\|p_{ik}\|) = \kappa_{ik}^{ob}(\|p_{ik}\|) \nabla_{p_i} \psi(\|p_{ik}\|) \text{ and } \vartheta_{ik}^{ob}(\|p_{ik}\|, v_{ik}) = \kappa_{ik}^{ob}(\|p_{ik}\|) \vartheta(v_{ik}), \quad (4.34)$$

where $\kappa_{ik}^{ob}(\|p_{ik}\|) \in \mathbb{R}_{>0}$ for all $\|p_{ik}\| \in [0, r]$. If the proximity graph $\mathcal{G}(p)_{t_0}$ is connected; the initial collective energy is such that $\bar{Q} < \min \{ \hat{V}_{ij}, \hat{\psi}_{ik}^{ob} \}$, where $\hat{V}_{ij} := \frac{\omega_i \hat{\psi}_{ij} + \omega_j \hat{\psi}_{ji}}{2}$; the values $\kappa_{ij}(s)$, for all $s \in [0, r]$ are such that

$$\sum_{j \in \mathcal{N}_i(p)} \kappa_{ij}(\|p_{ij}\|) + \sum_{k \in \mathcal{N}_i^{ob}(p)} \kappa_{ik}^{ob}(\|p_{ik}\|) \leq \frac{\hat{u}_i - h_i(\hat{\xi}_{i0} + \hat{\vartheta}_{i0})}{\hat{\varphi} + \hat{\vartheta}}, \quad i \in \mathcal{I}. \quad (4.35)$$

with $h_i \in \left(0, \frac{\hat{u}_i}{\hat{\xi}_{i0} + \hat{\vartheta}_{i0}}\right)$ for all $i \in \mathcal{I}_0$ and where $\hat{\varphi}_{ik}^{ob} = \hat{\varphi} := \max_{s \in [0, r]} \{ |\varphi(s)| \}$ and $\hat{\vartheta}$ is the value such that $\|\vartheta(x)\| \leq \hat{\vartheta}$ for all $x \in \mathbb{R}^n$. Then, the following statements hold for all $t \geq t_0$:

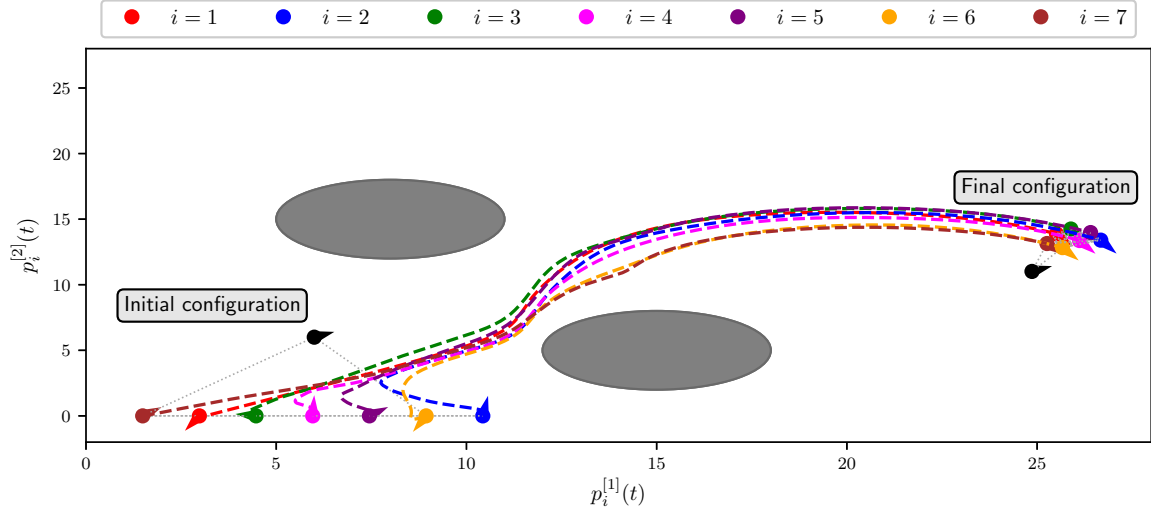
- i) *The proximity graph remains connected;*
- ii) *The multi-robot system is on leader-followers flocking motion while avoid environmental obstacles;*
- iii) *Every robot's control effort satisfy its own input constraint.*

The proof of this result is similar to the proof for the previous result so is not included.

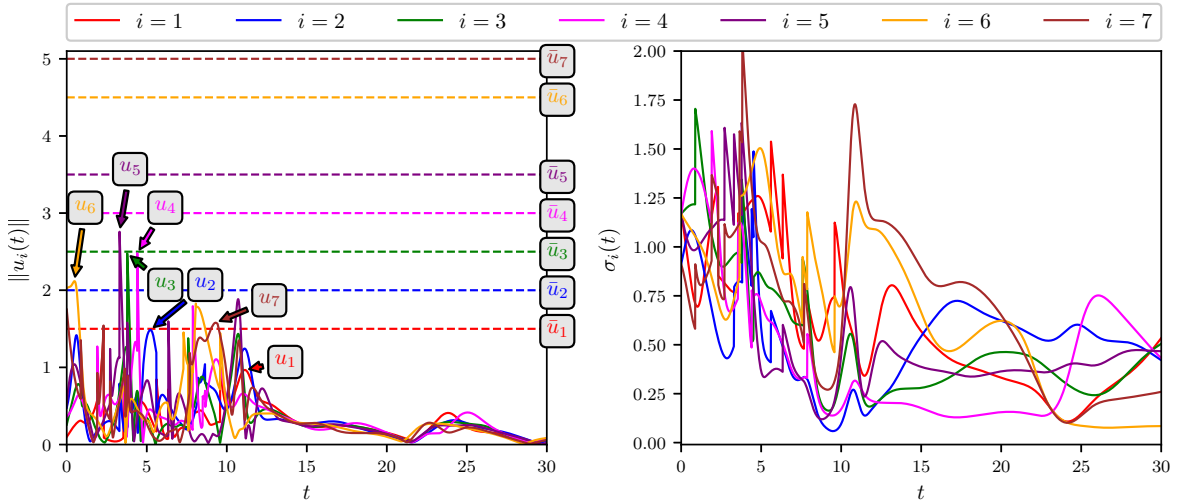
Example 4.4. *Again, consider the multi-agents system setup of Example 4.1. Let the obstacle avoidance terms be as defined for Example 4.3 and consider a virtual leader moving at a constant velocity towards the position of two nearby obstacles. This setup is illustrated in Figure 4.7a, where the virtual leader is in black. The set of informed agents is $\mathcal{I}_0 = \{6, 7\}$.*

In Figure 4.7a we illustrate how the multi-agent system navigates from an initial to a final position while evading nearby obstacles. Notice that, at all times, the distributed controller design preserves the proximity graph's connectivity. Meanwhile, Figure 4.7b shows the input constraints are satisfied at any time; We highlighted the maximum values of each control effort to illustrate this. Also, the inter-agent collision avoidance objective is fulfilled as shown by the indicators.

Remark 4.6. *By adding a couple of terms in our controller designs from equations (4.4) and (4.22), we included obstacle avoidance into the multi-agent systems behaviour. We computed these pieces in a fully distributed fashion using the notions described in [64, 120]. As such, the idea of using virtual agents to represent obstacles is not new. These notions, or slight modifications of them, are used extensively in previous researches [81, 83, 92, 121, 122]. However, we implemented it in a new multi-agent setup; Second-order multi-agent systems with heterogeneous input bounds.*



(a) System trajectories.



(b) Input norms (left) and collision avoidance indicators (right).

Figure 4.7: Leader followers flocking motion with obstacle avoidance.

4.2 Directed Proximity Graphs

Consider a multi-robot system consisting of N mobile robots where the position and velocity dynamics of the i th robot is described by the equations

$$\dot{p}_i = v_i, \quad \dot{v}_i = u_i, \quad i \in I := \{1, 2, \dots, N\}. \quad (4.36)$$

But now, let $r_i \in \mathbb{R}_{>0}$ be the sensing/communication radius of agent i and define the set of neighbours as

$$\mathcal{N}_i^{in}(p) := \{j \in \mathcal{V} : \|p_{ij}\| \leq r_i\}. \quad (4.37)$$

Notice that if $r_j < r_i$ then $j \in \mathcal{N}_i^{in}(p)$ but $i \notin \mathcal{N}_j^{in}(p)$. Proximity digraphs are a natural approach to model this kind of information exchange.

In the following sections, we discuss the implications of modelling information networks with proximity digraphs; Also, how we use a similar controller design to the previous section by introducing a digraph connectivity measure.

4.2.1 Connectivity measure

In previous sections, we discussed why network connectivity it's a milestone in the induction of collective behaviours on multi-agent systems. We ensured this property in bidirectional proximity graphs by assuming the initial information networks were connected and designed the distributed controllers to preserve every initial or newly added network edge. Using a balance condition, we were able to do this even though each agent has different control limitations. In consequence, agents don't need to know the global network configuration. However, in proximity digraphs, the existence of an edge does not imply the existence of its reciprocal. Much less the preservation of connectivity. Hence, we cannot rely on balance conditions nor neighbours acting to preserve reciprocal edges. We aim for a more flexible distributed controller design. To do so, we must have some local sense of the global network configuration.

Connectivity measures are functions of the network's connectivity indicators. The possible values the connectivity measure take reflects the global configuration of the network. Perhaps, the most well-known connectivity indicator on digraphs is the algebraic connectivity of the Laplacian matrix (defined in Section 2.1.3). If the digraph contains a spanning rooted tree, then the algebraic connectivity has a positive real part. Then, by defining the connectivity measure as the real part of the algebraic connectivity, our objective is to keep it positive. Thus, ensuring the existence of a rooted spanning tree in the digraph. Another connectivity indicator is the Laplacian matrix first left eigenvector. The vector entries of this eigenvalue are all positive if and only if the digraph is strongly connected. It is possible to define connectivity measures as functions of these entries. The domain of these functions for positive entries corresponds to strongly connected digraphs. Then, the objective is to keep the measure inside that domain.

The previously mentioned connectivity measures are based on indicators using global network information. That is, to all the link weights of the network that make up the inputs of the Laplacian matrix. However, there are methods to calculate, in a distributed way, the algebraic connectivity or the first left eigenvector. In [74, 84, 92, 93, 123], distributed algorithms are presented to compute the algebraic connectivity. The shortcoming is it requires the network to be, at least, strongly connected and balanced. To overcome this drawback, we propose to change the indicator to the first left-eigenvector. In which case, the network no longer needs to be balanced.

For presentation simplicity, we make the following assumption.

Assumption 4.2. *Every agent computes its corresponding entry of the network's Laplacian matrix first left-eigenvector and shares it with its out-neighbours.*

This assumption implies the i th agent computes the entry γ_i , of vector $\gamma \in \mathbb{R}^N$ such that $\gamma^T L = \mathbf{0}_N^T$, and have access to vector entries γ_j for all $j \in \mathcal{N}_i^{in}(p)$. Although this assumption is quite strong, there are algorithms to compute, in a distributed fashion,

matrix eigenvalues through their corresponding eigenvectors. The only missing piece is an algorithm to distributedly compute the transpose of the Laplacian matrix. We let this issue for future works.

Under assumption 4.2, we define the connectivity measure between the i th agent and its in-neighbor j , as a function $\mu(\gamma_i, \gamma_j) : \mathbb{R}_{\geq 0} \times \mathbb{R}_{\geq 0} \mapsto \mathcal{C}$ as follows:

$$\mu(\gamma_i, \gamma_j) := \frac{\gamma_i}{\gamma_j} + \frac{\gamma_j}{\gamma_i}. \quad (4.38)$$

Notice, function's image $\mathcal{C} := (1, \infty)$ with $\mu(\gamma_i, \gamma_j) \rightarrow \infty$ if and only if either $\gamma_i \rightarrow 0$ or $\gamma_j \rightarrow 0$. We will use, as a shorthand notation, $\mu_{ij} = \mu(\gamma_i, \gamma_j)$. We present some convenient properties of this connectivity measure in the following proposition.

Proposition 4.1. *Let digraph \mathcal{D} be strongly connected. Then, the connectivity measure (4.38), has the following properties:*

- i) $\text{Sign}\left(\frac{\partial \mu_{ij}}{\partial \gamma_i}\right) + \text{Sign}\left(\frac{\partial \mu_{ij}}{\partial \gamma_j}\right) = 0$;
- ii) $\gamma_i \frac{\partial \mu_{ij}}{\partial \gamma_i} + \gamma_j \frac{\partial \mu_{ij}}{\partial \gamma_j} = 0$;
- iii) $\gamma_i \left| \frac{\partial \mu_{ij}}{\partial \gamma_i} \right| = \gamma_j \left| \frac{\partial \mu_{ij}}{\partial \gamma_j} \right| = \mu_{ij}$;
- iv) $1 < \mu_{ij}$.

Proof. Statement i): First, notice that $\frac{\partial \mu_{ij}}{\partial \gamma_i} = \frac{1}{\gamma_j} - \frac{\gamma_j}{\gamma_i^2}$ and $\frac{\partial \mu_{ij}}{\partial \gamma_j} = \frac{1}{\gamma_i} - \frac{\gamma_i}{\gamma_j^2}$. Now, without lost of generality, suppose $\gamma_i \leq \gamma_j$. Notice that squaring both sides of the inequality and taking the reciprocal on both sides, we get $\frac{1}{\gamma_i^2} \geq \frac{1}{\gamma_j^2}$. Multiplying by γ_j both sides and changing a term to one side, we get

$$\frac{\partial \mu_{ij}}{\partial \gamma_i} = \frac{1}{\gamma_j} - \frac{\gamma_j}{\gamma_i^2} \leq 0.$$

Meanwhile, if we multiply $\frac{1}{\gamma_i^2} \geq \frac{1}{\gamma_j^2}$ by γ_i , we get

$$\frac{\partial \mu_{ij}}{\partial \gamma_j} = \frac{1}{\gamma_i} - \frac{\gamma_i}{\gamma_j^2} \geq 0.$$

Therefore, if $\gamma_i \leq \gamma_j$, both partials are of different sign. Following a similar reasoning, the case $\gamma_j < \gamma_i$, yields the same conclusion. Hence, our equality holds.

Statement ii): Recalling that $\frac{\partial \mu_{ij}}{\partial \gamma_i} = \frac{1}{\gamma_j} - \frac{\gamma_j}{\gamma_i^2}$ and $\frac{\partial \mu_{ij}}{\partial \gamma_j} = \frac{1}{\gamma_i} - \frac{\gamma_i}{\gamma_j^2}$, we have

$$\gamma_i \frac{\partial \mu_{ij}}{\partial \gamma_i} + \gamma_j \frac{\partial \mu_{ij}}{\partial \gamma_j} = \gamma_i \left(\frac{1}{\gamma_j} - \frac{\gamma_j}{\gamma_i^2} \right) + \gamma_j \left(\frac{1}{\gamma_i} - \frac{\gamma_i}{\gamma_j^2} \right) = \mu_{ij} - \mu_{ij} = 0.$$

Statement iii): Notice, by the triangle inequality, that

$$\gamma_i \left| \frac{\partial \mu_{ij}}{\partial \gamma_i} \right| = \gamma_i \left| \frac{1}{\gamma_j} - \frac{\gamma_j}{\gamma_i^2} \right| \leq \gamma_i \left(\frac{1}{\gamma_j} + \frac{\gamma_j}{\gamma_i^2} \right) = \mu_{ij}.$$

Following the reasoning for $\gamma_j \left| \frac{\partial \mu_{ij}}{\partial \gamma_j} \right|$, we get our result.

Statement *iv*): First, notice that $\mu_{ij} = \frac{\gamma_i^2 + \gamma_j^2}{\gamma_i \gamma_j}$. Now, without loss of generality, suppose $\gamma_i \leq \gamma_j$. Notice that the product $\gamma_i \gamma_j \leq \gamma_j^2$, therefore $1 + \frac{\gamma_i^2}{\gamma_j^2} \leq \mu_{ij}$. Due the fact that γ_i and γ_j are both positive, we yield to our result. \square

In what follows, we discuss a method to produce a position-dependent first left eigenvector and, in consequence, dynamic connectivity measure μ_{ij} .

Position-dependent first left eigenvector.

In this section, we set a relation between the multi-agent system's configuration p and the first left eigenvector γ of the matrix Laplacian for strongly connected digraphs. We do this through the edge weights definition. Then, we discuss some properties of γ related to the multi-agent system dynamics.

First, notice that proposition 2.1 gives us a clear relation between the eigenvector γ and the edge weights of the proximity digraph. The key idea here is to define interagent distance-dependent edge weights to produce position-dependent eigenvector entries. Since the edge weights set the adjacency matrix entries, we continue our discussion by defining those entries.

Let the ij -th element of the adjacency matrix $A(p)$ be defined as follows:

$$a_{ij}(\|p_{ij}\|) := \begin{cases} 1 & \text{if } \|p_{ij}\| < \rho_i, \\ \alpha_{ij}(\|p_{ij}\|) & \text{if } \rho_i \leq \|p_{ij}\| \leq r_i, \\ 0 & \text{if } r_i < \|p_{ij}\| \end{cases} \quad (4.39)$$

where $\alpha_{ij}(\cdot) : [\rho_i, r_i] \mapsto [0, 1]$ is a differentiable and strictly decreasing function such that $\frac{\partial a_{ij}(\|p_{ij}\|)}{\partial \|p_{ij}\|} = b_{ij}(\|p_{ij}\|) a_{ij}(\|p_{ij}\|)$. This definition allows us to have a time-varying position-dependent nonnegative value ranging from connectivity to non-connectivity between an agent and nearby agents. Notice also that the time-derivative of the adjacency matrix entry is:

$$\dot{a}_{ij}(\|p_{ij}\|) = v_{ij}^T \nabla_{p_i} a_{ij}(\|p_{ij}\|) = b_{ij}(\|p_{ij}\|) a_{ij}(\|p_{ij}\|) v_{ij}^T \frac{p_{ij}}{\|p_{ij}\|}, \quad (4.40)$$

where $\nabla_{p_i} a_{ij}(\|p_{ij}\|) = \frac{\partial a_{ij}(\|p_{ij}\|)}{\partial \|p_{ij}\|} \frac{p_{ij}}{\|p_{ij}\|}$ is the gradient respect to p_i of $a_{ij}(\|p_{ij}\|)$. Before we discuss the implications of this definition, we define a couple of sets and a function.

Let \mathcal{T} be a spanning tree contained on a digraph \mathcal{D} and denote as $\mathcal{E}(\mathcal{T})$ the edge set of \mathcal{T} , then the sets

$$\mathcal{E}_i^{in}(\mathcal{T}) := \{(j, i) \in \mathcal{E}(\mathcal{T}) : j \in \mathcal{N}_i^{in}\} \quad \text{and} \quad \mathcal{E}_i^{out}(\mathcal{T}) := \{(i, j) \in \mathcal{E}(\mathcal{T}) : j \in \mathcal{N}_i^{out}\}, \quad (4.41)$$

define, respectively, the set of edges of \mathcal{T} ending and starting at the i th node. Also, \mathcal{N}_i^{in} and \mathcal{N}_i^{out} are, respectively, the in- and out-neighbours of the i th agent on digraph \mathcal{D} . Now, consider an edge subset $\mathcal{S} \subseteq \mathcal{E}(\mathcal{D})$. The function

$$\mathbf{P}(\mathcal{S}) := \prod_{(k,j) \in \mathcal{S}} a_{jk}(\|p_{jk}\|) \quad (4.42)$$

defines the matrix adjacency entries product related to the edges in \mathcal{S} . Notice that, from the edge-weight definition (4.39), $\mathbf{P}(\mathcal{S}) \leq 1$ for any $\mathcal{S} \subseteq \mathcal{E}(\mathcal{D})$. Now, we use these sets and function definitions to analyze some properties of the γ eigenvector entries.

Let γ be the first left eigenvector for the matrix Laplacian L of the proximity digraph \mathcal{D} . Then, from proposition 2.1, the i th entry of γ is

$$\gamma_i = \sum_{\mathcal{T} \in \mathbb{T}_i(\mathcal{D})} \mathbf{P}(\mathcal{E}(\mathcal{T})) = \sum_{\mathcal{T} \in \mathbb{T}_i(\mathcal{D})} \mathbf{P}(\mathcal{E}_i^{\text{in}}(\mathcal{T})) \mathbf{P}(\bar{\mathcal{E}}(\mathcal{T})), \quad (4.43)$$

where $\mathbb{T}_i(\mathcal{D})$ is the set of all directed spanning trees in \mathcal{D} that are rooted at the i th node and $\bar{\mathcal{E}}(\mathcal{T}) = \mathcal{E}(\mathcal{T}) \setminus \mathcal{E}_i^{\text{in}}(\mathcal{T})$. A quick examination of this equation shows that $\gamma_i \leq |\mathbb{T}_i(\mathcal{D})|$. Also, if there is no directed spanning tree with the i th node as the root, then $\gamma_i = 0$. This case corresponds to one where proximity graph \mathcal{D} is not a strongly connected digraph. On the other hand, notice we can relate a vector entry γ_i with any other node, say $k \neq i$, of the information network through the sets defined in (4.41) as follows:

$$\gamma_i = \sum_{\mathcal{T} \in \mathbb{T}_i(\mathcal{D})} \mathbf{P}(\mathcal{E}_k^{\text{in}}(\mathcal{T})) \mathbf{P}(\mathcal{E}_k^{\text{out}}(\mathcal{T})) \mathbf{P}(\bar{\mathcal{E}}(\mathcal{T})), \quad (4.44)$$

where $\bar{\mathcal{E}}(\mathcal{T}) = \mathcal{E}(\mathcal{T}) \setminus \{\mathcal{E}_k^{\text{in}}(\mathcal{T}) \cup \mathcal{E}_k^{\text{out}}(\mathcal{T})\}$. This property allows us to relate vector entries of a node and the edges (and its weights) of its network neighbours.

Equation (4.43) allows us to compute the time derivative of γ_i and relate it to both inter-agent position and velocity vectors, and the edge weights gradient with respect to the agent's position as follows:

$$\begin{aligned} \dot{\gamma}_i &= \sum_{\mathcal{T} \in \mathbb{T}_i(\mathcal{D})} \sum_{(k,j) \in \mathcal{E}(\mathcal{T})} v_{jk}^T \nabla_{p_j} a_{jk}(\|p_{jk}\|) \mathbf{P}(\mathcal{E}(\mathcal{T}) \setminus \{(k,j)\}) \\ &= \sum_{\mathcal{T} \in \mathbb{T}_i(\mathcal{D})} \mathbf{P}(\mathcal{E}(\mathcal{T})) \sum_{(k,j) \in \mathcal{E}(\mathcal{T})} b_{kj}(\|p_{jk}\|) \frac{v_{jk}^T p_{jk}}{\|p_{jk}\|}. \end{aligned} \quad (4.45)$$

The second inequality uses the property shown in equation (4.39) and the fact that $\mathbf{P}(\mathcal{E}(\mathcal{T})) = a_{jk}(\|p_{jk}\|) \mathbf{P}(\mathcal{E}(\mathcal{T}) \setminus \{(k,j)\})$. Similarly, we can compute gradients for agent positions of the eigenvector entries. That is, the gradient of γ_i respect to agent's position p_i is

$$\begin{aligned} \nabla_{p_i} \gamma_i &= \sum_{\mathcal{T} \in \mathbb{T}_i(\mathcal{D})} \sum_{(k,i) \in \mathcal{E}_i^{\text{in}}(\mathcal{T})} \nabla_{p_i} a_{ik}(\|p_{ik}\|) \mathbf{P}(\mathcal{E}(\mathcal{T}) \setminus \{(k,i)\}) \\ &= \sum_{\mathcal{T} \in \mathbb{T}_i(\mathcal{D})} \mathbf{P}(\mathcal{E}(\mathcal{T})) \sum_{(k,i) \in \mathcal{E}_i^{\text{in}}(\mathcal{T})} b_{ik}(\|p_{ik}\|) \frac{p_{ik}}{\|p_{ik}\|}. \end{aligned} \quad (4.46)$$

In this case that the inner sum is over the set $\mathcal{E}_i^{\text{in}}(\mathcal{T})$ and not over $\mathcal{E}(\mathcal{T})$. This is because the i th node is the root of every spanning tree in \mathbb{T}_i , therefore, it only has incoming edges. If we compute the gradient of an entry γ_j respect to position p_i , with

$j \neq i$, we obtain

$$\begin{aligned}
 \nabla_{p_i} \gamma_j &= \sum_{\mathcal{T} \in \mathbb{T}_j(\mathcal{D})} \left[\sum_{(k,i) \in \mathcal{E}_i^{\text{in}}(\mathcal{T})} \nabla_{p_i} a_{ik}(\|p_{ik}\|) \mathbf{P}(\mathcal{E}(\mathcal{T}) \setminus \{(k,i)\}) \right. \\
 &\quad \left. + \sum_{(i,l) \in \mathcal{E}_i^{\text{out}}(\mathcal{T})} \nabla_{p_i} a_{li}(\|p_{li}\|) \mathbf{P}(\mathcal{E}(\mathcal{T}) \setminus \{(i,l)\}) \right] \quad (4.47) \\
 &= \sum_{\mathcal{T} \in \mathbb{T}_j(\mathcal{D})} \mathbf{P}(\mathcal{E}(\mathcal{T})) \left[\sum_{(k,i) \in \mathcal{E}_i^{\text{in}}(\mathcal{T})} b_{ik}(\|p_{ik}\|) \frac{p_{ik}}{\|p_{ik}\|} + \sum_{(i,l) \in \mathcal{E}_i^{\text{out}}(\mathcal{T})} b_{li}(\|p_{li}\|) \frac{p_{li}}{\|p_{li}\|} \right].
 \end{aligned}$$

Notice the sums are over all in- and out-edges of the i th node. In the case of node i being a leaf of the tree $\mathcal{T} \in \mathbb{T}_j$, the sum is over the out-edges only.

Remark 4.7. Equation (4.43), and those derived from it, depend on the set of the directed trees contained in \mathcal{D} and rooted at the node of interest. To the best of our knowledge, there is no reported distributed algorithm to identify the set $\mathbb{T}_i(\mathcal{D})$, for any $i \in \mathcal{V}_{\mathcal{D}}$. The well-known Dijkstra's and Edmond's algorithms identify the minimum weighted rooted tree on a digraph. However, a method to retrieve every tree in $\mathbb{T}_i(\mathcal{D})$ still is a case of study. This observation leads us to the following assumption.

Assumption 4.3. The i th agent computes the set $\mathbb{T}_i(\mathcal{D})$ and vectors $\nabla_{p_i} \gamma_i$ and $\nabla_{p_i} \gamma_j$, for all $j \in \mathcal{N}_i^{\text{in}}(p)$.

With this position-dependent first left eigenvector, we embed agent's positions into our connectivity measure. In consequence, connectivity measure (4.38) is position-dependent. We will discuss the consequences below.

Position-dependent connectivity measure

With the definition of the position-dependent first left eigenvector, we get a position-dependent connectivity measure. Therefore, we can compute time-derivatives and gradients of (4.38). In this section, we describe their properties and implications.

First, from Lemmas 2.6 and 2.7, notice that some entry of the first left eigenvector is zero, if and only if the digraph is not strongly connected. Then, there exist some configurations of multi-agent system (4.36) that lead to non-strongly connected proximity digraphs. The following Lemma relates the time-varying property of strongly connected proximity digraphs with the connectivity measure.

Lemma 4.5. Let $\mathcal{D}(c) = (\mathcal{V}, \mathcal{E})$ be a graph parametrized continuously by c such that $\mathcal{D}(c)$ is strongly connected $\forall c > 0$. Let $L(c)$ be its matrix Laplacian with first left eigenvector $\gamma(c)$. Let $\mathcal{D}(0)$ be the subgraph of $\mathcal{D}(c)$ obtained when $c = 0$, such that $\mathcal{D}(0)$ has at least one weakly connected component. Let \mathcal{E}_0 be the subset of edges in \mathcal{E} that are deleted when $c = 0$. Let $\mathcal{E}' \subset \mathcal{E}_0$ the set of edges belonging to a minimal connected edge set of $\mathcal{D}(0)$. Then, There exists $(i, j) \in \mathcal{E}'$ such that $\mu_{ij} \rightarrow 0$ as $c \rightarrow 0^+$.

This lemma's proof follows the same steps of Lemma IV.9 in [94]. Therefore, we omitted it here. Notice, Lemma 4.5 states that, for a strongly connected digraph \mathcal{D} , the connectivity measure μ_{ij} tends to infinity as \mathcal{D} approaches to a not strongly connected configuration. We'll use this fact later in our controller design.

Connectivity measure (4.38) change as eigenvector entries γ_i and γ_j does. We now present the rate change properties of μ_{ij} concerning time and agent's positions in terms of equations (4.43)-(4.47). The time derivative of connectivity measure (4.38) is

$$\dot{\mu}_{ij} = \frac{\partial \mu_{ij}}{\partial \gamma_i} \dot{\gamma}_i + \frac{\partial \mu_{ij}}{\partial \gamma_j} \dot{\gamma}_j. \quad (4.48)$$

Meanwhile, the gradient of μ_{ij} in the direction of the agent's position p_i is

$$\nabla_{p_i} \mu_{ij} = \frac{\partial \mu_{ij}}{\partial \gamma_i} \nabla_{p_i} \gamma_i + \frac{\partial \mu_{ij}}{\partial \gamma_j} \nabla_{p_i} \gamma_j. \quad (4.49)$$

where

$$\frac{\partial \mu_{ij}}{\partial \gamma_i} = \frac{1}{\gamma_j} - \frac{\gamma_j}{\gamma_i^2} \quad \text{and} \quad \frac{\partial \mu_{ij}}{\partial \gamma_j} = \frac{1}{\gamma_i} - \frac{\gamma_i}{\gamma_j^2}.$$

Notice, for this connectivity measure, we have that $\frac{\partial \mu_{ij}}{\partial \gamma_j} = -\frac{\gamma_i}{\gamma_j} \frac{\partial \mu_{ij}}{\partial \gamma_i}$.

So far, we have constructed and discussed the properties of a connectivity measure based on the first left eigenvector of the Laplacian matrix. In the next subsection, this measure is used to build a distributed controller to preserve the proximity digraph's strong connectivity while the group of agents maintain a flocking motion behaviour.

4.2.2 Controller design

We aim to design control actions to preserve proximity digraph's strong connectivity and induce a leaderless flocking motion, as described in Definition 2.5, in the multi-agent system (4.36). We will use an approach similar to that used for the bidirectional case (section 4.1), where the shape of the APF is key for our result. However, we will modify the APF's design. Since we will not preserve every single edge in $\mathcal{E}(p)$, we allow the APF to take different values as the inter-agent distance approach the sensing radius. The actual value of the APF will depend on both inter-agent distances and the connectivity measure described in section (4.38). We begin our design with the APF's definition, in charge of inter-agent position control. Then, we discuss a velocity consensus term used to fulfil the velocity alignment objective.

Let $\psi_{ij}(\cdot, \cdot) : [0, r_i] \times (1, \infty) \mapsto \mathbb{R}_{\geq 0}$ be an APF, with partial derivatives $\phi_{ij}(s_1, s_2) := \frac{\partial \psi_{ij}(s_1, s_2)}{\partial s_1}$ and $\varphi_{ij}(s_1, s_2) := \frac{\partial \psi_{ij}(s_1, s_2)}{\partial s_2}$, be defined with the following properties:

- (i) For all $s_1 \in [0, r_i]$ and $s_2 \in (1, \infty)$, $0 \leq \psi_{ij}(s_1, s_2)$;
- (ii) For all $s_1 \in [0, r_i]$ and any $s_2 \in (1, \infty)$, $\phi_{ij}(s_1, s_2) < 0$;
- (iii) For all $s_2 \in (1, \infty)$ and any $s_1 \in [0, r_i]$, $\varphi_{ij}(s_1, s_2) > 0$;
- (iv) $|\phi_{ij}(s_1, s_2)| \leq \bar{\phi}_{ij}$ with $\bar{\phi}_{ij} < \infty$;
- (v) $\varphi_{ij}(s_1, s_2) = \frac{1}{s_2} \chi_{ij}(s_1, s_2)$ with $|\chi_{ij}(s_1, s_2)| \leq \bar{\chi}_{ij} < \infty$.

Property (i) states the potential function is non-negative. Properties (ii-iii) states $\psi_{ij}(s_1, s_2)$ is a decreasing function of s_1 but increasing for s_2 . Property (iv) states $|\phi_{ij}(s_1, s_2)|$ is bounded for all values of s_1 and s_2 . Meanwhile, property (v) states $\varphi_{ij}(s_1, s_2)$ is bounded by a relation of s_2 and a bounded function of both inputs. Computing $\nabla_{p_i} \psi_{ij}(\|p_{ij}\|, \mu_{ij})$, we obtain a vector force in the direction of the minimum value of $\psi_{ij}(\|p_{ij}\|, \mu_{ij})$, *i.e.* towards the desired inter-robot distance and connectivity measure, as follows:

$$\nabla_{p_i} \psi_{ij}(\|p_{ij}\|, \mu_{ij}) = \phi_{ij}(\|p_{ij}\|, \mu_{ij}) \frac{p_{ij}}{\|p_{ij}\|} + \varphi_{ij}(\|p_{ij}\|, \mu_{ij}) \nabla_{p_i} \mu_{ij}. \quad (4.51)$$

On the other hand, the time-derivative of APF $\psi_{ij}(\cdot, \cdot)$ is

$$\dot{\psi}_{ij}(\|p_{ij}\|, \mu_{ij}) = \phi_{ij}(\|p_{ij}\|, \mu_{ij}) \frac{v_{ij}^T p_{ij}}{\|p_{ij}\|} + \varphi_{ij}(\|p_{ij}\|, \mu_{ij}) \dot{\mu}_{ij}. \quad (4.52)$$

The second controller's term, as in our previous controller designs, is a velocity consensus function. Here, the distance dependent edge weights defined in equation (4.39) are considered. The explicit form of this term can be seen in the definition of the controller shown below.

Consider the following controller:

$$u_i = -\frac{1}{\gamma_i} \sum_{j \in \mathcal{N}_i^{\text{in}}(p)} \nabla_{p_i} \psi_{ij}(\|p_{ij}\|, \mu_{ij}) - c \sum_{j \in \mathcal{N}_i^{\text{in}}(p)} a_{ij}(\|p_{ij}\|) (v_i - v_j), \quad i \in \mathcal{I}. \quad (4.53)$$

The key difference between this and previously defined controllers is due to the APF's dependency on the connectivity measure μ_{ij} and the non-constant distance dependent edge weights. We also drop the use of the neighborhood hysteresis process. Here, the addition/deletion of in-neighbors is a continuous process, as can be seen from the adjacency matrix elements definition from equation (4.39).

4.2.3 Stability analysis

In this section, we discuss the stability of the closed loop system (4.36)-(4.53). First, we define a velocity disagreement vector; The way it is defined and its properties will be useful for our stability analysis. Then, the collective energy, through which we will analyze the closed-loop stability, is described.

Disagreement vector

Let $\gamma \in \mathbb{R}$ be the first left eigenvector of the matrix Laplacian $L(\mathcal{D})$ associated with a strongly connected proximity graph $\mathcal{D}(p)$. Denote as $v = [v_1^T, \dots, v_N^T]^T$ the stack velocity vector of the whole multi-agent system (4.36). Introduce a new variable

$$\delta = [(I_N - \mathbf{1}_N \gamma^T) \otimes I_n] v, \quad (4.54)$$

where notice $\mathbf{1}_N \gamma^T \in \mathbb{R}^{N \times N}$. Each entry of δ is

$$\delta_i = v_i - \sum_{k=1}^N \gamma_k v_k, \quad i \in \mathcal{I}. \quad (4.55)$$

Notice δ_i sets a difference between the i th agent's velocity and the weighted sum of all other agent velocities; The weights are, in fact, the entries of vector γ . The time-derivative of δ_i its given by the following equation

$$\dot{\delta}_i = u_i - \sum_{k=1}^N (\dot{\gamma}_k v_k + \gamma_k u_k), \quad i \in \mathcal{I}, \quad (4.56)$$

where $\dot{\gamma}_k$ is described by the equation (4.45).

Remark 4.8. *Previous works use the disagreement vector δ in the stability analysis for consensus problems over directed graphs (see [103] and references therein). However, they consider fixed information networks. Here, we deal with proximity digraphs of moving agents and, therefore, time-varying eigenvectors.*

The following lemma summarizes some properties of the disagreement vector.

Lemma 4.6. *Consider a strongly connected proximity digraph $\mathcal{D}(p)$ with matrix Laplacian $L(\mathcal{D})$. Let $\gamma \in \mathbb{R}_{>0}^N$ be such that $\gamma^T L(\mathcal{D}) = \mathbf{0}_N^T$ and satisfy $\gamma^T \mathbf{1}_N = 1$. Then the following statements/equalities hold:*

- i) $\delta = \mathbf{0}_{Nn}$ if and only if $v_1 = \dots = v_N$.
- ii) $\sum_{i=1}^N \gamma_i \delta_i = \mathbf{0}_n$.
- iii) $\sum_{i=1}^N \dot{\gamma}_i (\delta_i - v_i) = \mathbf{0}_n$.
- iv) If $\|v\| \leq \bar{v}$, then $\|\delta_i\| \leq (1 - \gamma_i) \bar{v}$ for all $i \in \mathcal{I}$.

Proof. Proof of statement i): By definition of γ , it is easy to verify that δ satisfies

$$(\gamma^T \otimes I_n) \delta = \mathbf{0}_{Nn}.$$

Also, by the definition of γ , it is not difficult to see that 0 is a simple eigenvalue of matrix $I_N - \mathbf{1}_N \gamma^T$ with $\mathbf{1}_N$ as the corresponding eigenvector and 1 is another eigenvalue with multiplicity $N - 1$. Then, it follows from (4.54) that $\delta = \mathbf{0}_{Nn}$ if and only if $v_1 = \dots = v_N$.

Proof of statement ii): From the definition of δ_i we have that

$$\begin{aligned} \sum_{i=1}^N \gamma_i \delta_i &= \sum_{i=1}^N \gamma_i \left(v_i - \sum_{k=1}^N \gamma_k v_k \right), \\ &= \sum_{i=1}^N \gamma_i v_i - \left(\sum_{i=1}^N \gamma_i \right) \sum_{k=1}^N \gamma_k v_k, \\ &= \sum_{i=1}^N \gamma_i v_i - \sum_{k=1}^N \gamma_k v_k = \mathbf{0}_n. \end{aligned}$$

where for the last equality we use the fact that $\gamma^T \mathbf{1}_N = 1$.

Proof of statement *iii*): From statement *ii*) we know that $\sum_{i=1}^N \gamma_i \delta_i = 0$, *i.e.* a constant, this implies that $\frac{d}{dt} \sum_{i=1}^N \gamma_i \delta_i = 0$. Now, notice

$$\begin{aligned} \frac{d}{dt} \sum_{i=1}^N \gamma_i \delta_i &= \sum_{i=1}^N \left(\dot{\gamma}_i \delta_i + \gamma_i \left[u_i - \sum_{k=1}^N (\dot{\gamma}_k v_k + \gamma_k u_k) \right] \right), \\ &= \sum_{i=1}^N (\dot{\gamma}_i \delta_i + \gamma_i u_i) - \left(\sum_{i=1}^N \gamma_i \right) \left(\sum_{k=1}^N (\dot{\gamma}_k v_k + \gamma_k u_k) \right), \\ &= \sum_{i=1}^N \dot{\gamma}_i (\delta_i - v_i) = \mathbf{0}_n, \end{aligned}$$

where, again, for the last inequality, we use that fact that $\gamma^T \mathbf{1}_N = 1$.

Proof of statement *iv*): Assumption $\|v\| \leq \bar{v}$ implies that $\|v_i - v_k\| \leq \bar{v}$ for all $i, k \in \mathcal{I}$ with $k \neq i$. From the definition of δ_i and assumption $\gamma^T \mathbf{1}_N = 1$ we have

$$\|\delta_i\| = \left\| \sum_{k=1}^N \gamma_k (v_i - v_k) \right\| \leq \sum_{k \neq i} \gamma_k \|v_i - v_k\| = (1 - \gamma_i) \bar{v},$$

where for the last inequality we use the fact that $\sum_{k \neq i} \gamma_k = 1 - \gamma_i$. \square

Disagreement vector properties are key to the close-loop system's stability analysis. We discuss this relationship in the following section.

Collective energy

In this section, we present the energy function with which we will study the stability of the closed-loop system (4.36)-(4.53). We discuss its relation with the flocking motion and connectivity preservation objectives. Then, we analyze its time-derivative, which leads us to a lemma, essential for our main result.

Define the collective energy of the closed-loop system (4.36)-(4.53), as follows

$$V(p, v) := \frac{1}{2} \sum_{i=1}^N \sum_{j \in \mathcal{N}_i^{\text{in}}(p)} \psi_{ij}(\|p_{ij}\|, \mu_{ij}) + \frac{1}{2} \sum_{i=1}^N \gamma_i \|\delta_i\|^2. \quad (4.57)$$

This equation summarizes the artificial potential and kinetic energies of the overall closed-loop system. The minimum collective energy takes place in a configuration p^* such that the sum of APFs is locally minimal and a velocity vector v^* , such that $v_1 = \dots = v_N$. On the other hand, for strongly connected proximity digraphs $\mathcal{D}(p)$, configurations p such that $\|p_{ij}\| > 0$ for all $i, j \in \mathcal{I}$ with $j \neq i$, and bounded velocity vector v , there exists a $\bar{V} \in \mathbb{R}_{>0}$ such that $V(p, v) \leq \bar{V} < \infty$.

Before we continue our analysis of the collective energy function, and to keep the notation as short as possible, we will write $V(p, v) = V$, $\psi_{ij} = \psi_{ij}(\|p_{ij}\|, \mu_{ij})$, $\phi_{ij} = \phi_{ij}(\|p_{ij}\|, \mu_{ij})$, $\varphi_{ij} = \varphi_{ij}(\|p_{ij}\|, \mu_{ij})$ and so on.

Take the time-derivative of equation (4.57), we get

$$\dot{V} = \frac{1}{2} \sum_{i=1}^N \sum_{j \in \mathcal{N}_i^{\text{in}}(p)} \dot{\psi}_{ij} + \frac{1}{2} \sum_{i=1}^N \left(\dot{\gamma}_i \|\delta_i\|^2 + 2\gamma_i \delta_i^T \dot{\delta}_i \right),$$

where the terms $\dot{\gamma}_i$, $\dot{\psi}_{ij}$ and $\dot{\delta}_i$, are described in equations (4.45), (4.52) and (4.56), respectively. Notice that

$$\begin{aligned} \sum_{i=1}^N \gamma_i \delta_i^T \dot{\delta}_i &= \sum_{i=1}^N \gamma_i \delta_i^T \left(u_i - \sum_{k=1}^N (\dot{\gamma}_k v_k + \gamma_k u_k) \right), \\ &= \sum_{i=1}^N \gamma_i \delta_i^T u_i - \sum_{i=1}^N \gamma_i \delta_i^T \left(\sum_{k=1}^N (\dot{\gamma}_k v_k + \gamma_k u_k) \right), \\ &= \sum_{i=1}^N \gamma_i \delta_i^T u_i, \end{aligned}$$

where, for the last inequality, we use Lemma 4.6 property *ii*) to eliminate the latest term of the second inequality. Therefore, collective energy time-derivative is

$$\dot{V} = \frac{1}{2} \sum_{i=1}^N \sum_{j \in \mathcal{N}_i^{\text{in}}(p)} \dot{\psi}_{ij} + \frac{1}{2} \sum_{i=1}^N \dot{\gamma}_i \|\delta_i\|^2 + \sum_{i=1}^N \gamma_i \delta_i^T u_i, \quad (4.58)$$

As we are considering proximity digraphs, the information network's topology might change over time. Suppose the topology of $\mathcal{D}(p)$ switches every time instant t_k with $k = 1, 2, \dots$, and remains fixed over the time interval $[t_{k-1}, t_k)$. At each time instant t_k , edges might be added or removed from $\mathcal{E}(p)$. The following lemma studies the time-derivative of the collective energy function (4.57) in the time interval $[t_{k-1}, t_k)$.

Lemma 4.7. *Consider the closed-loop system (4.36)-(4.53) for the time interval $[t_{k-1}, t_k)$ where no edges are added nor deleted. Denote V_{k-1} the collective energy at time instant t_{k-1} . Suppose at time instant t_{k-1} configuration p is such that the proximity digraph $\mathcal{D}(p)$ is strongly connected, vector v is bounded and, for all $t \in [t_{k-1}, t_k)$,*

$$c \geq \frac{\bar{b}}{\tilde{\gamma}\alpha(t)} (4N(N-1)^2(\bar{\phi} + \bar{\chi}) + \bar{v}) \quad (4.59)$$

where $\tilde{\gamma} = \min_{i \in \mathcal{I}} \{\gamma_i\}$. Then $V_k \leq V_{k-1}$ for all $t \in [t_{k-1}, t_k)$.

Proof. Before we begin our collective energy analysis, notice that, from our assumptions, there exists some \bar{v} such that $\|v\| \leq \bar{v}$. Then, from Lemma 4.6, $\|\delta_i\|$ is bounded for all $i \in \mathcal{I}$.

Plugging in controller (4.53) into the last term of equation (4.58), we get

$$\begin{aligned} \sum_{i=1}^N \gamma_i \delta_i^T u_i &= - \sum_{i=1}^N \delta_i^T \sum_{j \in \mathcal{N}_i^{\text{in}}(p)} \nabla_{p_i} \psi_{ij} - c \sum_{i=1}^N \gamma_i \delta_i^T \sum_{j \in \mathcal{N}_i^{\text{in}}(p)} a_{ij} (\|p_{ij}\|) (\delta_i - \delta_j), \\ &= - \sum_{i=1}^N \delta_i^T \sum_{j \in \mathcal{N}_i^{\text{in}}(p)} \nabla_{p_i} \psi_{ij} - \frac{c}{2} \delta^T \left([\Gamma \mathcal{L}(p) + \mathcal{L}^T(p) \Gamma] \otimes I_n \right) \delta \end{aligned}$$

where notice $\delta_i - \delta_j = v_i - v_j$ and for the second equality matrix $\Gamma = \text{diag}(\gamma_1, \dots, \gamma_N)$. Therefore, equation (4.58) is

$$\begin{aligned} \dot{V} = & \sum_{i=1}^N \sum_{j \in \mathcal{N}_i^{\text{in}}(p)} \left(\frac{1}{2} \dot{\psi}_{ij} - \delta_i^T \nabla_{p_i} \psi_{ij} \right) + \frac{1}{2} \sum_{i=1}^N \dot{\gamma}_i \|\delta_i\|^2 \\ & - \frac{c}{2} \delta^T \left([\Gamma \mathcal{L}(p) + \mathcal{L}^T(p) \Gamma] \otimes I_n \right) \delta. \end{aligned} \quad (4.60)$$

We analyze each term of this equation separately.

Let us center our attention to the first term. From equations (4.51) and (4.52), notice

$$\begin{aligned} \sum_{i=1}^N \sum_{j \in \mathcal{N}_i^{\text{in}}(p)} \left(\frac{1}{2} \dot{\psi}_{ij} - \delta_i^T \nabla_{p_i} \psi_{ij} \right) = & \sum_{i=1}^N \sum_{j \in \mathcal{N}_i^{\text{in}}(p)} \phi_{ij} \left(\frac{v_{ij}^T p_{ij}}{2 \|p_{ij}\|} - \delta_i^T \frac{p_{ij}}{\|p_{ij}\|} \right) \\ & + \sum_{i=1}^N \sum_{j \in \mathcal{N}_i^{\text{in}}(p)} \varphi_{ij} \left(\frac{\dot{\mu}_{ij}}{2} - \delta_i^T \nabla_{p_i} \mu_{ij} \right). \end{aligned} \quad (4.61)$$

We now study the properties of both terms in the right hand side of the equations. For the first term of the right hand side of equation (4.61) is easy to show that, for all pair of agents $i, j \in \mathcal{I}$ such that $\|p_{ij}\| \leq \min\{r_i, r_j\}$, *i.e.* $(i, j), (j, i) \in \mathcal{E}(p)$, the sum

$$\phi_{ij} \left(\frac{v_{ij}^T p_{ij}}{2 \|p_{ij}\|} - \delta_i^T \frac{p_{ij}}{\|p_{ij}\|} \right) + \phi_{ji} \left(\frac{v_{ji}^T p_{ji}}{2 \|p_{ji}\|} - \delta_j^T \frac{p_{ji}}{\|p_{ji}\|} \right) = 0.$$

Now, define the set $\vec{\mathcal{E}}(p) := \{(l, k) \in \mathcal{E}(p) \mid (k, l) \notin \mathcal{E}(p)\}$, clearly $\vec{\mathcal{E}}(p) \subseteq \mathcal{E}(p)$. Then, the sum

$$\sum_{i=1}^N \sum_{j \in \mathcal{N}_i^{\text{in}}(p)} \phi_{ij} \left(\frac{v_{ij}^T p_{ij}}{2 \|p_{ij}\|} - \delta_i^T \frac{p_{ij}}{\|p_{ij}\|} \right) = \frac{1}{2} \sum_{(j,i) \in \vec{\mathcal{E}}(p)} \phi_{ij} (v_{ij} - 2\delta_i)^T \frac{p_{ij}}{\|p_{ij}\|}$$

is the sum of every edge of $\mathcal{D}(p)$ that has no reciprocal. Notice $v_{ij} - 2\delta_i = -(\delta_i + \delta_j)$ and the previous sum is bounded as

$$\begin{aligned} \left\| \sum_{(j,i) \in \vec{\mathcal{E}}(p)} \phi_{ij} (v_{ij} - 2\delta_i)^T \frac{p_{ij}}{\|p_{ij}\|} \right\| & \leq \sum_{(j,i) \in \vec{\mathcal{E}}(p)} |\phi_{ij}| \|\delta_i + \delta_j\|, \\ & \leq \sum_{(j,i) \in \vec{\mathcal{E}}(p)} |\phi_{ij}| (2[1 - (\gamma_i + \gamma_j)] \bar{v} + |\gamma_j - \gamma_i| \|v_i - v_j\|), \\ & \leq 2\bar{v} \sum_{(j,i) \in \vec{\mathcal{E}}(p)} |\phi_{ij}| (1 - 2\bar{\gamma}_{ij}), \end{aligned}$$

where $\bar{\gamma}_{ij} = \max\{\gamma_i, \gamma_j\}$. Therefore,

$$\begin{aligned} \left| \sum_{i=1}^N \sum_{j \in \mathcal{N}_i^{in}(p)} \phi_{ij} \left(\frac{v_{ij}^T p_{ij}}{2 \|p_{ij}\|} - \delta_i^T \frac{p_{ij}}{\|p_{ij}\|} \right) \right| &\leq 2\bar{v} \sum_{(j,i) \in \bar{\mathcal{E}}(p)} |\phi_{ij}| (1 - 2\bar{\gamma}_{ij}), \\ &\leq 2\bar{v}\bar{\phi} |\bar{\mathcal{E}}(p)|, \end{aligned}$$

where $\bar{\phi} = \max_{(j,i) \in \mathcal{E}(p)} \{|\phi_{ij}|\}$. As for the second term of the right-hand side of equation (4.61), all pair of agents such that $(i, j), (j, i) \in \mathcal{E}(p)$, the sum

$$\varphi_{ij} \left(\frac{\dot{\mu}_{ij}}{2} - \delta_i^T \nabla_{p_i} \mu_{ij} \right) + \varphi_{ji} \left(\frac{\dot{\mu}_{ji}}{2} - \delta_j^T \nabla_{p_j} \mu_{ji} \right) = \varphi_{ij} \left(\dot{\mu}_{ij} - \delta_i^T \nabla_{p_i} \mu_{ij} - \delta_j^T \nabla_{p_j} \mu_{ji} \right),$$

where notice $\varphi_{ij} = \varphi_{ji}$ and $\dot{\mu}_{ij} = \dot{\mu}_{ji}$, and the sum on the right-hand side of this equation

$$\begin{aligned} \dot{\mu}_{ij} - \delta_i^T \nabla_{p_i} \mu_{ij} - \delta_j^T \nabla_{p_j} \mu_{ji} &= \frac{\partial \mu_{ij}}{\partial \gamma_i} (\dot{\gamma}_i - \delta_i^T \nabla_{p_i} \gamma_i - \delta_j^T \nabla_{p_j} \gamma_i) \\ &\quad + \frac{\partial \mu_{ij}}{\partial \gamma_j} (\dot{\gamma}_j - \delta_j^T \nabla_{p_j} \gamma_j - \delta_i^T \nabla_{p_i} \gamma_j) \end{aligned}$$

where

$$\begin{aligned} \dot{\gamma}_i - \delta_i^T \nabla_{p_i} \gamma_i - \delta_j^T \nabla_{p_j} \gamma_i &= - \sum_{\mathcal{T} \in \mathbb{T}_i(\mathcal{D})} \mathbf{P}(\mathcal{E}(\mathcal{T})) \left(\sum_{\substack{(k,i) \in \mathcal{E}_i^{in}(\mathcal{T}) \\ k \neq j}} b_{ik}(\|p_{ik}\|) \frac{\delta_k^T p_{ik}}{\|p_{ik}\|} \right. \\ &\quad \left. + \sum_{(l,j) \in \mathcal{E}_j^{in}(\mathcal{T})} b_{jl}(\|p_{jl}\|) \frac{\delta_l^T p_{jl}}{\|p_{jl}\|} - \sum_{(n,m) \in \bar{\mathcal{E}}(\mathcal{T})} b_{mn}(\|p_{mn}\|) \frac{\delta_{mn}^T p_{mn}}{\|p_{mn}\|} \right), \end{aligned}$$

with $\bar{\mathcal{E}}(\mathcal{T}) = \mathcal{E}(\mathcal{T}) \setminus \{\mathcal{E}_i^{in}(\mathcal{T}) \cup \mathcal{E}_j^{in}(\mathcal{T})\}$, and

$$\begin{aligned} \dot{\gamma}_j - \delta_j^T \nabla_{p_j} \gamma_j - \delta_i^T \nabla_{p_i} \gamma_j &= - \sum_{\mathcal{T} \in \mathbb{T}_j(\mathcal{D})} \mathbf{P}(\mathcal{E}(\mathcal{T})) \left(\sum_{\substack{(k,j) \in \mathcal{E}_j^{in}(\mathcal{T}) \\ k \neq i}} b_{jk}(\|p_{jk}\|) \frac{\delta_k^T p_{jk}}{\|p_{jk}\|} \right. \\ &\quad \left. + \sum_{(l,i) \in \mathcal{E}_i^{in}(\mathcal{T})} b_{il}(\|p_{il}\|) \frac{\delta_l^T p_{il}}{\|p_{il}\|} - \sum_{(n,m) \in \hat{\mathcal{E}}(\mathcal{T})} b_{mn}(\|p_{mn}\|) \frac{\delta_{mn}^T p_{mn}}{\|p_{mn}\|} \right), \end{aligned}$$

with $\hat{\mathcal{E}}(\mathcal{T}) = \mathcal{E}(\mathcal{T}) \setminus \{\mathcal{E}_j^{in}(\mathcal{T}) \cup \mathcal{E}_i^{in}(\mathcal{T})\}$. Notice, both of the previous terms are bounded as follows

$$\begin{aligned} |\dot{\gamma}_i - \delta_i^T \nabla_{p_i} \gamma_i - \delta_j^T \nabla_{p_j} \gamma_i| &\leq \gamma_i \bar{b}\bar{v}(N-2) \text{ and} \\ |\dot{\gamma}_j - \delta_j^T \nabla_{p_j} \gamma_j - \delta_i^T \nabla_{p_i} \gamma_j| &\leq \gamma_j \bar{b}\bar{v}(N-2), \end{aligned}$$

where $\bar{b} = \max_{(y,x) \in \mathcal{E}(\mathcal{D}(p))} \{ \|b_{xy}(\|p_{xy}\|) \}$. Finally, notice

$$\begin{aligned} |\varphi_{ij} (\dot{\mu}_{ij} - \delta_i^T \nabla_{p_i} \mu_{ij} - \delta_j^T \nabla_{p_j} \mu_{ji})| &\leq |\varphi_{ij}| \left(\left| \frac{\partial \mu_{ij}}{\partial \gamma_i} \right| (\gamma_i \bar{b} \bar{v} (N-2)) + \left| \frac{\partial \mu_{ij}}{\partial \gamma_j} \right| (\gamma_j \bar{b} \bar{v} (N-2)) \right) \\ &\leq 2 |\varphi_{ij}| \mu_{ij} \bar{b} \bar{v} (N-2), \\ &\leq 2 \bar{\chi} \bar{b} \bar{v} (N-2) \end{aligned}$$

where, for the last two inequalities, we use properties *iii*) in Proposition 4.1 and *iv*) of equation (4.50). On the other hand, for those edges in the set $\bar{\mathcal{E}}(p)$, we have

$$\varphi_{ij} \left(\frac{\dot{\mu}_{ij}}{2} - \delta_i^T \nabla_{p_i} \mu_{ij} \right) = \varphi_{ij} \left(\frac{\partial \mu_{ij}}{\partial \gamma_i} (\dot{\gamma}_i - \delta_i^T \nabla_{p_i} \gamma_i) + \frac{\partial \mu_{ij}}{\partial \gamma_j} (\dot{\gamma}_j - \delta_i^T \nabla_{p_i} \gamma_j) \right)$$

where

$$\begin{aligned} \dot{\gamma}_i - \delta_i^T \nabla_{p_i} \gamma_i &= - \sum_{\mathcal{T} \in \mathbb{T}_i(\mathcal{D})} \mathbf{P}(\mathcal{E}(\mathcal{T})) \left(\sum_{(k,i) \in \mathcal{E}_i^{in}(\mathcal{T})} b_{ik}(\|p_{ik}\|) \frac{\delta_k^T p_{ik}}{\|p_{ik}\|} \right. \\ &\quad \left. - \sum_{(y,x) \in \bar{\mathcal{E}}(\mathcal{T})} b_{xy}(\|p_{xy}\|) \frac{\delta_{xy}^T p_{xy}}{\|p_{xy}\|} \right) \end{aligned}$$

where $\bar{\mathcal{E}}(\mathcal{T}) = \mathcal{E}(\mathcal{T}) \setminus \mathcal{E}_i^{in}(\mathcal{T})$, and

$$\begin{aligned} \dot{\gamma}_j - \delta_i^T \nabla_{p_i} \gamma_j &= - \sum_{\mathcal{T} \in \mathbb{T}_j(\mathcal{D})} \mathbf{P}(\mathcal{E}(\mathcal{T})) \left(\sum_{(k,i) \in \mathcal{E}_i^{in}(\mathcal{T})} b_{ik}(\|p_{ik}\|) \frac{\delta_k^T p_{ik}}{\|p_{ik}\|} \right. \\ &\quad \left. - \sum_{(i,l) \in \mathcal{E}_i^{out}(\mathcal{T})} b_{li}(\|p_{li}\|) \frac{(\delta_l - 2\delta_i)^T p_{li}}{\|p_{li}\|} - \sum_{(y,x) \in \bar{\mathcal{E}}(\mathcal{T})} b_{xy}(\|p_{xy}\|) \frac{\delta_{xy}^T p_{xy}}{\|p_{xy}\|} \right) \end{aligned}$$

with $\hat{\mathcal{E}}(\mathcal{T}) = \mathcal{E}(\mathcal{T}) \setminus \{\mathcal{E}_i^{in}(\mathcal{T}) \cup \mathcal{E}_i^{out}(\mathcal{T})\}$. Taking the absolute value of both equations, we get

$$|\dot{\gamma}_i - \delta_i^T \nabla_{p_i} \gamma_i| \leq 2\gamma_i \bar{b} \bar{v} (N-1) \quad \text{and} \quad |\dot{\gamma}_j - \delta_i^T \nabla_{p_i} \gamma_j| \leq 2\gamma_j \bar{b} \bar{v} (N-1).$$

Hence

$$\begin{aligned} \left| \varphi_{ij} \left(\frac{\dot{\mu}_{ij}}{2} - \delta_i^T \nabla_{p_i} \mu_{ij} \right) \right| &\leq |\varphi_{ij}| \left(\left| \frac{\partial \mu_{ij}}{\partial \gamma_i} \right| (2\gamma_i \bar{b} \bar{v} (N-1)) + \left| \frac{\partial \mu_{ij}}{\partial \gamma_j} \right| (2\gamma_j \bar{b} \bar{v} (N-1)) \right) \\ &\leq 4 |\varphi_{ij}| \mu_{ij} \bar{b} \bar{v} (N-1), \\ &\leq 4 \bar{\chi} \bar{b} \bar{v} (N-1), \end{aligned}$$

where again, for the last two inequalities, we use properties *iii*) in Proposition 4.1 and *iv*) of equation (4.50). Therefore,

$$\begin{aligned} \left| \sum_{i=1}^N \sum_{j \in \mathcal{N}_i^{in}(p)} \varphi_{ij} \left(\frac{\dot{\mu}_{ij}}{2} - \delta_i^T \nabla_{p_i} \mu_{ij} \right) \right| &\leq \bar{\chi} \bar{b} \bar{v} (N-2) |\mathcal{E}(p) \setminus \bar{\mathcal{E}}(p)| + 4 \bar{\chi} \bar{b} \bar{v} (N-1) |\bar{\mathcal{E}}(p)|, \\ &\leq 4 \bar{\chi} \bar{b} \bar{v} (N-1) |\mathcal{E}(p)| \end{aligned}$$

where, for the second inequality, notice $2\bar{\chi}\bar{b}\bar{v}(N-2) \leq 4\bar{\chi}\bar{b}\bar{v}(N-1)$. Finally, plugging in all these inequalities into equation (4.61) we get an upper bound as follows

$$\begin{aligned} \left| \sum_{i=1}^N \sum_{j \in \mathcal{N}_i^{\text{in}}(p)} \left(\frac{1}{2} \dot{\psi}_{ij} - \delta_i^T \nabla_{p_i} \psi_{ij} \right) \right| &\leq 2\bar{v}\bar{\phi} |\vec{\mathcal{E}}(p)| + 4\bar{\chi}\bar{b}\bar{v}(N-1) |\mathcal{E}(p)|, \\ &\leq 4\bar{b}\bar{v}(N-1) |\mathcal{E}(p)| (\bar{\phi} + \bar{\chi}), \\ &\leq 4\bar{b}\bar{v}^2 N(N-1)^2 (\bar{\phi} + \bar{\chi}), \end{aligned}$$

where we should notice that $|\mathcal{E}(p)| \leq N(N-1)$ with the equality holding only when $\mathcal{D}(p)$ is a fully connected digraph.

With the previous analysis, we are able to bound every term in the time-derivative of collective energy (4.58) as follows

$$\dot{V} \leq \sum_{i=1}^N 4\bar{b}\bar{v}^2(N-1)^2 (\bar{\phi} + \bar{\chi}) + \frac{1}{2} \sum_{i=1}^N \dot{\gamma}_i \|\delta_i\|^2 - \frac{c}{2} \delta^T ([\Gamma \mathcal{L}(p) + \mathcal{L}^T(p) \Gamma] \otimes I_n) \delta.$$

Its easy to show that

$$\frac{1}{2} \sum_{i=1}^N \dot{\gamma}_i \|\delta_i\|^2 \leq \bar{b}\bar{v} \sum_{i=1}^N \gamma_i \|\delta_i\|^2 \leq \bar{b}\bar{v}^3.$$

And, from Lemma 2.9, we know that

$$\begin{aligned} \frac{c}{2} \delta^T ([\Gamma \mathcal{L}(p) + \mathcal{L}^T(p) \Gamma] \otimes I_n) \delta &\geq c\alpha(t) \delta^T (\Gamma \otimes I_n) \delta = c\alpha(t) \sum_{i=1}^N \gamma_i \|\delta_i\|^2 \\ &\geq c\alpha(t) \bar{\gamma} \bar{v}^2, \end{aligned}$$

where $\alpha(t) = \alpha(\mathcal{L}(p)) > 0$ is the generalized algebraic connectivity. Thus, we can resume the previous inequality for \dot{V} as follows

$$\dot{V} \leq 4\bar{b}\bar{v}^2 N(N-1)^2 (\bar{\phi} + \bar{\chi}) + \bar{b}\bar{v}^3 - c\alpha(t) \bar{\gamma} \bar{v}^2 \leq 0,$$

where the non-positivity is due to our assumption from equation (4.59). \square

Remark 4.9. Notice, from equation (4.59), the lower bound for a suitable control gain c is time-varying. That is, it changes as the proximity digraph's topology does. While $\mathcal{D}(p)$ remains strongly connected, from Lemma 2.9, we know $\alpha(t)$ is positive. Therefore, there exists a suitable finite control gain. However, up to date, there is no known lower bound of it. Moreover, the lower bound of c also changes over switching time intervals. When new edges are added or removed from $\mathcal{E}(p)$, the values of $\alpha(t)$ also switch. Therefore, for the terms involving the APFs within \dot{V} in our proof for Lemma 4.7, we consider the upper bound of the possible number of edges in $\mathcal{E}(p)$. But, we still need a constant lower bound for $\alpha(t)$ to keep our result in Lemma 4.7 over every topology switching time instant.

With this supporting Lemma, we build up our main result of this section.

Theorem 4.5. *Consider the multi-agent system (4.36)-(4.53). Suppose at t_0 multi-agent's configuration p is such that $\mathcal{D}(p)$ is strongly connected and the collective energy is bounded. Also, for controller (4.53), choose gain c such that fulfills inequality (4.59) for all $t \geq t_0$. Then, the following statements hold:*

- (i) *Proximity digraph $\mathcal{D}(p)$ is strongly connected for all $t \geq t_0$;*
- (ii) *The multi-agent system is on leaderless flocking motion.*

Proof. Proof of statement (i): Suppose the proximity digraph $\mathcal{D}(p)$ switches at every time instant t_k , with $k = 1, 2, \dots$, and remains fixed over the time interval $[t_{k-1}, t_k)$. We carry out the following analysis for $k = 1$ and then it will be extended to every time interval.

Given the topology of $\mathcal{D}(p)$ doesn't change for all $t \in [t_0, t_1)$, from Lemma 4.7, the collective energy doesn't increase, *i.e.* $V_t \leq V_{t_0}$ for all $t \in [t_0, t_1)$. Hence, V_t is bounded above by some constant value and there are no APFs approaching infinity in (4.57). From our APFs definition, this implies there are no connectivity measures approaching infinity. In consequence, the entries of eigenvector γ are such that $\gamma_i > 0$, for all $i \in \mathcal{I}$. That is, proximity digraph $\mathcal{D}(p)$ remains strongly connected for all $t \in [t_0, t_1)$.

Now, consider the time instant t_1 , where the topology of $\mathcal{D}(p)$ change. Denote, respectively, as \mathcal{E}^- and \mathcal{E}^+ the set of edges added to and removed from $\mathcal{E}(p)$ at instant t_1 . Since the remotion of edges reduce the collective energy, is clear that V_{t_1} will be smaller than V_{t_0} and our statement of the previous paragraph will still hold true. However, for edge additions, this is not the case. Notice, the collective energy at t_1 is such that

$$V_{t_1} \leq V_{t_0} + \sum_{(k,i) \in \mathcal{E}^+} \psi_{ik}.$$

However, addition of edges will not decrease the values of eigenvector entries, as we can see from their definition in equation (4.43). That is, connectivity measures μ_{ik} are bounded for all $(k, i) \in \mathcal{E}^+$ and also does the potentials ψ_{ik} . Hence, the collective energy at instant t_1 is finite, thus $\mathcal{D}(p)$ is strongly connected.

By similar reasoning over each time interval, we conclude the collective energy is finite for all time intervals. That is, there exists $\bar{V} < \infty$ such that $V_t \leq \bar{V}$ for all $t \geq 0$. Thus, the proximity digraph $\mathcal{D}(p)$ remains strongly connected for all $t \geq 0$.

Proof of statement (ii): For the multi-agent system to be in leaderless flocking motion, it must satisfy the properties described in Definition 2.5. We discuss them separately.

(The group is cohesive) We already show $\mathcal{D}(p)$ remains strongly connected for all $t \geq 0$. Therefore, the maximum distance between any pair of agents is the sum of their sensing radius, *i.e.* $\rho = \sum_{i=1}^N r_i$ for all $t \geq 0$. Hence the group is cohesive.

(Inter-robot collisions are avoided) Notice from the definition of APFs that the values of $\psi_{ij} \rightarrow \infty$ as $\|p_{ij}\| \rightarrow 0$. However, we already show, in our proof of statement (i), that there exists $\bar{V} < \infty$ such that $V_t \leq \bar{V}$ for all $t \geq 0$. In consequence, there are no distances $\|p_{ij}\|$ approaching zero for all $i, j \in \mathcal{I}$ and $t \geq 0$. Hence, inter-robot collisions are avoided.

(Inter-robot velocity mismatches are bounded) Notice vectors δ_i can be rewritten as ponderated inter-agent velocity differences as $\delta_i = \sum_{k=1}^N \gamma_k v_{ik}$. We already show the proximity digraph $\mathcal{D}(p)$ is strongly connected and the collective energy (4.57) remains bounded for all $t \geq 0$. On the one hand, this implies that every eigenvector entry is positive. And, on the other hand, the disagreement velocity vectors are bounded, that is $\|\delta_i\| \leq \sqrt{\frac{2\bar{V}}{\gamma_i}}$. With these observations, we conclude that, at any time $t \geq 0$, velocity differences $\|v_{ij}\| \leq \bar{v}$ for some $\bar{v} < \infty$. Thus, inter-robot velocity mismatches are bounded. \square

Remark 4.10. *Conclusions in Theorem 4.5 relies on the properties exhibited by the collective energy; More specifically, on its boundedness, which allowed us to ensure the strong connectivity property of $\mathcal{D}(p)$ and, at the same time, the leaderless flocking motion behaviour. However, in this case, and different from our results in Section 4.1, we cannot ensure the multi-agent system reaches a rigid configuration. Due to the proximity digraph's topology flexibility, we can't establish a positively invariant set to use Lasalle's invariance principle as we did before. Instead, we concluded the system is stable; Although this is sufficient to prove satisfaction of the flocking motion properties, we can't ensure asymptotic velocity alignment as we did in our previous results.*

Remark 4.11. *Connectivity measure (4.38) was presented in [94]. There, the objective was to preserve the strong connectivity of digraph $\mathcal{D}(p)$ and no more. The dynamics of every agent was of first-order and inter-agent collisions were allowed. The controller's design uses a sort of constrained bidirectionality over each network edge; Each agent is aware of being sensed by another with a bigger sensing radius and uses this information to compute its control actions. In contrast, we consider second-order dynamic agents and inter-agent collisions are avoided. Also, the agents are unaware of others outside their sensing radius and, therefore, compute their control actions only with local information. With these considerations/restrictions, we also ensure the strong connectivity preservation of $\mathcal{D}(p)$.*

Remark 4.12. *As we discussed in Remark 4.7, the computation of $\nabla_{p_i} \gamma_i$ and $\nabla_{p_i} \gamma_j$ requires the local knowledge of sets \mathbb{T}_i and \mathbb{T}_j . Without this information, we cannot compute $\nabla_{p_i} \mu_{ij}$ and, in consequence, neither the distributed controller (4.53). Therefore, up to date, we cannot provide any illustration for the effectiveness of the distributed controller (4.53).*

In this chapter, we studied flocking motion in multi-robot systems. Even though having different combinations of robot- and environmental-related constraints, our distributed controller designs allow multi-robot systems to exhibit flocking behaviour. These constructions extend the already existing controllers present in the literature. We also presented the first use of a first-left eigenvector based connectivity measure in combination with the gradient-descent method in a multi-robot system with heterogeneous sensing limitations. The following chapter resume this thesis' results in some final comments.

Final Comments

In this thesis, we investigated the motion coordination of a finite set of mobile robots. We designed distributed controllers under a behavioural approach while considering both robot and environmental constraints such as limited communication/sensing and motion capabilities, non-unitary inertias and environmental obstacles. Our proposed controller designs induce a desired collective behaviour in the multi-robot system.

In this work, we controlled the motion of a point of interest within two kinds of mobile robots: differential mobile robots and quadrotors. The dynamics of each of these points of interest are nonlinear; We discussed control schemes allowing us to describe their motion as a second-order system. Then, we defined consensus and flocking motion in leaderless and leader-followers configurations.

Our controller designs for consensus motion contemplated two scenarios: Fixed and proximity graphs. In the first scenario, we considered robots with uneven inertias exchanging information through a fixed directed network. Our controller designs allowed us to consider, through minor modifications, the leaderless and the leader-followers configurations, even if the leader's acceleration is time-varying. Also, sufficient and necessary conditions to achieve consensus behaviour were derived. As a result, we extended many previous works, such as [50, 51, 116, 124]. In the second scenario, we included homogeneous robot communication/sensing constraints. This limitation leads us to time-varying information networks. We used the concept of proximity graphs to model information exchange among robots. A combination of the gradient-descent method along with velocity consensus functions and a neighbourhood hysteresis process establish our controller designs. With it, we guaranteed the proximity graph's connectivity and asymptotic consensus behaviour in the multi-robot system in both leaderless and leader-followers scenarios. Here, the leader's states are available only to a portion of informed robots in the group. Also, the leader's velocity might be time-varying. Our results extend [58], where every robot must know the leader's acceleration.

On the other hand, our study on flock behaviour for multi-robot systems focused on combinations of three physical constraints: limited communication/detection ranges, input constraints, and obstacles in the workspace. We modelled the information network with proximity graphs. Since we contemplated both homogeneous and heterogeneous communication/sensing ranges, proximity graphs were either bidirectional or

directed. When the proximity graph was bidirectional, our controller designs allowed flocking motion when robots had individual input constraints, even in the presence of obstacles. With the developed designs we improve previously reported results such as [78, 117] where predictive control schemes were used, or as [80, 119], where a target determination process is needed. Our controller designs took advantage of heterogeneous input constraints and allowed robots with higher capabilities to compensate for neighbours that are less capable of meeting the group's requirements. Meanwhile, when the proximity graph was directed, our designs exploited the properties of a proposed connectivity measure. The proposed controllers are the first of their kind, as they combine the gradient descent method with a connectivity measure based on the first-left eigenvector of the matrix Laplacian. We proved the leaderless flocking motion behaviour to be stable. Nonetheless, a distributed method to compute the first-left eigenvector entries gradient is needed; And thus obtain a clear illustration of the controller effectiveness.

Multi-robot systems motion control seemed to be a colossal task; Especially when motion constraints include physical restrictions such as those considered in this work. To tackle it, we took a behavioural approach. Our design objective was to embed local heuristical rules into distributed controllers that steer the multi-robot system into the desired behaviour. The tool to do so was the gradient descent method. With a careful design of APFs, this method allowed us to control the motion of each robot. Then, using tools from graph and control theory, we showed multi-robot system states trajectories fulfil the properties of the desired behaviour. With this, we positively answer our hypothesis; It is possible to design, using a behavioural approach, distributed controllers to drive multi-robot systems into a constrained coordinated motion.

5.1 Future work

There are, possibly, several extensions to our work. We described some ideas to improve/extend the results here presented.

In Chapter 3 we solved consensus problems for both leaderless and leader followers scenarios. For the fixed information network case, our design supports constant state deviations between connected robots. Being able to change the state deviations on the fly would be helpful under environmental constrained scenarios. For the proximity graphs case, we might consider obstacle avoidance objectives as well. Robots with input constraints is another possible extension. For this last case, time-varying neighbourhood hysteresis processes would be of great help to keep control efforts below prescribed limitations. These are some possible modifications regarded to future works.

In Chapter 4, we solved leaderless and leader-follower flocking motion problems. For the bidirectional proximity graph case, there are some further research directions. To deal with heterogeneous input constraints, we had to make a detailed balance assumption. With an adaptive rule, we might remove this assumption. Consequently, this should relax the conditions to satisfy the heterogeneous input constraints. Also, a time-varying hysteresis process might be helpful in this regard. Another possible improvement is the use of connectivity measures. As we discussed, these allow more

flexible final network configurations. Especially important in the case of workspace obstacles. As for the directed proximity graphs case, there are still some aspects to consider. To compute the entire of the first-left eigenvector of the matrix Laplacian, we need a distributed algorithm to compute the transpose of this matrix. On the other hand, we need an algorithm to identify the rooted tree sets in each robot; A requirement to get the corresponding vector entries gradient to the robot's position. These are some possible improvements to our work and our future research objectives.

There are still many other challenges to be tackled in multi-robot systems control. For example, robots of different kinds lead to more heterogeneous groups - in comparison to our study. Also, many possible phenomenons might occur in the information network like communication time delays, data loss or edge intermittence, to name a few. In this thesis, we consider three of the critical constraint in multi-robot systems; However, there is still much to do.

Either relegating humans from dangerous environments such as disaster zones or finding victims of these events, improving the performance of surveillance tasks, or supporting space explorations, implementations of multi-robot systems will bring many benefits to society. There is no doubt that, over the coming years, many advances in technology will appear and support future multi-robot systems implementations. They are likely the future of robotics and robots implementations. However, none of them will be possible without mathematicians and controller designers tackling the seemly colossal task of developing theoretical frameworks to study multi-robot systems. It's up to us to pave the way and make it possible.

Bibliography

- [1] K. Čapek, P. Selver, and N. Playfair. *R.U.R: (Rossum's universal robots): a Fantastic Melodrama in Three Acts and an Epilogue*. S. French, New York, NY, 1923.
- [2] B. Siciliano, L. Sciavicco, L. Villani, and G. Oriolo. *Robotics*. Advanced Textbooks in Control and Signal Processing. Springer London, London, 2009.
- [3] T. Bajd, M. Mihelj, J. Lenarčič, A. Stanovnik, and M. Munih. *Robotics*. Springer Dordrecht Heidelberg, London New York, 2010.
- [4] M. Ben-Ari and F. Mondada. *Elements of Robotics*. Springer International Publishing, Cham, 2017.
- [5] G. Bekey and J. Yuh. The status of robotics. *IEEE Robot. Autom. Mag.*, 14(4): 76–81, dec 2007.
- [6] E. Garcia, M. A. Jimenez, P. G. De Santos, and M. Armada. The evolution of robotics research. *IEEE Robot. Autom. Mag.*, 14(1):90–103, mar 2007.
- [7] G. Bekey and J. Yuh. The Status of Robotics: Report on the WTEC International Study: Part II. *IEEE Robot. Autom. Mag.*, 15(1):80–86, mar 2008.
- [8] *Oxford English dictionary*. Oxford University Press, Oxford, 2021.
- [9] *Cambridge dictionary*. Cambridge University Press, Cambridge, 2021.
- [10] *Random House Webster's dictionary of American English*. Random House Reference, New York, NY, 1997.
- [11] B. Siciliano and O. Khatib. *Springer handbook of robotics*, volume 46. Springer Berlin Heidelberg, Berlin, Heidelberg, 2009.
- [12] H. Skubch. *Modelling and controlling of behaviour for autonomous mobile robots*. Springer, 2013.

- [13] S. N. Young and J. M. Peschel. Review of Human-Machine Interfaces for Small Unmanned Systems with Robotic Manipulators. *IEEE Trans. Human-Machine Syst.*, 50(2):131–143, 2020.
- [14] K. Nakadai, M. Kumon, H. G. Okuno, K. Hoshiba, M. Wakabayashi, K. Washizaki, T. Ishiki, D. Gabriel, Y. Bando, T. Morito, R. Kojima, and O. Sugiyama. Development of microphone-array-embedded UAV for search and rescue task. In *IEEE Int. Conf. Intell. Robot. Syst.*, volume 2017-Sept, pages 5985–5990. IEEE, sep 2017.
- [15] T. I. Zohdi. Multiple UAVs for Mapping: A Review of Basic Modeling, Simulation, and Applications. *Annu. Rev. Environ. Resour.*, 43(1):523–543, oct 2018.
- [16] E. Simetti, F. Wanderlingh, S. Torelli, M. Bibuli, A. Odetti, G. Bruzzone, D. L. Rizzini, J. Aleotti, G. Palli, L. Moriello, and U. Scarcia. Autonomous Underwater Intervention: Experimental Results of the MARIS Project. *IEEE J. Ocean. Eng.*, 43(3):620–639, 2018.
- [17] J. Cao, D. Lu, D. Li, Z. Zeng, B. Yao, and L. Lian. Smartfloat: A Multimodal Underwater Vehicle Combining Float and Glider Capabilities. *IEEE Access*, 7: 77825–77838, 2019.
- [18] E. Simetti and G. Casalino. Manipulation and Transportation With Cooperative Underwater Vehicle Manipulator Systems. *IEEE J. Ocean. Eng.*, 42(4):782–799, 2017.
- [19] C. Potena, R. Khanna, J. Nieto, R. Siegwart, D. Nardi, and A. Pretto. AgriColMap: Aerial-Ground Collaborative 3D Mapping for Precision Farming. *IEEE Robot. Autom. Lett.*, 4(2):1085–1092, apr 2019.
- [20] A. Pretto, S. Aravecchia, W. Burgard, N. Chebrolu, C. Dornhege, T. Falck, F. V. Fleckenstein, A. Fontenla, M. Imperoli, R. Khanna, F. Liebis, P. Lottes, A. Milioto, D. Nardi, S. Nardi, J. Pfeifer, M. Popovic, C. Potena, C. Pradalier, E. Rothacker-Feder, I. Sa, A. Schaefer, R. Siegwart, C. Stachniss, A. Walter, W. Winterhalter, X. Wu, and J. Nieto. Building an Aerial-Ground Robotics System for Precision Farming: An Adaptable Solution. *IEEE Robot. Autom. Mag.*, 28(3):29–49, 2021.
- [21] T. Sasaki, K. Otsu, R. Thakker, S. Haesaert, and A. A. Agha-Mohammadi. Where to map? Iterative rover-copter path planning for mars exploration. *IEEE Robot. Autom. Lett.*, 5(2):2123–2130, 2020.
- [22] S. J. Russell and P. Norving. *Artificial Intelligence: A Modern Approach*. Prentice Hall Press, Upper Saddle River, NJ, USA, 1995.
- [23] M. Wooldridge. *An Introduction to Multiagent Systems*. John Wiley & Sons, 2002.
- [24] J. Cortés and M. Egerstedt. Coordinated Control of Multi-Robot Systems: A Survey. *SICE J. Control. Meas. Syst. Integr.*, 10(6):495–503, 2017.

-
- [25] E. Sahin. Swarm Robotics: From Sources of Inspiration to Domains of Application. In E. ahin, , and W. M. Spears, editors, *Swarm Robot.*, pages 10–20, Berlin, Heidelberg, 2005. Springer, Berlin, Heidelberg.
- [26] H. Hamann. *Swarm Robotics: A Formal Approach*. Springer International Publishing, Cham, 2018.
- [27] G. Vásárhelyi, C. Virágh, G. Somorjai, T. Nepusz, A. E. Eiben, and T. Vicsek. Optimized flocking of autonomous drones in confined environments. *Sci. Robot.*, 3(20), jul 2018.
- [28] E. Ordaz-Rivas, A. Rodriguez-Liñan, M. Aguilera-Ruíz, and L. Torres-Treviño. Collective Tasks for a Flock of Robots Using Influence Factor. *J. Intell. Robot. Syst. Theory Appl.*, 94(2):439–453, 2019.
- [29] M. Coppola, K. N. McGuire, C. De Wagter, and G. C. H. E. de Croon. A Survey on Swarming With Micro Air Vehicles: Fundamental Challenges and Constraints. *Front. Robot. AI*, 7:18, feb 2020.
- [30] E. Ordaz-Rivas, A. Rodriguez-Liñan, and L. Torres-Treviño. Flock of Robots with Self-Cooperation for Prey-Predator Task. *J. Intell. Robot. Syst. Theory Appl.*, 101(2), 2021.
- [31] H. Oh, A. Ramezan Shirazi, C. Sun, and Y. Jin. Bio-inspired self-organising multi-robot pattern formation: A review. *Rob. Auton. Syst.*, 91:83–100, may 2017.
- [32] I. Slavkov, D. Carrillo-Zapata, N. Carranza, X. Diego, F. Jansson, J. Kaandorp, S. Hauert, and J. Sharpe. Morphogenesis in robot swarms. *Sci. Robot.*, 3(25), dec 2018.
- [33] E. B. Ferreira-Filho and L. C. Pimenta. Abstraction based approach for segregation in heterogeneous robotic swarms. *Rob. Auton. Syst.*, 122:103295, dec 2019.
- [34] A. Howard, L. E. Parker, and G. S. Sukhatme. Experiments with a large heterogeneous mobile robot team: Exploration, mapping, deployment and detection. *Int. J. Rob. Res.*, 25(5-6):431–447, may 2006.
- [35] M. Dorigo, D. Floreano, L. M. Gambardella, F. Mondada, S. Nolfi, T. Baaboura, M. Birattari, M. Bonani, M. Brambilla, A. Brutschy, D. Burnier, A. Campo, A. L. Christensen, A. Decugniere, G. Di Caro, F. Ducatelle, E. Ferrante, A. Forster, J. M. Gonzales, J. Guzzi, V. Longchamp, S. Magnenat, N. Mathews, M. Montes de Oca, R. O’Grady, C. Pinciroli, G. Pini, P. Retornaz, J. Roberts, V. Sperati, T. Stirling, A. Stranieri, T. Stutzle, V. Trianni, E. Tuci, A. E. Turgut, and F. Vaussard. Swarmanoid: A Novel Concept for the Study of Heterogeneous Robotic Swarms. *IEEE Robot. Autom. Mag.*, 20(4):60–71, dec 2013.

- [36] M. Langerwisch, T. Wittmann, S. Thamke, T. Remmersmann, A. Tiderko, and B. Wagner. Heterogeneous teams of unmanned ground and aerial robots for reconnaissance and surveillance - A field experiment. In *2013 IEEE Int. Symp. Safety, Secur. Rescue Robot. SSRR 2013*, pages 1–6. IEEE, oct 2013.
- [37] N. Bezzo, B. Griffin, P. Cruz, J. Donahue, R. Fierro, and J. Wood. A cooperative heterogeneous mobile wireless mechatronic system. *IEEE/ASME Trans. Mechatronics*, 19(1):20–31, feb 2014.
- [38] T. Gunn and J. Anderson. Dynamic heterogeneous team formation for robotic urban search and rescue. *J. Comput. Syst. Sci.*, 81(3):553–567, may 2015.
- [39] W. Ren and C. Yongcan. *Distributed Coordination of Multi-agent Networks: Emergent Problems, Models, and Issues*. Springer-Verlag London, 1 edition, 2011.
- [40] I. Navarro and F. Matía. A survey of collective movement of mobile robots. *Int. J. Adv. Robot. Syst.*, 10(1):73, jan 2013.
- [41] T. Balch and R. C. Arkin. Behavior-based formation control for multirobot teams. *IEEE Trans. Robot. Autom.*, 14(6):926–939, 1998.
- [42] W. Ren and R. W. Beard. *Distributed Consensus in Multi-vehicle Cooperative Control: Theory and Applications*. Springer-verlag, 2008.
- [43] R. Olfati-Saber, J. A. Fax, and R. M. Murray. Consensus and cooperation in networked multi-agent systems. *Proc. IEEE*, 95(1):215–233, jan 2007.
- [44] M. H. Degroot. Reaching a consensus. *J. Am. Stat. Assoc.*, 69(345):118–121, 1974.
- [45] T. Vicsek, A. Czirok, E. Ben-Jacob, I. Cohen, and O. Shochet. Novel Type of Phase Transition in a System of Self-Driven Particles. *Phys. Rev. Lett.*, 75:1226–1229, 1995.
- [46] A. Jadbabaie, J. Lin, and A. S. Morse. Mobile Autonomous Agents Using Nearest Neighbor Rules*. *Proc. 41st IEEE Conf. Decis. Control*, (December):2953–2958, 2002.
- [47] K. K. Oh, M. C. Park, and H. S. Ahn. A survey of multi-agent formation control. *Automatica*, 53:424–440, mar 2015.
- [48] J. Qin, Q. Ma, Y. Shi, and L. Wang. Recent advances in consensus of multi-agent systems: A brief survey. *IEEE Trans. Ind. Electron.*, 64(6):4972–4983, jun 2017.
- [49] P. Shi and B. Yan. A Survey on Intelligent Control for Multiagent Systems. *IEEE Trans. Syst. Man, Cybern. Syst.*, 51(1):161–175, 2021.
- [50] Y. Liu, Y. Jia, J. Du, and F. Yu. Consensus problem of multiple inertial agents with fixed and switching topologies. *Proc. World Congr. Intell. Control Autom.*, pages 1470–1475, 2008.

-
- [51] W. Li and M. W. Spong. Stability of general coupled inertial agents. *IEEE Trans. Automat. Contr.*, 55(6):1411–1416, 2010.
- [52] G. Chen and F. L. Lewis. Leader-following control for multiple inertial agents. *Int. J. Robust Nonlinear Control*, 21(8):925–942, may 2011.
- [53] M. M. Zavlanos, M. B. Egerstedt, and G. J. Pappas. Graph-theoretic connectivity control of mobile robot networks. In *Proc. IEEE*, volume 99, pages 1525–1540, sep 2011.
- [54] M. Ji and M. Egerstedt. Distributed Coordination Control of Multiagent Systems While Preserving Connectedness. *IEEE Trans. Robot.*, 23(4):693–703, aug 2007.
- [55] M. M. Zavlanos and G. J. Pappas. Distributed Connectivity Control of Mobile Networks. *IEEE Trans. Robot.*, 24(6):1416–1428, 2008.
- [56] M. M. Zavlanos, H. G. Tanner, A. Jadbabaie, and G. J. Pappas. Hybrid control for connectivity preserving flocking. *IEEE Trans. Automat. Contr.*, 54(12):2869–2875, dec 2009.
- [57] N. Michael, M. M. Zavlanos, V. Kumar, and G. J. Pappas. Maintaining Connectivity in Mobile Robot Networks. In *Springer Tracts Adv. Robot.*, volume 54, pages 117–126. Springer, Berlin, Heidelberg, 2009.
- [58] H. Su, X. Wang, and G. Chen. Rendezvous of multiple mobile agents with preserved network connectivity. *Syst. Control Lett.*, 59:313–322, 2010.
- [59] A. Ajorlou, A. Momeni, and A. G. Aghdam. A class of bounded distributed control strategies for connectivity preservation in multi-agent systems. *IEEE Trans. Automat. Contr.*, 55(12):2828–2833, dec 2010.
- [60] P. Li, S. Xu, W. Chen, Y. Wei, and Z. Zhang. A connectivity preserving rendezvous for unicycle agents with heterogenous input disturbances. *J. Franklin Inst.*, 355(10):4248–4267, jul 2018.
- [61] Y. Dong, Y. Su, Y. Liu, and S. Xu. An internal model approach for multi-agent rendezvous and connectivity preservation with nonlinear dynamics. *Automatica*, 89:300–307, mar 2018.
- [62] Y. Dong and S. Xu. Rendezvous problem of multiple linear uncertain systems under state-dependent dynamic networks. *J. Franklin Inst.*, 356(15):8325–8343, 2019.
- [63] C. W. Reynolds. Flocks, herds and schools: A distributed behavioral model. In *ACM SIGGRAPH Comput. Graph.*, volume 21, pages 25–34, 1987.
- [64] R. Olfati-Saber. Flocking for Multi-Agent Dynamic Systems: Algorithms and Theory. *IEEE Trans. Automat. Contr.*, 51(3):401–420, mar 2006.

- [65] L. E. Beaver and A. A. Malikopoulos. An overview on optimal flocking. *Annu. Rev. Control*, 51(March):88–99, 2021.
- [66] G. Wen, Z. Duan, Z. Li, and G. Chen. Flocking of multi-agent dynamical systems with intermittent nonlinear velocity measurements. *Int. J. Robust Nonlinear Control*, 22(16):1790–1805, nov 2012.
- [67] F. Sun, R. Wang, W. Zhu, and Y. Li. Flocking in nonlinear multi-agent systems with time-varying delay via event-triggered control. *Appl. Math. Comput.*, 350: 66–77, 2019.
- [68] Z. Feng and G. Hu. Connectivity-preserving flocking for networked Lagrange systems with time-varying actuator faults. *Automatica*, 109:108509, 2019.
- [69] Z. Chen, M.-C. Fan, and H.-T. Zhang. How Much Control is Enough for Network Connectivity Preservation and Collision Avoidance? *IEEE Trans. Cybern.*, 45 (8):1647–1656, aug 2015.
- [70] Housheng Su, Xiaofan Wang, and Zongli Lin. Flocking of multi-agents with a virtual leader. *IEEE Trans. Automat. Contr.*, 54(2):293–307, 2009.
- [71] W. Yu, G. Chen, and M. Cao. Distributed leader-follower flocking control for multi-agent dynamical systems with time-varying velocities. *Syst. Control Lett.*, 59(9):543–552, 2010.
- [72] G. Wen, Z. Duan, H. Su, G. Chen, and W. Yu. A Connectivity-preserving flocking algorithm for multi-agent dynamical systems with bounded potential function. *IET Control Theory Appl.*, 6(6):813, 2012.
- [73] Y. Mao, L. Dou, H. Fang, and J. Chen. Bounded Connectivity-Preserving Leader-Follower Flocking Algorithms Without Acceleration Measurements. *Asian J. Control*, 17, 2015.
- [74] A. Gasparri, L. Sabattini, and G. Ulivi. Bounded control law for global connectivity maintenance in cooperative multirobot systems. *IEEE Trans. Robot.*, 33 (3):700–717, jun 2017.
- [75] P. Li, S. Xu, W. Chen, Y. Wei, and Z. Zhang. Adaptive finite-time flocking for uncertain nonlinear multi-agent systems with connectivity preservation. *Neurocomputing*, 275:1903–1910, jan 2018.
- [76] K. Khateri, M. Pourgholi, M. Montazeri, and L. Sabattini. A connectivity preserving node permutation local method in limited range robotic networks. *Rob. Auton. Syst.*, 129:103540, 2020.
- [77] H.-T. Zhang, Z. Cheng, G. Chen, and C. Li. Model predictive flocking control for second-order multi-agent systems with input constraints. *IEEE Trans. Circuits Syst. I Regul. Pap.*, 62(6):1599–1606, jun 2015.

-
- [78] H. T. Zhang, B. Liu, Z. Cheng, and G. Chen. Model Predictive Flocking Control of the Cucker-Smale Multi-Agent Model with Input Constraints. *IEEE Trans. Circuits Syst. I Regul. Pap.*, 63(8):1265–1275, aug 2016.
- [79] R. Maeda, T. Endo, and F. Matsuno. Decentralized Navigation for Heterogeneous Swarm Robots With Limited Field of View. *IEEE Robot. Autom. Lett.*, 2(2):904–911, apr 2017.
- [80] M. Yoshimoto, T. Endo, R. Maeda, and F. Matsuno. Decentralized navigation method for a robotic swarm with nonhomogeneous abilities. *Auton. Robots*, 42(8):1583–1599, dec 2018.
- [81] X. Li, D. Sun, and J. Yang. A bounded controller for multirobot navigation while maintaining network connectivity in the presence of obstacles. *Automatica*, 49(1):285–292, jan 2013.
- [82] J. Li, W. Zhang, H. Su, and Y. Yang. Flocking of partially-informed multi-agent systems avoiding obstacles with arbitrary shape. *Auton. Agent. Multi. Agent. Syst.*, 29(5):943–972, sep 2015.
- [83] D. Sakai, H. Fukushima, and F. Matsuno. Leader-Follower Navigation in Obstacle Environments While Preserving Connectivity Without Data Transmission. *IEEE Trans. Control Syst. Technol.*, pages 1–16, 2017.
- [84] P. Yang, R. Freeman, G. Gordon, K. Lynch, S. Srinivasa, and R. Sukthankar. Decentralized estimation and control of graph connectivity for mobile sensor networks. *Automatica*, 46(2):390–396, feb 2010.
- [85] M. Franceschelli, A. Gasparri, A. Giua, and C. Seatzu. Decentralized estimation of Laplacian eigenvalues in multi-agent systems. *Automatica*, 49(4):1031–1036, apr 2013.
- [86] R. Aragues, G. Shi, D. V. Dimarogonas, C. Sagiús, K. H. Johansson, and Y. Mezouar. Distributed algebraic connectivity estimation for undirected graphs with upper and lower bounds. *Automatica*, 50(12):3253–3259, dec 2014.
- [87] T. M. D. Tran and A. Y. Kibangou. Distributed estimation of Laplacian eigenvalues via constrained consensus optimization problems. *Syst. Control Lett.*, 80: 56–62, jun 2015.
- [88] H. A. Poonawala and M. W. Spong. Decentralized estimation of the algebraic connectivity for strongly connected networks. In *2015 Am. Control Conf.*, pages 4068–4073, Chicago, IL, 2015. IEEE.
- [89] L. Sabattini, C. Secchi, and N. Chopra. Decentralized Estimation and Control for Preserving the Strong Connectivity of Directed Graphs. *IEEE Trans. Cybern.*, 45(10):2273–2286, oct 2015.

- [90] L. Sabattini, N. Chopra, and C. Secchi. Decentralized connectivity maintenance for cooperative control of mobile robotic systems. *Int. J. Rob. Res.*, 32(12): 1411–1423, 2013.
- [91] L. Sabattini, C. Secchi, N. Chopra, and A. Gasparri. Distributed control of multirobot systems with global connectivity maintenance. *IEEE Trans. Robot.*, 29(5):1326–1332, 2013.
- [92] H. Fang, Y. Wei, J. Chen, and B. Xin. Flocking of Second-Order Multiagent Systems With Connectivity Preservation Based on Algebraic Connectivity Estimation. *IEEE Trans. Cybern.*, 47(4):1067–1077, apr 2017.
- [93] K. Li, R. Gong, S. Wu, C. Hu, and Y. Wang. Decentralized Robust Connectivity Control in Flocking of Multi-Robot Systems. *IEEE Access*, 8:105250–105262, jun 2020.
- [94] H. A. Poonawala and M. W. Spong. Preserving Strong Connectivity in Directed Proximity Graphs. *IEEE Trans. Automat. Contr.*, 62(9):4392–4404, sep 2017.
- [95] E. J. Ávila-Martínez and J. G. Barajas-Ramírez. Consenso con líder virtual en sistemas de múltiples agentes inerciales. In *Congr. Nac. Control Automático*, page 6, Monterrey, Nuevo León, 2017.
- [96] E. J. Ávila-Martínez and J. G. Barajas-Ramírez. Distributed control for consensus on leader-followers proximity graphs. In *IFAC-PapersOnLine*, volume 51, pages 240–245, Guadalajara, Jalisco, México, 2018.
- [97] E. J. Ávila-Martínez and J. G. Barajas-Ramírez. Flocking motion in swarms with limited sensing radius and heterogeneous input constraints. *J. Franklin Inst.*, 358(4):2346–2366, mar 2021.
- [98] J. R. Silvester. Determinants of block matrices. *Math. Gaz.*, 84(501):460–467, nov 2000.
- [99] Z. Qu. *Cooperative Control of Dynamical Systems: Applications to Autonomous Vehicles*. 2009.
- [100] C. W. Wu. *Synchronization in Complex Networks of Nonlinear Dynamical Systems*. World Scientific, Singapore, oct 2007.
- [101] C. Godsil and G. Royle. *Algebraic Graph Theory*, volume 207 of *Graduate Texts in Mathematics*. Springer New York, New York, NY, 2001.
- [102] M. Mesbahi and M. Egerstedt. *Graph theoretic methods in multiagent networks*. Princeton University Press, 2010.
- [103] Z. Li. *Cooperative Control of Multi-agent System Consensus Region Approach*. CRC Press, Boca Raton, Florida, 1st editio edition, 2015.

-
- [104] H. Guo, M. Y. Li, and Z. Shuai. A graph-theoretic approach to the method of global Lyapunov functions. *Proc. Am. Math. Soc.*, 136(08):2793–2802, 2008.
- [105] A. Bara and S. Dale. Dynamic modeling and stabilization of wheeled mobile robot. *Proc. 5th WSEAS Int. Conf. Dyn. Syst. Control*, (CONTROL'09):87–92, 2009.
- [106] R. W. Brockett. Asymptotic stability and feedback stabilization. In *Differ. Geom. Control Theory*, pages 181–191, 1983.
- [107] J. B. Pomet. Explicit design of time-varying stabilizing control laws for a class of controllable systems without drift. *Syst. Control Lett.*, 18(2):147–158, feb 1992.
- [108] C. C. de Wit and O. J. Sordalen. Exponential Stabilization of Mobile Robots with Nonholonomic Constraints. In *Proc. 30th IEEE Conf. Decis. Control*, volume 1, pages 692–697, 1991.
- [109] C. Samson. Time-varying Feedback Stabilization of Car-like Wheeled Mobile Robots. *Int. J. Rob. Res.*, 12(1):55–64, feb 1993.
- [110] A. Astolfi. Exponential stabilization of a wheeled mobile robot via discontinuous control. *J. Dyn. Syst. Meas. Control. Trans. ASME*, 121(1):121–126, mar 1999.
- [111] A. Isidori. *Nonlinear Control Systems*. Communications and Control Engineering. Springer London, London, 1995.
- [112] R. Rahimi, F. Abdollahi, and K. Naqshi. Time-varying formation control of a collaborative heterogeneous multi agent system. *Rob. Auton. Syst.*, 62(12):1799–1805, dec 2014.
- [113] Q. Quan. *Introduction to multicopter design and control*. Springer Singapore, jun 2017.
- [114] L. R. García Carrillo, A. E. Dzúl López, R. Lozano, and C. Pégard. *Quad Rotorcraft Control: Vision-Based Hovering and Navigation*. Advances in Industrial Control. Springer London, London, 2013.
- [115] E. G. Hernandez-Martinez, G. Fernandez-Anaya, E. D. Ferreira, J. J. Flores-Godoy, and A. Lopez-Gonzalez. Trajectory Tracking of a Quadcopter UAV with Optimal Translational Control. *IFAC-PapersOnLine*, 48(19):226–231, 2015.
- [116] D. Lee and M. W. Spong. Flocking of Multiple inertial systems on Balanced Graph. In *Proc. 2006 Am. Control Conf.*, pages 2136–2141, 2006.
- [117] H.-T. Zhang, Z. Cheng, G. Chen, and C. Li. Model predictive flocking control for second-order multi-agent systems with input constraints. *IEEE Trans. Circuits Syst. I Regul. Pap.*, 62(6):1599–1606, jun 2015.

- [118] T. Chu, L. Wang, T. Chen, and S. Mu. Complex emergent dynamics of anisotropic swarms: Convergence vs oscillation. *Chaos, Solitons & Fractals*, 30(4):875–885, nov 2006.
- [119] R. Maeda, T. Endo, and F. Matsuno. Decentralized Navigation for Heterogeneous Swarm Robots With Limited Field of View. *IEEE Robot. Autom. Lett.*, 2(2):904–911, apr 2017.
- [120] R. Olfati-Saber. Flocking for multi-agent dynamic systems: Algorithms and theory. Technical report, California Institute of Technology, Control and Dynamical Systems, Pasadena, California, jun 2004.
- [121] J. Wang, H. Zhao, Y. Bi, S. Shao, Q. Liu, X. Chen, R. Zeng, Y. Wang, and L. Ha. An Improved Fast Flocking Algorithm with Obstacle Avoidance for Multiagent Dynamic Systems. *J. Appl. Math.*, 2014(1992), 2014.
- [122] D. Sakai, H. Fukushima, and F. Matsuno. Flocking for Multirobots Without Distinguishing Robots and Obstacles. *IEEE Trans. Control Syst. Technol.*, 25(3):1019–1027, may 2017.
- [123] D. Cai, S. Wu, and J. Deng. Distributed Global Connectivity Maintenance and Control of Multi-Robot Networks. *IEEE Access*, 5:9398–9414, 2017.
- [124] W. Li and M. W. Spong. Analysis of Flocking of Cooperative Multiple Inertial Agents via A Geometric Decomposition Technique. *IEEE Trans. Syst. Man, Cybern. Syst.*, 44(12):1611–1623, dec 2014.